INTERFACIAL COMPOSITIONS OF LONG-CHAIN MICELLES MEASURED BY THE CHEMICAL TRAPPING METHOD. DISCOVERY OF WEAK HYDROGEN BONDS IN 1-N-1•2BR BOLAFORM SALT CRYSTALS

by

YAN CAI

A dissertation submitted to the

Graduate School-New Brunswick

Rutgers, The State University of New Jersey

In partial fulfillment of the requirements

For the degree of

Doctor of Philosophy

Graduate Program in Chemistry and Chemical Biology

Written under the direction of

Professor Laurence S. Romsted

And approved by

_____

_____

_____

_____

New Brunswick, New Jersey

October, 2013

ABSTRACT OF THE DISSERTATION

INTERFACIAL COMPOSITIONS OF LONG-CHAIN MICELLES MEASURED BY THE CHEMICAL TRAPPING METHOD. DISCOVERY OF WEAK HYDROGEN BONDS IN 1-N-1•2BR BOLAFORM SALT CRYSTALS

By Yan Cai

Dissertation Director:

Laurence S. Romsted

Long-chain surfactants form micelles when the concentration reaches cmc. Micelles are composed of a hydrophobic core and an interfacial region containing head groups in contact with water molecules and counterions. Recent research shows that the interfacial region plays an important role in micellar properties and structures. The change of composition in the micellar solution shifts the balance of forces and changes the micelle size and shape as a result. Chemical trapping method is applied to estimate the interfacial compositions of micelles. The probe, 16-ArN_2^+, reacts with the weakly basic nucleophiles in the interfacial region, and the products are analyzed with HPLC.

Changes in interfacial concentrations of water and counterions through the sphere-to-rod transitions of CTAB and CTAC solutions have been studied by the

chemical trapping method, and the results have been published. In the second chapter of the thesis, the chemical trapping method was applied to long chain micellar solutions DTAB and CTAToS. When counterion salts are added in the surfactant solutions, the counterion concentration in micellar interfacial region increases incrementally.

Chapter 3 introduces non-conventional gemini surfactants 12-n-12•2Br (n = 2, 3 and 4) and their simple model bolaform sals 1-n-1•2Br (n = 2, 3 and 4). The twin-tailed structures have rather small 1^{st} and 2^{nd} cmcs comparing to their single-tailed analog DTAB. Single crystal X-ray diffraction technique is used to analyze bolaform salts. Weak hydrogen bonds are discovered in 1-2-1•2Br and 1-3-1•2Br crystals.

ACKNOWLEDGEMENT

I would like to thank Professor Laurence S. Romsted, who is my research advisor. I also want to thank Professor Ralf Warmuth and Professor Kai Hultzsch, who served as my committee members. I would like to thank Professor Peter C. Kahn as my outfield thesis committee member.

My bolaform salt crystals would not be obtained without the help of Doctor Tom Emge. Professor Joe Potenza also gave great suggestion on the explanation of crystal structures.

I also want to thanks the Romsted's group. They worked with me, discussed with me, and made the time I spent in Rutgers fun.

Finally, I would like to thank my parents, my husband, and my lovely little daughter Audrey. Thanks for their love and support in all these years.

DEDICATION

To my families.

Table of Contents

LIST OF FIGURES

LIST OF TABLES

Chapter 1. Chemical Trapping method

1.1 Surfactants

Surfactants are surface-active molecules. They are composed of hydrophilic head groups and hydrophobic tails, Figure 1. Surfactants are generally characterized by their head group types, such as cationic, anionic, nonionic, and zwitterionic. Depending upon surfactant structure and solution composition, surfactants spontaneously form assemblies with different structures, such as spherical and rod-like micelles, bilayers and vesicles, Figure 1.[1-3]

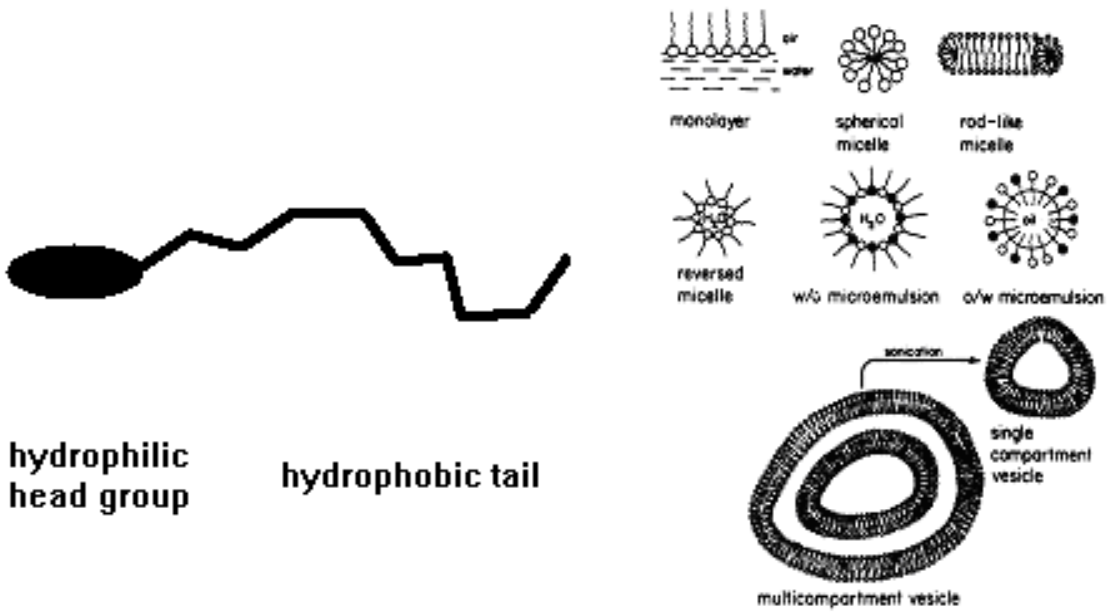

Figure 1. Common shape of a surfactant (left), and several assemblies that surfactants form (right).[3]

When the surfactant concentration exceeds a critical value, virtually all additional surfactant added spontaneously forms spherical micelles. This concentration is called the critical micelle concentration, or cmc. In general, the cmc depends on surfactant structure such as head group size, hydrophobic chain length, temperature, and electrolyte and other additive concentrations.

Table 1. Surfactant cmcs and sphere-to-rod transition concentrations of cationic surfactants with different tail lengths, headgroup structures and counterions.[4]

Surfactant*	No.C's Tail	Head Group, X	Cmc/mM	2^{nd} cmc/M	Reference
CTAB	16	$-N(Me)_3^+ Br^-$	0.98	~0.1	Okuda, 1987
CTAC	16	$-N(Me)_3^+ Cl^-$	1.3	~1.0	Raston, 1947
DTAB	12	$-N(Me)_3^+ Br^-$	16	~1.8	Klevens, 1948
DTAC	12	$-N(Me)_3^+ Cl^-$	20	none	Osugi, 1995
DDAB	12	$-NH(Me)_2^+ Br^-$	12.4	~0.1	Ikeda, 1984
DDAC	12	$-NH(Me)_2^+ Cl^-$	14.9	~0.8	Ikeda, 1984

*CTAB: cetyltrimethylammonium bromide

CTAC: cetyltrimethylammonium chloride

DTAB: dodecyltrimethylammonium bromide

DTAC: dodecyltrimethylammonium chloride

DDAB: dedecyldimethylammonium bromide

DDAC: dodecyldimethylammonium chloride

Table 1 lists the cmcs and sphere-to-rod transition concentrations of cationic surfactants with different head groups and tail lengths. The cmcs decrease as tail lengths increase, e.g. the cmc of DTAB is 16 mM, higher than the cmc of CTAB, 0.98 mM. The cmcs increase as the size of the head group increases and the anhydrous radius of the counterions decrease, e.g. the cmc of DTAB is higher than the cmc of DDAB, and the cmcs of chlorides are higher than the cmcs of bromides with the same tail lengths and headgroup sizes. Sphere-to-rod transitions are covered below.

The sphere-to-rod transition is a result of micelle growth. When spherical micelles form, counterions associate with the interface. As more surfactants or salts are added in the bulk solution, micelle starts to grow, and the concentration of counterions in the interface increases. When the concentration of counterions in the micellar interfacial region reaches a certain value, a sphere-to-rod transition takes place. This value is called the 2nd cmc, Figure 2.[5,6]

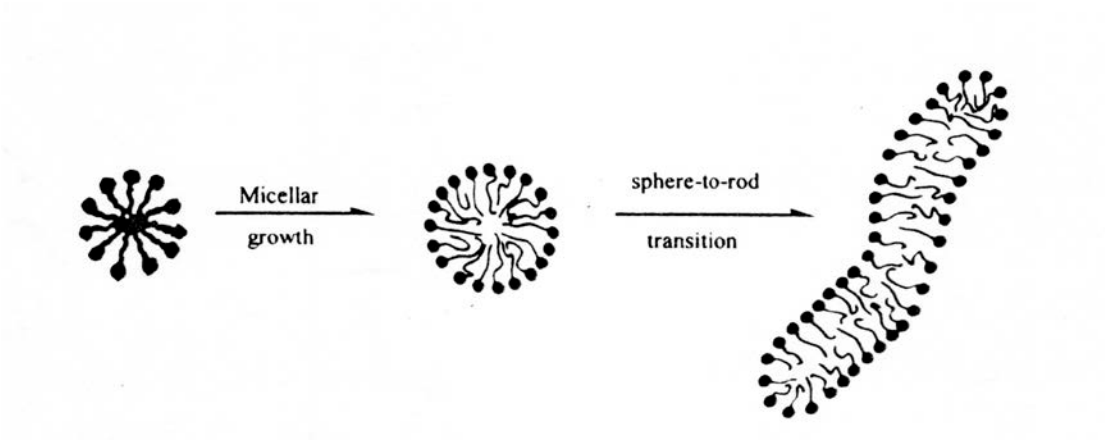

Figure 2. Cartoon of micellar growth and the sphere-to-rod Transition.[5]

Table 1 also lists the 2nd cmcs of surfactants for different head groups and tail lengths. The 1st and 2nd cmcs show parallel dependence on surfactant structure. The 2nd

cmcs decrease as tail lengths increase, e.g. the 2nd cmc of DTAB is 1.8 M, higher than the 2nd cmc of CTAB, 0.1 M. The 2nd cmcs increase as the size of the head group increases and the anhydrous radius of the counterions decrease, e.g. the 2nd cmc of DTAB is higher than the 2nd cmc of DDAB, and the 2nd cmcs of chlorides are higher than the 2nd cmcs of bromides with the same tail lengths and head group sizes.

1.2 Packing

Why do surfactant molecules aggregate into micelles but only to a limited size and aggregation number? Figure 3 shows a two-dimensional cartoon of micelle packing based on the concept that surfactant shape determines aggregate shape.[7,8] Cone-shaped surfactants pack to form spherical micelles. In water, the hydrophobic tails of the surfactants gather into a hydrophobic core with the hydrophilic head groups pack around the core to form an interfacial layer that also contains counterions and water.

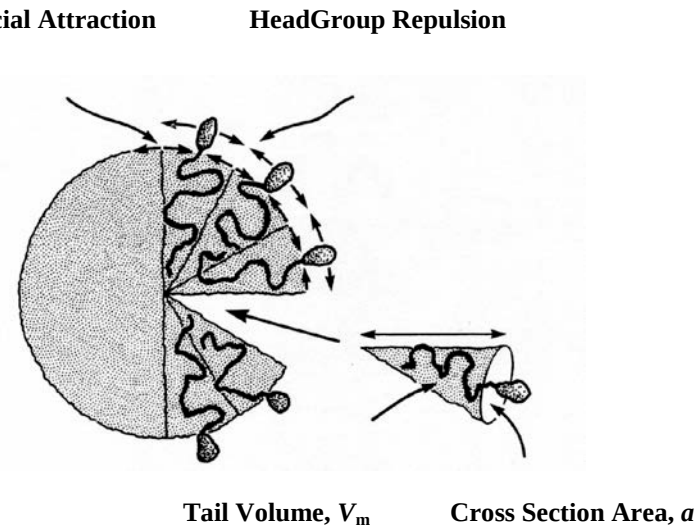

Figure 3. Factors contributing to micelle stability[7]

The packing parameter $p = V_h/l_c a_0$ correlates surfactant shape with aggregate shape. V_h is the volume of hydrophobic tail, l_c is the length of hydrophobic tail, and a_0 is the area of hydrophilic headgroup, Figure 3. Different packing parameters are associated with different aggregate shapes, Table 2.[1,6,7,9]

Table 2. Different micelle structures and their packing parameters

Value of $V_h/l_c a_0$	Micelle Structure
0~1/3	Spheroidal in aqueous media
1/3~1/2	Cylindrical in aqueous media
1/2~1	Lamellar in aqueous media
>1	Inverse (reversed) in nonpolar media

As p increases, micelle surface curvature decreases until at $p > 1$ the surface becomes concave. However, many surfactants form multiple structures, e.g. spherical, rod-like and at high concentrations lamellar mesophase which is inconsistent with a strict surfactant structure aggregate correlation and the change in balance of forces responsible for such transitions is an unsolved problem. [7]

The aggregation numbers (N) for most of ionic micelles are around 60~100. N depends on surfactant structure, e.g., the length of hydrophobic tail and hydrophilic headgroup, salt concentration and temperature. Table 3 lists values of N for a variety of ionic surfactants at different temperatures, chain lengths and counterion concentrations.[1] Surfactants with longer chain lengths have bigger aggregation numbers, e.g. DTAB (42)

< CTAB (75). Bigger head groups decrease aggregation numbers, e.g. in tetradecyltrialkylammonium bromide series C_4H_9 (35) < C_2H_5 (55) < CH_3 (106). The addition of counterions increases aggregation numbers, shown clearly for both DTAB and CTAB with added Br^- at the same surfactant concentration. Increasing the temperature reduces N, which is illustrated clearly for TTAB. However, the packing parameter does not explain the change of micelle shape and size.

Table 3. Aggregation numbers of surfactants at different temperatures, counterion concentrations, and chain lengths

Compound	Solvent	Temp. (ºC)	Aggregation number, N	Reference
$C_{12}H_{25}N^{+}(CH_3)_3Br^{-}$	H_2O (0.04 M conc.)	25	42	Rodenas, 1994
$C_{12}H_{25}N^{+}(CH_3)_3Br^{-}$	H_2O (0.10 M conc.)	25	69	Rodenas, 1994
$C_{12}H_{25}N^{+}(CH_3)_3Br^{-}$	0.02M KBr(0.04 M conc.)	25	49	Rodenas, 1994
$C_{12}H_{25}N^{+}(CH_3)_3Br^{-}$	0.08M KBr(0.04 M conc.)	25	59	Rodenas, 1994
$C_{12}H_{25}N^{+}(CH_3)_3Cl^{-}$	H_2O	25	50	Sowada, 1994
$[C_{12}H_{25}N^{+}(CH_3)_3]_2SO_4^{2-}$	H_2O	23	65	Tartar, 1955
$C_{14}H_{29}N^{+}(CH_3)_3Br^{-}$	H_2O ($1.05x10^{-1}$ M conc.)	5	131	Gorski, 2001
$C_{14}H_{29}N^{+}(CH_3)_3Br^{-}$	H_2O ($1.05x10^{-1}$ M conc.)	10	122	Gorski, 2001
$C_{14}H_{29}N^{+}(CH_3)_3Br^{-}$	H_2O ($1.05x10^{-1}$ M conc.)	20	106	Gorski, 2001
$C_{14}H_{29}N^{+}(CH_3)_3Br^{-}$	H_2O ($1.05x10^{-1}$ M conc.)	40	88	Gorski, 2001
$C_{14}H_{29}N^{+}(CH_3)_3Br^{-}$	H_2O ($1.05x10^{-1}$ M conc.)	60	74	Gorski, 2001
$C_{14}H_{29}N^{+}(CH_3)_3Br^{-}$	H_2O ($1.05x10^{-1}$ M conc.)	80	73	Gorski, 2001
$C_{14}H_{29}N^{+}(C_2H_5)_3Br^{-}$	H_2O	20	55	Lianos, 1982
$C_{14}H_{29}N^{+}(C_4H_9)_3Br^{-}$	H_2O	20	35	Lianos, 1982
$C_{16}H_{33}N^{+}(CH_3)_3Br^{-}$	H_2O (0.005 M conc.)	25	44	Rodenas, 1994
$C_{16}H_{33}N^{+}(CH_3)_3Br^{-}$	H_2O (0.021 M conc.)	25	75	Rodenas, 1994
$C_{16}H_{33}N^{+}(CH_3)_3Br^{-}$	0.1M KBr (0.005 M conc.)	25	57	Rodenas, 1994
$C_{16}H_{33}N^{+}(CH_3)_3Br^{-}$	0.1M KBr (0.021 M conc.)	25	71	Rodenas, 1994

1.3 Balance of forces

Micelles are stable, typically spherical or spheroidal structures in dilute, aqueous solution with aggregation numbers on the order of 50-150.[10,11] The hydrophobic tails organize spontaneously to form a hydrophobic core. The interfacial region composed of hydrophilic head groups, counterions, and water is formed between the hydrophobic core and polar aqueous solution, Figure 4.

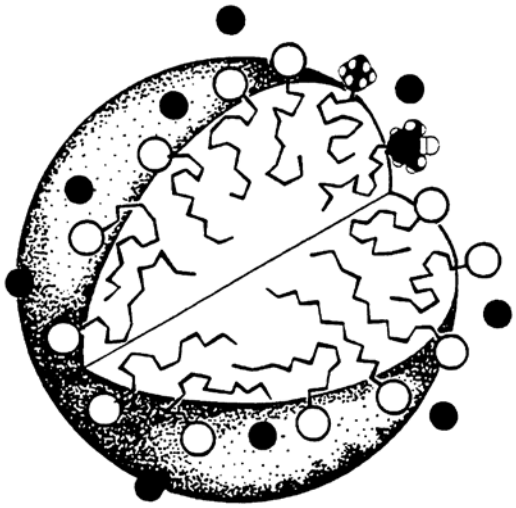

Figure 4. Cartoon of the composition of a cationic spherical micelle showing hydrophobic tails, headgroups (○), and counterions (●). Water molecules are not shown.[12]

The driving force for aggregation is the hydrophobic effect, sometimes called hydrophobic attraction.[12] Hydrophobic attraction induces the aggregation of hydrocarbon tails. In bulk solution, hydrophobic tails of surfactants are surrounded by water. When the concentration of surfactant is above cmc, the hydrocarbon chains associate with each other to form micelles. The free energy change at room temperature is give by $\Delta G_{micelle} =$

$\Delta H_{micelle} - T\Delta S_{micelle,}$ the energy difference between hydrophobic tails interacting with water and between each other is generally small ($\Delta H_{micelle} \sim 0$). However, $\Delta S_{micelle}$ is large and positive because water is released into the aqueous solution when micelle forms such that $\Delta G_{micelle} \approx - T\Delta S_{micelle} < 0$.

The balancing forces opposing the hydrophobic attraction are complicated, which can be the columbic repulsion between cationic headgroup, and the tendency to avoid contact between hydrophobic core and the solvent.[13] At equilibrium, the balance of forces determines the micelle size and shape.[14-16]

The change of composition in the micellar solution shifts the balance of forces and changes the micelle size and shape as a result. As more surfactants and counterion as salt are added to a micellar solution, micelles grow. Chemical trapping results are consistent with counterions entering the interfacial region to form ion pairs and more water is released, which lead to tighter packing of surfactant molecules and the shrinkage of interfacial region.[7,12] Figure 5 illustrates the hypothetic interfacial compositions of spherical and rod-like micelles.[17] The boundaries of interfacial regions are hypothetical, and the volumes of the interfacial regions are unknown because there is no method to measure them. Surfactants move frequently in and out of the micelles and come to kinetic equilibrium in both spherical and rod-like micelles. Sphere-to-rod transition occurs at the 2^{nd} cmc.

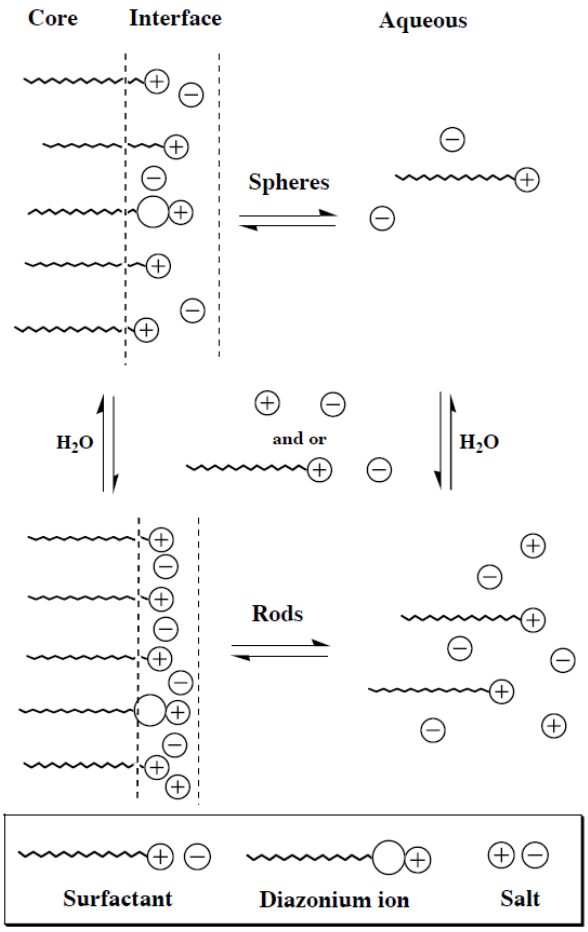

Figure 5. Hypothetic interfacial regions of spherical (top) and rod-like (bottom) micelles. Added surfactant and salt increase the counterion concentration in interfacial region and induce sphere-to-rod transition.[17]

Micelle growth is often attributed to coulombic interactions, i.e., added counterions screen repulsive interactions between headgroups, but the change in micellar shape and size can not be interpreted only in terms of coulombic effects because they also depend on counterion type. Ion specific effects have been observed in both chemistry and biology. In 1888, Hofmeister showed that a series of anions differ in their ability to solubilize proteins.[18] More ions have been added to Hofmeister's original series over the

last century. A common sequence of the series is: $I^- > ClO_4^- \approx NO_3^- > Br^- > Cl^- > OH^- \approx F^- \approx SO_4^{2-}$.[18] In this series, for example, Br^- is more polarized, less strongly hydrated, and has a stronger tendency to form ion pairs than Cl^-. Experimental results confirmed that Br^- forms rod-like micelles more easily than Cl^-, and has smaller 1st and 2nd cmc, Table 1.

1.4 Pseudophase ion exchange model

Understanding the relationships between aggregate structure and solution composition requires the determination of the composition of the micellar interfacial region. The pseudophase ion exchange model (PIE) describes counterion distributions in solution. The PIE considers the totality of the micelles in the water solution as a second phase different from the water phase. Counterions are either associated with the micellar pseudophase or free in aqueous solution. The degree of ionization, α, defines the fraction of counterions contributed by the interfacial region to the ion concentration of the aqueous pseudophase.

$$\alpha = \frac{[X_w] - \text{cmc}}{[D_t] - \text{cmc}} \qquad (1)$$

$[X_w]$ is concentration of free ion, and $[D_t]$ is concentration of surfactant. The degree of counterion association is $\beta = 1 - \alpha$. Square brackets indicate mole per liter of solution here and throughout the thesis.

The pseudophase ion exchange model is based on two assumptions. First, α is constant, independent of surfactant and salt concentrations.[19] Second, counterions exchange on a 1:1 basis,[20] one counterion enters the micellar interfacial region and one

counterion leaves simultaneously. In a spherical micelle with n surfactant monomers, (1-α) n counterions are in the Stern layer with the headgroups in interfacial region, and αn counterions are distributed in aqueous solution. Generally, α increases with increasing temperature, nonelectrolyte concentration, surfactant headgroup size, and the hydrated radius of the hydrophilic counterion, and decreases with increasing surfactant chain length. However, the measured α values are different for different methods.[21]

Figure 6. Pseudophase model applied to a dediazoniation reaction.[22]

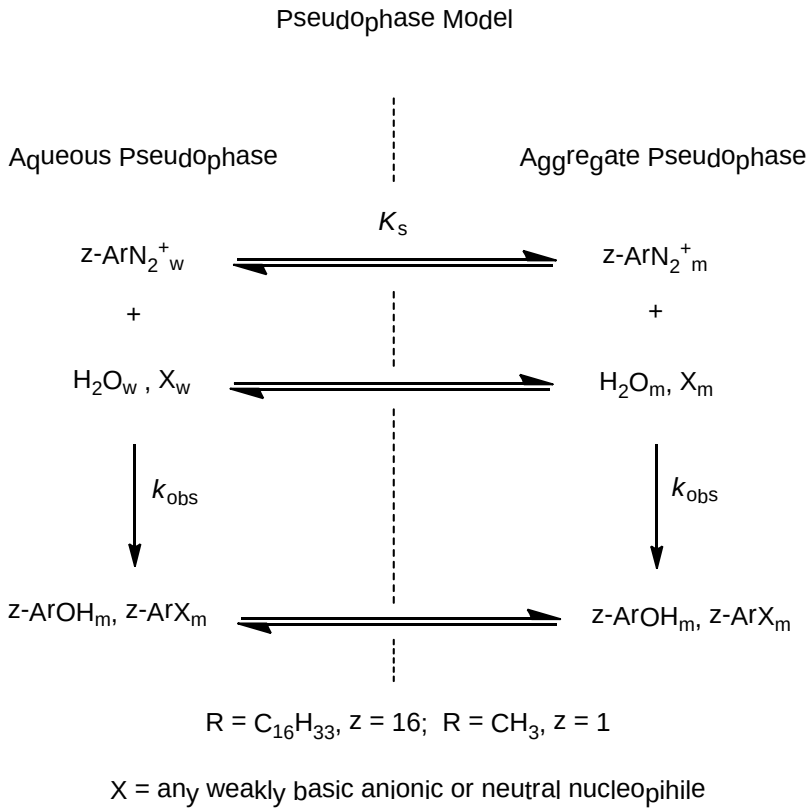

Figure 6 illustrates the pseudophase model as applied to a dediazoniation reaction, which will be introduced later, in interfacial region and bulk solution. The components

are located in either the aqueous or micellar pseudophase, i.e. a two site model. All the components including the probe are in dynamic equilibrium in the micellar solution, so the observed reaction rate is defined as:

$$k_{obs} = k_m[16\text{-}ArN_2^+]_m X_m + k_w[16\text{-}ArN_2^+]_w X_w \quad (2)$$

X is nucleophiles, i.e. H_2O, Br-, ROH, X_m indicates concentration in mole/L interfacial volume. The subscript w means in the water, and the subscript m means in the micelle. k_m and k_w are rate constants in micelles and in water. The distribution constant k_s for 16-ArN_2^+ is difficult to determine because it decomposes spontaneously.[23] However, assuming k_s of 16-ArN_2^+ is close to the k_s of a cationic surfactant ion with similar molecular structure, such as *N*-1-hexadecyl-3-carbamoylpyridinium bromide, then more than 97% of 16-ArN_2^+ is bound to the micelles at CTAB = 0.01 M.[24] Thus, k_{obs} at this and higher concentrations represents reaction in the micelles. The contribution from reaction in aqueous pseudophase solution is negligible.

In original PIE model, the counterion concentration in interfacial region is defined as

$$X_m = \frac{[X_m]}{[D_n]\,V_m} = \frac{\beta}{V_m} \quad (3)$$

where $[X_m]$ indicates concentration of counterion X^- contributed by micellar surfactant in the interfacial region, V_m is the volume available to X^- in the micellar interfacial region in liter per mole, $[D_n]$ is the micellized surfactant concentration, which equals $[D_t]$ – cmc. $[D_t]$ is the total surfactant concentration in the solution. $[X_m]/[D_n]$ is the definition of β. If β and V_m are constant, X_m is constant.

In the pseudophase ion exchange model as described above, X_m is assumed to be constant and independent of added salt. The original pseudophase assumption works when all the counterions in solution are contributed by reactive counterion surfactants, and in the absence of reactive counterion added as salt. Reactive counterion surfactants have only one counterion, which is also the nucleophile in the reaction, e.g., Br^- in CTAB micelles. Increasing the surfactant concentration increases the binding of the organic substrate to the micellar pseudophase. When the micellar concentration is high enough, the substrate is completely micelle bound, and the contribution to the observed reaction rate in the aqueous phase is negligible.[25-27]

However, a number of experiments demonstrate that this is not true. Early in 1979, Bunton and co-workers reported the failure of PIE for reactions of 2,4-dinitrochlorobenzene and –naphthalene in *p*-$C_8H_{17}O_6H_4CH_2N^+Me_3OH^-$, which in relatively high concentrations, k_{obs} continues to increase[28]. Nome and co-workers also discovered a similar deviation for dehydrochlorination results from the expected PIE model in CTAOH solutions with added NaOH as counterion salt. They suggested that k_{obs} also depended on the concentration of X^- in aqueous pseudophase.[29]

To interpret the chemical trapping in the thesis, we use a two-site pseudophase model in which both bound and free counterions are included in the interfacial region. The definition of X_m becomes

$$X_m = \frac{[X_m]}{[D_n]\,V_m} + [X_w] = \frac{\beta}{V_m} + [X_w] \qquad (4)$$

$[X_w]$ is counterion concentration in aqueous pseudophase solution.

This definition states that concentration of counterion in micellar interfacial region is the sum of interfacial and aqueous salt concentrations. The addition of counterion added as salt to the solution produces an equivalent increase of counterion concentration in micellar interfacial region.

1.5 Chemical Trapping Method

A variety of techniques have been used to determine compositions of micellar assemblies, e.g. conductometry, potentiometry, and spectrometry (NMR, UV-Vis, fluorescence, ESR, IR and circular dichroism)[22]. Some determine only one component at a time, some detect narrow composition ranges, and others report only physical properties, e.g. polarities, instead of compositions.

The chemical trapping method provides a new approach for determining molarities of water and counterions in micellar interfacial regions. In this method, the probe associates with the micelles with its reactive head group in the interfacial region and reacts with weakly basic nucleophiles such as water and halide ions. HPLC is used to determine the product yields.

1.5.1 Probe used in chemical trapping experiments

The probe is an arenediazonium ion, 4-hexadecyl-2,6-dimethylbenzenediazonium ion, 16-ArN_2^+, prepared as its tetrafluoroborate (BF_4^-) salt.

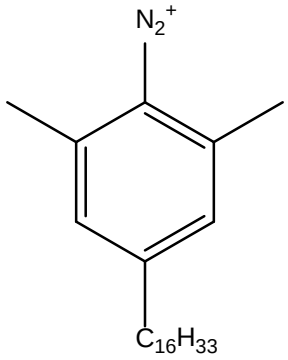

There are several reasons why arenediazonium ions are good, reliable probes in micelles. First, dediazoniation chemistry has been studied extensively and is well understood[22,24,30]. In arenadiazonium ions, nitrogen is replaced by nucleophiles including especially by nucleophilic solvents e.g. H_2O and EtOH.[31] Second, the products of dediazoniation reactions are generally very stable, permitting quantitative analysis. Third, the dediazoniation reaction rate is remarkably medium insensitive, which means the product yields from competitive reaction with nucleophiles are almost directly proportional to the conncentrations of nucleophiles. Fourth, the selectivities of nucleophiles are relatively low, which ensures that there are reasonable amounts of each product to be detected. Fifth, a variety of weakly basic functional groups, neutral and anionic, have been trapped by arenediazonium ions, showing the applicability of this method to a variety of biochemical and commercial surfactant systems, Figure 7.[4,22,24]

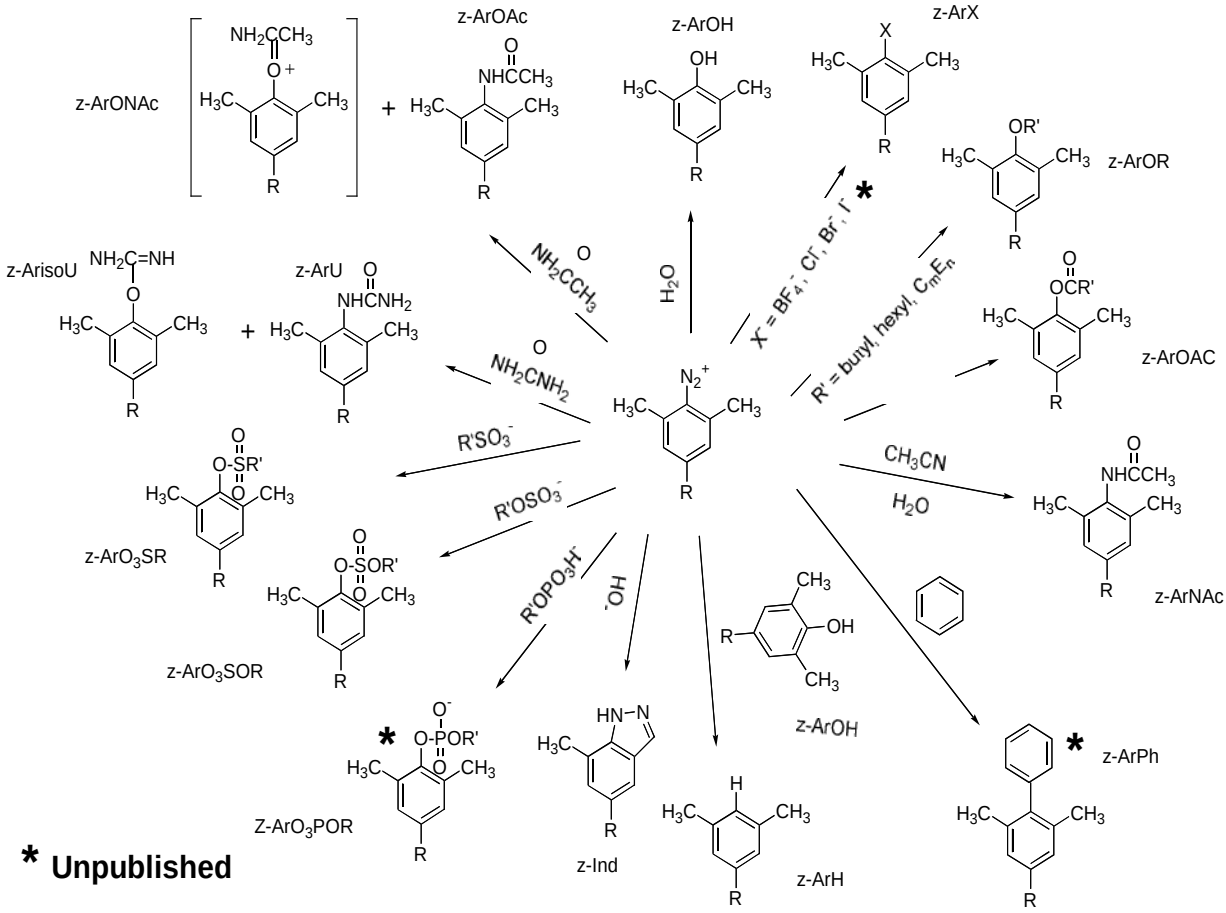

Figure 7. Arenediazonium ion reactions with a variety of functional groups. Reactions with OH^- and z-ArOH proceed via different mechanisms.

Water and halide ions replace the nitrogens to form a phenol and halide products. The phenol product reduces the arenediazonium ion to form a benzene derivative, and z-Ind is formed by a base-induced cyclization, as shown at the bottom of the figure. Other weakly basic nucleophiles, e.g. amides, RCO_2^-, CN^-, RSO_3^-, also react with the arenediazonium ion.

1.5.2 Reaction of *z*-ArN_2BF_4

16-ArN_2^+ is only slightly water soluble, and its long hydrocarbon chain is sufficiently hydrophobic to associate with the hydrophobic cores of micelles. The cationic head group, ArN_2^+, is assumed to be located in the micellar interfacial region with the similarly sized surfactant head groups, $CH_2N(CH_3)_4^+$. The amount of the probe added to the micellar solution is relatively small, typically 10^{-4} M, which means it has a negligible effect on micelle structure. The arenediazonium ion remains in the interfacial region and reacts with nucleophiles, Figure 8.[5]

Figure 8. Typical products from the dediazoniation reaction.

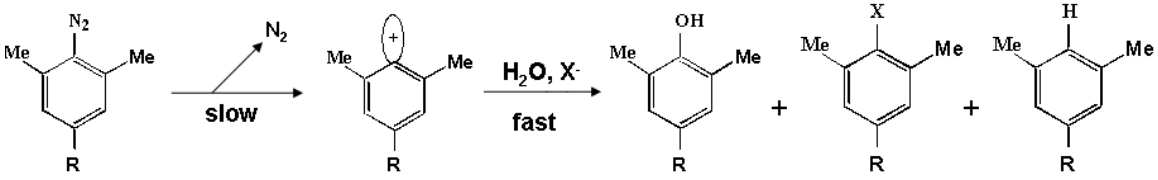

***z*-ArN_2^+** ***z*-Ar^+** ***z*-ArOH** ***z*-ArX** ***z*-ArH**

***z* =1, R = CH_3 ; *z* = 16, R = $C_{16}H_{33}$; X is a weakly basic nucleophile, e.g., Cl, Br**

In the dediazoniation reaction, the slow step is the loss of the diazonio group, followed by rapid reaction of the intermediate aryl cation with weakly basic nucleophiles, e.g., Br^- and H_2O, in the interfacial region of CTAB micelles, producing 16-ArBr and 16-ArOH, which are stable. The total yield approaches 100%. 16-ArH is the reduced product from the reaction of 16-ArOH and unreacted 16-ArN_2^+, which can be suppressed in acidic solution.[14] The short chain arenediazonium ion, 1-ArN_2^+, is used as the reference

for the reaction in micelles because its aqueous salt solutions can be prepared at same molarities of counterion and water as the micellar interfacial region.[14]

1.5.3 Basic Assumptions of the Chemical Trapping Method

The chemical trapping method is based on the assumption that the selectivity of 16-ArN_2^+ toward different nucleophiles, S_w^x, in the micellar interfacial region is the same as that of 1-ArN_2^+ toward those nucleophiles in aqueous bulk solution at the same concentrations of the nucleophile equations. That is, if the yields are the same, the concentrations are the same.

$$S_w^x = \frac{[H_2O](\%1\text{-ArX})}{[TMAX](\%1\text{-ArOH})} = \frac{H_2O_m(\%16\text{-ArX})}{X_m(\%16\text{-ArOH})} \quad (5)$$

Figure 9 illustrates the reactions of 16-ArN_2^+ and 1-ArN_2^+ in the micellar and the aqueous reference solutions, respectively.[32] The reactive group of 16-ArN_2^+ is located within the micellar interface and is oriented like the surfactant, because its structure is almost the same as a surfactant, and 1-ArN_2^+ is dissolved in bulk aqueous solution in the absence of surfactant. The components of interfacial region in micellar solution are comparable to the components in aqueous solution, both of which have cationic headgroups, arenediazonium ion, water, and counterions.

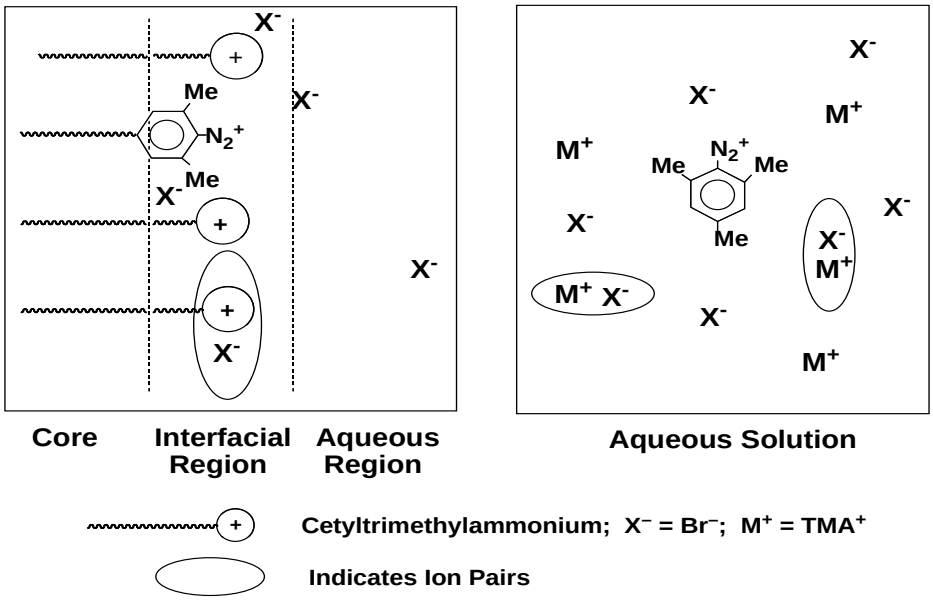

Figure 9. Reactions of 16-ArN_2^+ and 1-ArN_2^+ in the micellar and the aqueous reference solutions. 16-ArN_2^+ is located at the micelle interface, and 1-ArN_2^+ is aqueous reference solution containing the same nucleophiles.

Chapter 2. Chemical Trapping Method Applied to Micellar Solutions

Spherical micelles undergo sphere-to-rod transition when the counterion concentration in micellar interfacial region exceeds the 2nd cmc. Romsted's group applied chemical trapping method to a variety of surfactant solutions in which the sphere-to-rod transition was reported, e.g., CTAB, CTAC and the benzoate counterions, and some gemini surfactants with twin tails.[14,24,25] The interfacial counterion concentrations are observed to jump for these surfactants, and the water concentrations decrease abruptly when the sphere-to-rod transition concentration is reached.

This chapter focuses on applying the chemical trapping method to some other surfactants with shorter tail lengths and less hydrophobicity, e.g., DTAB, and with different counterion, e.g. ToS^-. The results tell us the composition changes of H_2O and counterions (Br^-, ToS^-) in the micellar interfacial regions with different surfactant and counterion concentrations. However, around the reported 2nd cmc region, the expected counterion and water concentration jumps were not observed.

2.1 Published Results on CTAB and CTAC

The chemical trapping method has been applied to CTAB and CTAC. The products of dediazoniation reaction are analyzed with HPLC. The total percentage yields of dediazoniation reaction between the arenediazonium probe and the components in micellar interfacial regions are 100 ± 5 %. Sudden changes of interfacial counterion concentrations are observed as salts are added.

Figure 10 shows the chemical trapping results on cetyltrimethylammonium bromide (CTAB or CTMAB), cetyltriethylammonium bromide (CTEAB), cetyltripropylammonium bromide (CTPAB) and cetyltributylammonium bromide (CTBAB).

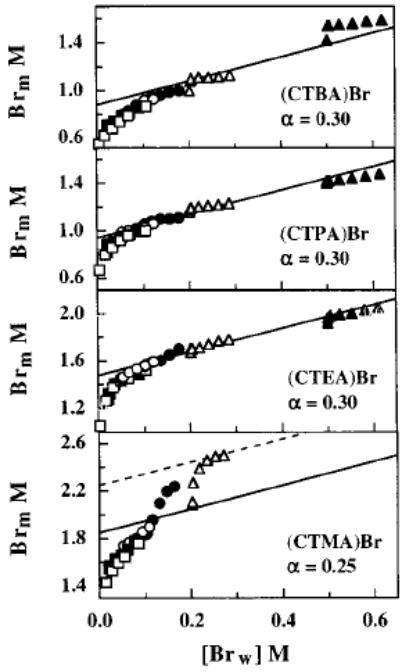

Figure 10. Plots of Br_m versus $[Br_w]$ at optimal α values for the four CTRAB(R = methyl, ethyl, propyl, and butyl) surfactants with added TMAB. Straight lines have a slope of 1 and intercepts were selected to give optimal contact with the linear portions of the curves.[25]

Figure 10 shows the Br^- concentration change in the micellar interfacial regions as a result of increasing the Br^- concentration in the aqueous solutions for CTMAB, CTEAB, CTPAB and CTBAB. In this figure, Br_m is the Br^- concentration in micellar interfacial region, and $[Br_w]$ is the Br^- concentration in aqueous solution, which is calculated from

$$[Br_w] = \frac{\alpha\{([CTRAB] - cmc)\} + cmc + [HBr] + [TMAB]}{1 - V[CTRAB]} \qquad (6)$$

where V is the mole volume of the surfactants in mole per liter assuming the density of the surfactant is 1 g/mL.[25] α has different values when the measuring method is different.[33,34] But the α values for the CTRAB surfactants are determined by treating α as disposable parameters and selecting the best values that make smooth curves.[25] Figure 11 illustrates the example of how α is determined using equation 6 from the plots of Br_m versus $[Br_w]$.[25]

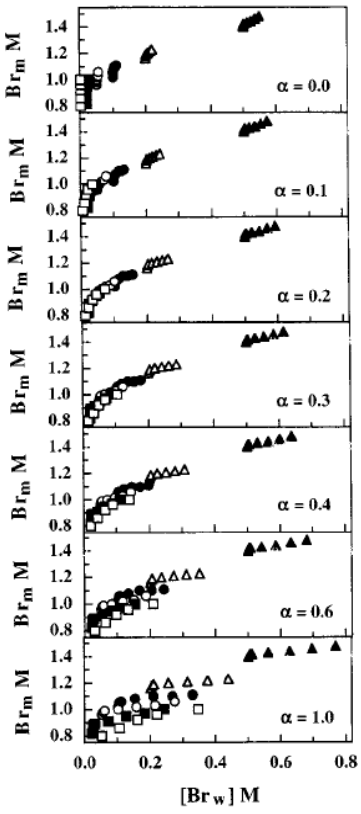

Figure 11. Effects of increasing α values in CTPAB/TMAB solutions on plots of Br_m versus $[Br_w]$.[25]

In Figure 11, α values increase from 0 to 1. When α is 0.2 – 0.4, all the data points fall on smooth curves. But the data points are more dispersed when α has larger or smaller values, so α = 0.3 was selected as optimal value for CTPAB. The optimal value of α is determined the same way for CTBAB and CTAEB. And for CTMAB, the optimal α value is 0.25.[25]

In Figure 10, when [Br_w] increases, Br_m for CTEAB, CTPAB and CTBAB increase smoothly. The Br_m increases more rapidly below 0.1 M [Br_w], and above about 0.1 M [Br_w], the data fits a straight line with slope of 1. For CTMAB, there is a break in the Br_m above 0.1 M of [Br_w]. CTMAB has a 2nd cmc of 0.1 M, and the break of concentration changes suggests that when the sphere-to-rod transition occurs, there is a significant increase of the counterion (Br^-) concentration in the micellar interfacial region. The straight line with slope of 1 means that when an increment of [Br_w] is added to the aqueous solution, there is an incremental increase in the concentration of Br_m in the micellar interfacial region. The fitting of data points on the straight line meets the definition of X_m (m = Br) in equation 4.

Plots of water molarity in micellar interfacial region, H_2O_m, are shown in Figure 12. H_2O_m decrease as [Br_w] increases. The break of H_2O_m for CTMAB appears above 0.1 M of [Br_w], which is at the same molarity as Br_m in Figure 10. CTEAB, CTPAB and CTBAB have continuous decrease of H_2O_m, which show no break.

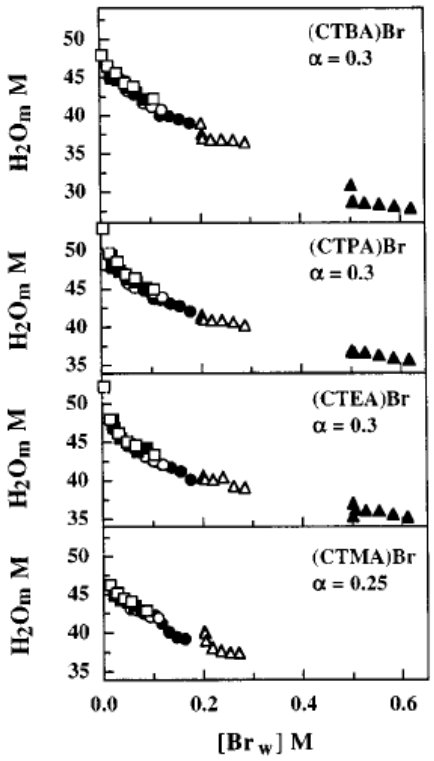

Figure 12. Plots of H_2O_m versus $[Br_w]$ at optimal α values for the four CTRAB surfactants with added TMAB.[25]

The chemical trapping method was also applied to CTAC/TMAC. Figure 13 shows the final results of plots of Cl_m and H_2O_m versus $[Cl_w]$ being the same process as with Br^-.

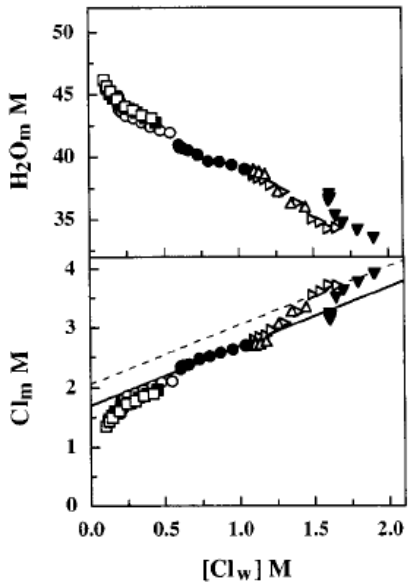

Figure 13. Plots of Cl_m and H_2O_m versus $[Cl_w]$ at the optimal α value of 0.4 for CTAC/TMAC solutions. The straight line has a slope of 1 and the intercept was selected to give optimal contact with the linear portion of the curve.[25]

Figure 13 shows that when more CTAC or TMAC is added in the solution, concentration of Cl^- in the interfacial region increases. The break occurs above c.a. 1.2 M and the literature value of 2nd cmc of CTAC is 1.0 M, which are numerically similar. The increase of Br_m in CTAB is more rapid than the increase of Cl_m in CTAC solution, and the result shows that the concentration jump of Cl_m occurs at a higher concentration over a broader range than Br_m.

The chemical trapping results to both CTRAB and CTAC show clearly that when the sphere-to-rod transition occurs on the micelles, the counterion composition in the interfacial region increases rapidly, instead of smoothly before and after the transition. From Chapter 1, we know that the adding of more counterions in the micellar solution changes the balance of forces for aggregation. When the counterion concentration

increases to the critical point, the 2nd cmc, a shift to a new balance of forces occurs, which leads to dehydration of the interface, tighter packing of surfactant molecules, and counterions and the shape change. Because CTAB and CTAC are common and widely used surfactants, the successful application of chemical trapping method to them made us wonder whether the similar counterion concentration jumps happen on micellar interfacial regions of surfactants with shorter hydrophobic chain length or different counterions.

2.2 Chemical Trapping Method Applied to DTAB

DTAB is similar in structure to CTAB, except the hydrocarbon chain has 12 instead of 16 carbons. When the hydrophobic tail is shorter, the driving force for aggregation is smaller, so more surfactant molecules are packed in the micelles to make the forces balanced. The reported cmc of DTAB is 16 mM and the 2nd cmc is 1.8 M, Table 1, both of which are significantly higher than those of CTAB. In this section, the chemical trapping method is applied to DTAB micelles in an attempt to determine the concentration change of water and counterion when sphere-to-rod transition occurs. The results shown in Figure 10 and 13 for CTAB and CTAC were expected to be seen for DTAB. The reaction is carried out at 25°C for 24 h, and the reaction half life is c.a. 90 min. The short chain dediazoniation reaction in TMAB solution is used as reference. Table 4 shows the data for the chemical trapping method in DTAB solutions, and Figures 14 and 15 are drawn from the data.

Table 4

Chemical trapping results in DTAB solution and added TMAB with 2.5×10^{-4} M of 16-ArN_2BF_4 in 0.001 M HBr at 25°C[a]

[TMAB] (M)	[DTAB] (M)	Total %yield	Normalized %yield[b]		$[Br_w]$[c] (M)	Br_m[d] (M)	S_w^{Br}[e]	H_2O_m[f] (M)
			16-ArOH	16-ArBr				
0	0.05	98.0	78.6	21.4	0.03	1.11	11.7	47.5
0	0.1	97.5	76.3	23.7	0.04	1.28	11.2	46.3
0	0.2	100.4	74.4	25.6	0.07	1.43	10.9	45.3
0	0.3	99.3	73.3	26.7	0.10	1.52	10.7	44.7
0	0.4	99.1	72.9	27.1	0.13	1.55	10.7	44.5
0	0.5	104.8	70.6	29.4	0.16	1.75	10.3	43.3
0.1	0.05	104.6	73.3	26.7	0.13	1.52	10.7	44.7
0.2	0.05	105.0	70.6	29.4	0.23	1.75	10.3	43.3
0.3	0.05	104.7	70.2	29.8	0.33	1.78	10.3	43.1
0.4	0.05	102.5	67.9	32.1	0.43	1.98	10.0	41.8
0.5	0.1	104.5	66.5	33.5	0.56	2.11	9.8	41.0
0.5	0.4	108.4	63.2	36.8	0.70	2.41	9.5	39.2
0.6	0.05	103.1	67.8	32.2	0.64	1.99	10.0	41.8
1	0.05	99.5	60.1	39.9	1.04	2.71	9.2	37.4
1	0.1	112.1	62.1	37.9	1.07	2.52	9.3	38.5
1	0.5	108.7	60.3	39.7	1.35	2.69	9.2	37.5
1.5	0.05	96.5	57.3	42.7	1.55	2.99	8.9	35.8
1.5	0.1	102.5	57.9	42.1	1.59	2.93	9.0	36.1
1.5	0.3	104.5	56.0	44.0	1.75	3.12	8.8	35.0
2	0.05	104.3	55.0	45.0	2.06	3.22	8.7	34.4
2	0.1	99.7	54.4	45.6	2.10	3.29	8.7	34.1
2.5	0.05	103.0	50.5	49.5	2.57	3.70	8.4	31.7
2.5	0.1	102.6	50.2	49.8	2.62	3.73	8.4	31.6
2.5	0.2	103.4	48.4	51.6	2.73	3.93	8.3	30.5

a. Reaction time 24 hours. Each sample injected in triplicate. HPLC method: 55% methanol / 45% isopropanol. Flow rate = 0.4 mL/min over 60 min, λ = 220 nm, injection volume = 100 µL. Typical retention times: 16-ArOH ~ 13 min, 16-ArBr ~ 30 min. Calibration Curves: 16-ArOH: [16-ArOH] = 1.08×10^{-10} (peak area); 16-ArBr: [16-ArBr] = 7.35×10^{-11} (peak area). The yield of 16-ArH has been normalized as indicated in Appendix I. b. Normalized yield: %16-ArX (X = OH, Br) = 100(%16-ArX)/(total yields). c. $[Br_w]$ is calculated with equation (6), where V is the molar volume of DTAB in mole per liter assuming that the density of DTAB is 1.0 g/mL.[25] d. Br_m: estimated from fitting a plot of %(1-ArBr) vs [TMAB]: $Br_m = (\%16\text{-ArBr} / 19.95)^{1.439}$.[24] e. S_w^{Br} is obtained from fitting a plot of S_w^{Br} vs [TMAB]: $S_w^{Br} = 12.01 \times Br_m^{-0.272}$.[24] f. $H_2O_m = S_w^{Br} Br_m$ %16-ArOH / %16-ArBr

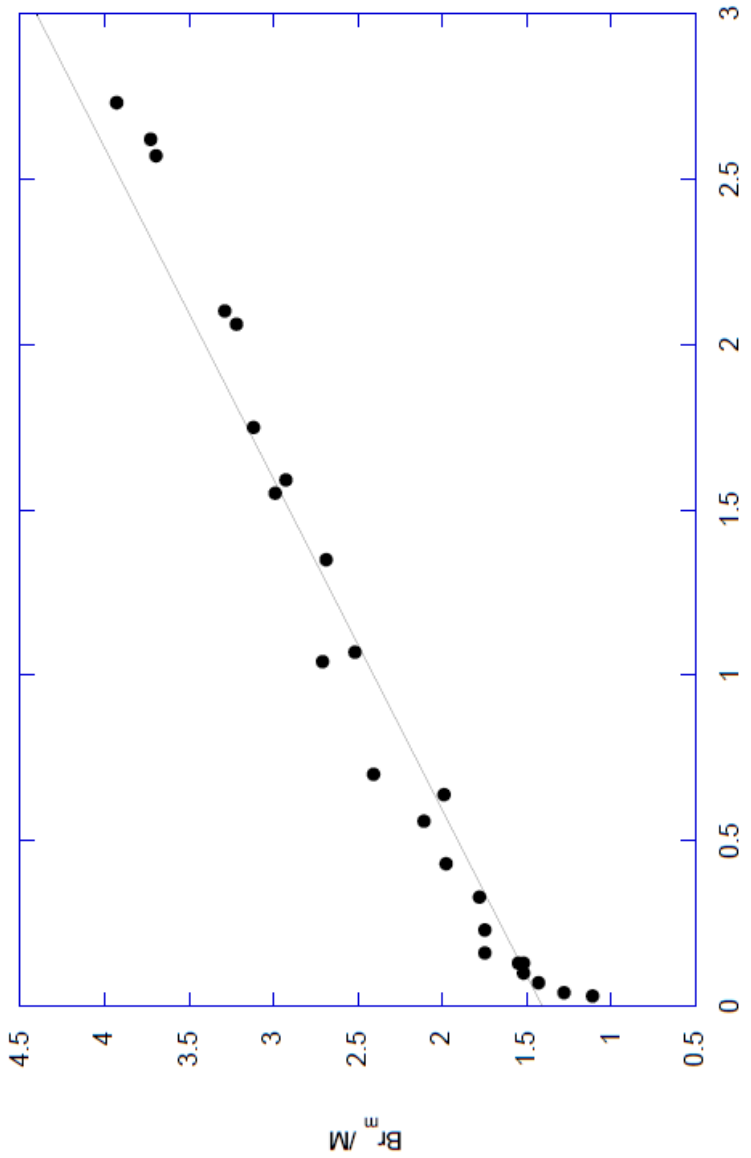

Figure 14. Plot of Br_m versus $[Br_w]$ for chemical trapping in DTAB solutions at 25°C. Straight line has a slope of 1 and the intercept is selected to give optimal contact with the linear portion of the curve.

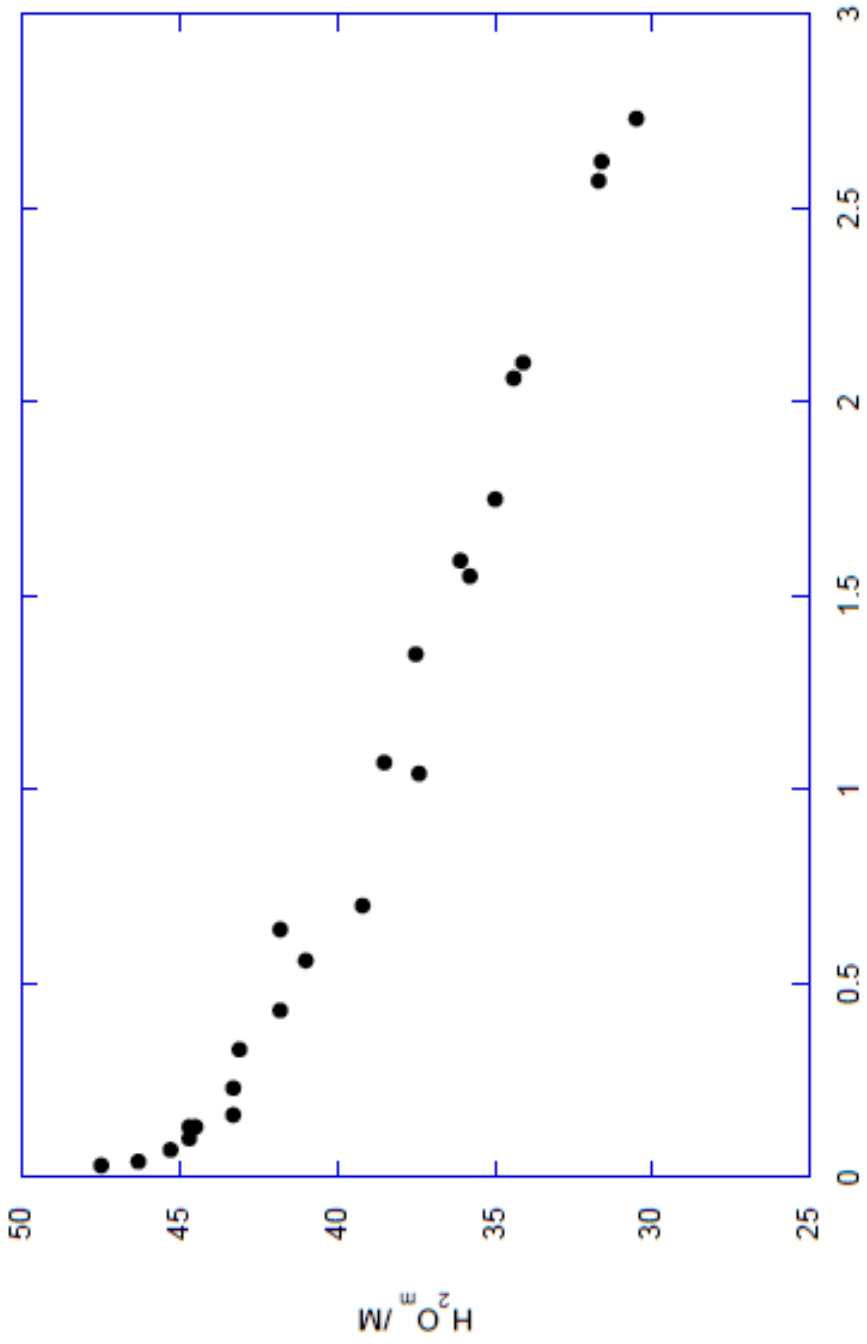

Figure 15. Plot of H_2O_m versus $[Br_w]$ for chemical trapping in DTAB solution at 25°C.

In table 4, [TMAB] increases from 0 to 2.5 M. [DTAB] is varied as well. The dediazoniation products are analyzed by HPLC. Each solution was injected three times, and the average deviation of peak areas are small, as shown in Appendix. The total percentage yields of products are 100 ± 5%, which means all the arenediazonium ions react with either Br^- or H_2O. The normalized yields of 16-ArOH decrease from the top to the bottom, and the corresponding normalized yields of 16-ArBr increase. The normalized yields are used to compute $[Br_w]$, Br_m and H_2O_m by the methods in the footnotes of Table 4. When more TMAB is added in the solution, $[Br_w]$ and Br_m increase, and H_2O_m decreases. The basic trends are the same as in CTAB and CTAC solution shown in Figure 10, 12 and 13.

The $[Br_w]$, Br_m and H_2O_m data for DTAB are plotted in Figure 14 and 15. Figure 14 is the plots of Br_m versus $[Br_w]$. The straight line is imposed and has a slope of 1. When $[Br_w] < 0.1$ M, Br_m increases rapidly. Above 0.1 M, Br_m increases smoothly and most of the data points follow the straight line. Comparing to Figure 10 for CTAB, the rapid increase below cmc is similar to the results for CTAB, Figure 10, but near the 2nd cmc of DTAB, 1.8 M,[4] no break occurs in Br_m, which is different from CTAB. Figure 15 shows the plots of H_2O_m versus $[Br_w]$. Correspondingly, when $[Br_w] < 0.1$ M, H_2O_m decreases rapidly, and above 0.1 M, H_2O_m decreases smoothly. There is no break for H_2O_m either. The change in slope for H_2O_m in CTAB is not as dramatic as in Figure 10.

2.3 Chemical trapping method applied to CTAToS

Toluenesulfonate ion (ToS^-) is a bigger anion than Br^- and more hydrophobic, and should be even less strongly hydrated especially at the aromatic rings. The Krafft

temperature of CTAToS is 23°C determined by dye solubilization.[35] The degree of ionization of CTAToS is 0.13 measured by free electrophoresis.[36] The cmc of CTAToS is 0.26 mM as measured by electrical conductivity and surface tension method.[37] The sphere-to-rod transition is reported to occur at 2.0 mM measure with static light scattering.[37-39]

Cetyltrimethylammonium *p*-toluenesulfonate (CTAToS) solution has a special property that is different from other surfactants. When NaToS is added, the viscosity of the solution increases to a maximum and then decreases. Bunton and co-workers reported the viscosity measurements in 1973, Figure 16.[40,41]

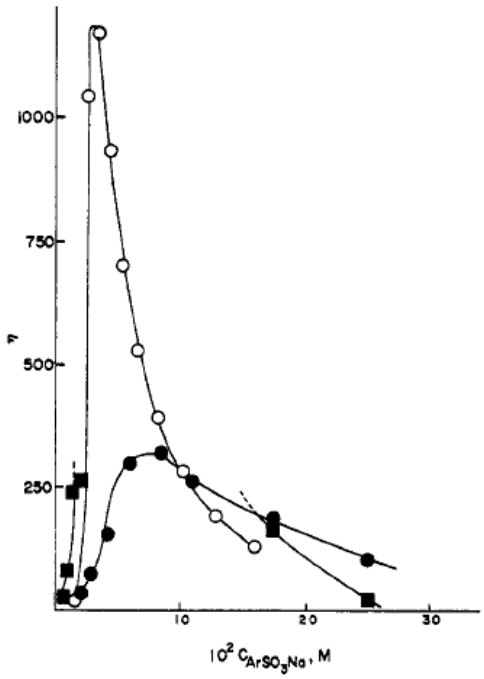

Figure 16. The effect of sodium arenesulfonates on the solution viscosity of 0.02 M of CTAB at 25°C. (●) $NaC_6H_5SO_3$; (○) NaToS; (■) Na-*p*-$(CH_3)_2CHC_6H_4SO_3$.[41]

Added sodium benzenesulfonate has little effect on the viscosity of CTAB. Added sodium *p*-isopropylbenzenesulfonate increases the viscosity over a wide range of concentrations with increases that are too big to be measured. The addition of sodium toluenesulfonate, discussed in this chapter also, causes a marked increase to the viscosity. The viscosity is the greatest when the concentrations of CTAB and NaToS are about equal, and it decreases when more NaToS is added.

In our lab, CTAB solutions were mixed with NaToS stock solutions with increasing concentrations for visual observation. The viscosity maximum appears when the NaToS and CTAB concentration ratio is about 1:1, which agrees with Bunton's result, and then the solutions become more fluid as more NaToS is added. The reason for viscosity maximum is not known.

Since ToS^- is much larger and more hydrophobic than Br^- and Cl^-, there is no educated guess on what the chemical trapping result would be. Additional experiments are needed. Dichlorobenzoate ion (OBz) is similar in size to ToS^-, and it also has an aromatic ring, which makes the hydrophobicity similar too. Chemical trapping on OBz ion may help to get an idea on ToS^-. Geng et al. ran chemical trapping experiments on mixed micelles of CTA3,5OBz/CTAC and CTA2,6OBz/CTAC, Figure 17.[32]

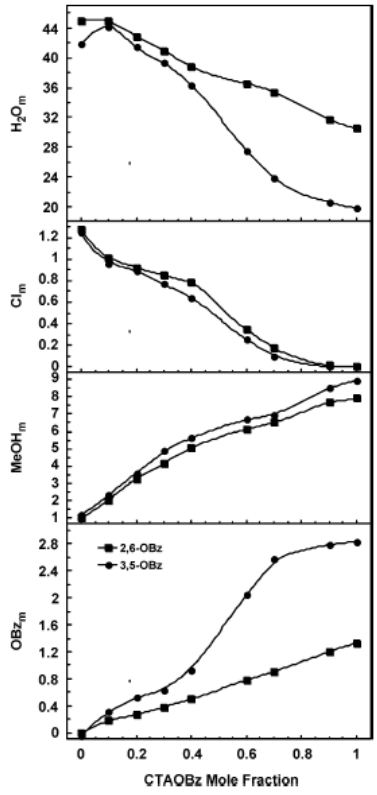

Figure 17. Changes in interfacial molarities of water, chloride ion, methanol and dichlorobenzoate ions (2,6OBz$_m$ and 3,5OBz$_m$) with increasing mole fraction (0 to 1) of CTAOBz (decreasing CTAC mole fraction from 1 to 0) in 10 mM mixed micelles of CTAOBz/CTAC at 25^{o}C. Lines are drawn to aid the eye.[32]

Figure 17 compares cetyltrimethylammonium surfactants with two different counterions, 2,6OBz and 3,5OBz. The chemical trapping method is applied in 10 mM mixed micelles of CTAOBz/CTAC with increasing mole fraction of CTAOBz. The marked increase of 3,5OBz$_m$ indicates the sphere-to-rod transition when CTA3,5OBz mole fraction increases and CTAC mole fraction decreases, and the steady increase of 2,6OBz$_m$ shows no shape change of the surfactant.

ToS^- and OBz are similar in size and hydrophobicity. If the chemical trapping method was applied to 10 mM mixed micelles of CTAToS/CTAC with increasing mole fraction of CTAToS (0 to 1) and decreasing mole fraction of CTAC (1 to 0), to mimic the CTAOBz/CTAC experiments, the experimental results might show the counterion concentration increase in ToS_m. Dediazoniation reaction of 1-$ArN_2BF_4^-$ in aqueous NaToS were carried out and used as a reference to calculate ToS_m,. The data are listed in Table 5 and plotted in Figures 18 and 19.

Table 5
Chemical trapping results in NaToS solution
with 2.5×10^{-4} M of 1-ArN_2BF_4 in 0.01 M HBr at 25°C[a]

[NaToS]/M	[H_2O]/M	%total	%1-ArOH	%1-ArToS	normalized %1-ArOH[b]	normalized %1-ArToS	S_w^{ToS} [c]
0.5	52.9	75.8	63.2	12.6	83.4	16.6	21.05851
1.0	49.2	74.7	55.0	19.7	73.6	26.4	17.64783
1.5	45.5	73.1	48.1	25.0	65.8	34.2	15.76596
2.0	42.0	74.2	43.8	30.4	59.0	41.0	14.59322
2.5	38.8	68.9	36.9	32.0	53.6	46.4	13.43522

a. Reaction time 24 hours. Each sample injected in triplicate.
HPLC method: 80% methanol / 20% H_2O. Flow rate = 0.8 mL/min over 20 min, λ = 230 nm, injection volume = 100 µL.
Typical retention times: 1-ArOH ~ 4 min, 1-ArToS ~ 6 min.
Calibration Curves: 1-ArOH: [1-ArOH] = 5.10×10^{-11} (peak area)
1-ArToS: [1-ArToS] = 1.06×10^{-11} (peak area).
b. Normalized yield %1-ArX (X = OH, ToS) = 100(%1-ArX)/(total yields)
c. S_w^{ToS} is calculated as S_w^{ToS} = [H_2O](normalized %1-ArToS)/([NaToS](normalized %1-ArOH)).

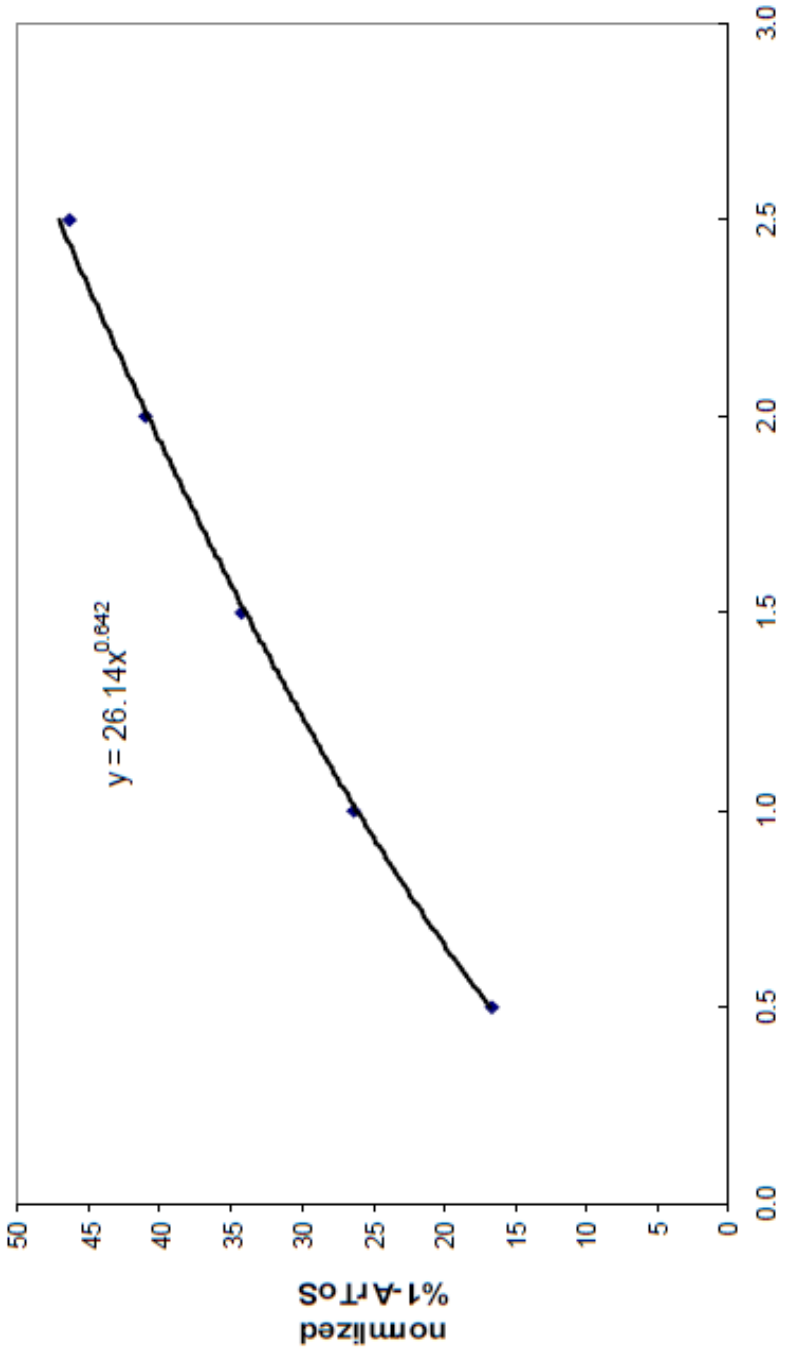

Figure 18. Plot of normalized percentage yield of 1-ArToS *vs* [NaToS] for the chemical trapping reaction in NaToS with 2.5 x 10^{-4} M of 1-ArN_2BF_4 in 0.01 M HBr at 25°C. The line is drawn to aid the eye.

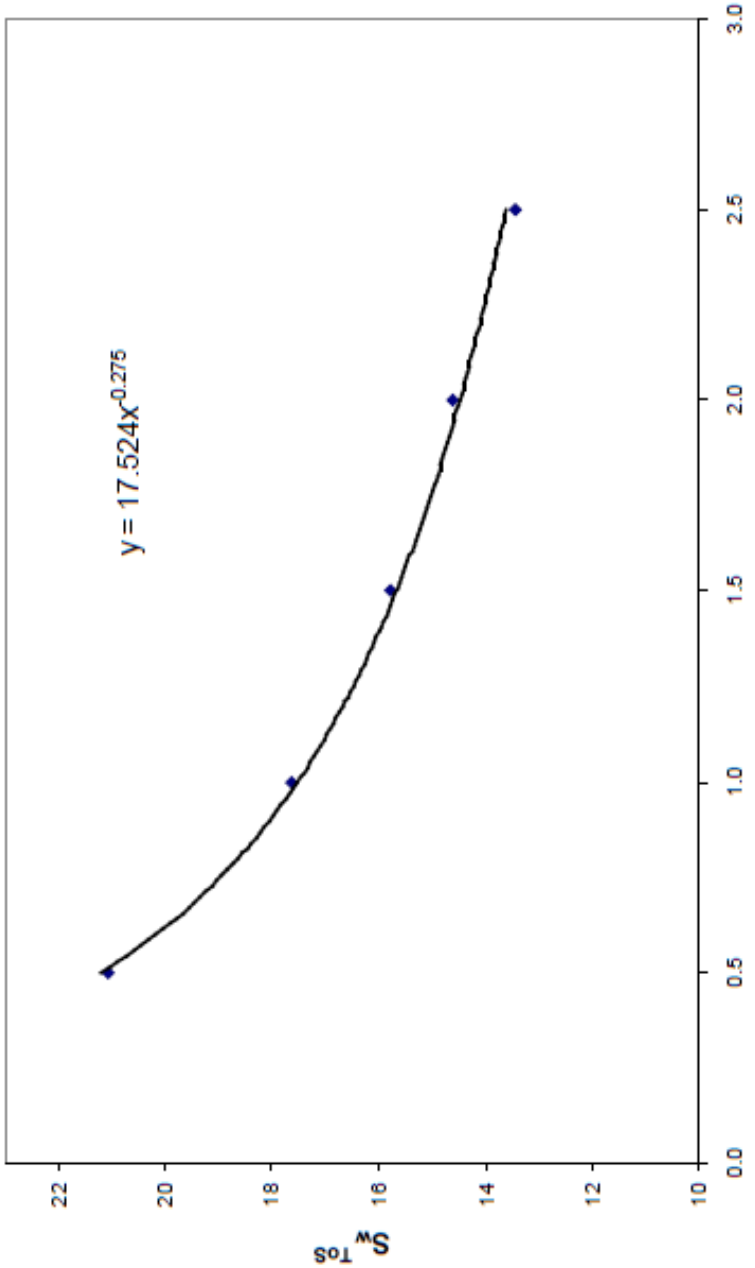

Figure 19. Plot of selectivity of 1-ArToS vs [NaToS] for the chemical trapping reaction in NaToS with 2.5 x 10^{-4} M of 1-ArN_2BF_4 in 0.01 M HBr at 25°C. The line is drawn to aid the eye.

In Table 5, [NaToS] ranges from 0.5 – 2.5 M, and [H_2O] is calculated from the weights of water added. Product yields of 1-ArToS and 1-ArOH were determined by HPLC. The total percentage yields are as low as 75% for a number of repeats. The possibilities that might lead to such low yields, e.g. impurity of 1-ArN_2BF_4, unfinished reaction, outdated calibration curves, and HPLC malfunction, were eliminated. The 1-ArN_2BF_4 was pure by NMR, and the product peaks were clear and clean on HPLC graphs over a number of repeats, as shown in Appendix 2. Compared to the reported product yields of 1-ArBr and 1-ArOH in reaction of 1-ArN_2BF_4 and TMAB, 1-ArBr yield increases gradually, and 1-ArOH yield decreases gradually.[24] The yield increase of 1-ArToS is similar to 1-ArBr, and the yield decrease of 1-ArOH is similar to 1-ArOH in TMAB. Combining all analysis above, the trapping results in Table 5 are believed to be trustworthy. Both 1-ArToS and 1-ArOH yields are normalized, and the normalized yields increase for 1-ArToS and decrease for 1-ArOH when at higher [NaToS]. The selectivity of ToS^-, equation 5, decreases gradually, Figure 19.

The normalized percentage yields of 1-ArToS versus [NaToS] are used as reference for chemical trapping in CTAToS solutions, to calculate ToS_m. Because the micellar interfacial region of CTAToS has the same composition as its short chain bulk solution, ToS^-, ToS_m can be estimated from fitting the plots, $\%16\text{-ArToS}=26.14[ToS_m]^{0.642}$. For the same reason, Figure 19 shows the plots of selectivity of 1-ArToS versus [NaToS]. S_w^{ToS} for ToS^- can be obtained form fitting the plots, $S_w^{ToS} = 17.52[ToS_m]^{-0.275}$.

These short chain dediazoniation results are used to estimate the interfacial molarities in CTAToS/CTAC mixed surfactants. The data are listed in Table 6, and plotted in various ways in Figures 20 to 25.

Table 6.
Chemical trapping in CTAToS and CTAC mixture surfactants with 16-ArN_2^+ 2.5 x 10^{-4} M in 0.01 M HCl at 25°C[a]

[CTAToS] (mM)	[CTAC] (mM)	total %yield	Normalized % yield			ToS_m[b] (M)	Cl_m[c] (M)	S_w^{ToS}[d]	S_w^{Cl}[e]	H_2O_m[f]
			16-ArOH	16-ArToS	16-ArCl					
0	10	101.3	87.8	0.0	12.2	0.000	1.054		6.33	47.83
1	9	90.9	90.7	0.9	8.4	0.005	0.643	73.32	7.25	49.49
2	8	91.9	90.3	2.4	7.2	0.024	0.534	48.68	7.64	49.23
3	7	104.5	86.6	5.7	7.7	0.092	0.582	33.72	7.46	48.11
4	6	82.3	89.7	6.7	3.6	0.119	0.219	31.45	9.78	51.13
5	5	104.7	85.2	10.1	4.7	0.228	0.306	26.31	8.91	50.04
6	4	98.8	85.4	11.6	3.2	0.281	0.182	24.83	10.29	51.25
7	3	90.2	81.7	14.6	3.7	0.405	0.220	22.47	9.76	50.21
8	2	107.4	80.1	17.3	2.6	0.527	0.140	20.89	11.06	50.50
9	1	109.9	79.5	18.8	1.8	0.596	0.087	20.20	12.62	50.80
10	0	96.0	80.6	19.4	0.0	0.627	0.000	19.92		51.96

a. Reaction time 24 hours. Each sample injected in triplicate.
HPLC method: 55% methanol / 45% isopropanol. Flow rate = 0.4 mL/min over 80 min, λ = 220 nm, injection volume = 100 µL.
Typical retention times: 16-ArOH ~ 25 min, 16-ArToS ~ 36 min, 16-ArCl ~ 72 min
Calibration curves: [16-ArOH]=1.08 x 10^{-10}(peak area)
[16-ArTOS]=4.78 x 10^{-12}(peak area)
[16-ArCl]=6.51 x 10^{-11}(peak area)
b. ToS_m: estimated from fitting a plot of %(1-ArToS) vs [NaToS]. %1-ArToS=26.14$[NaToS]^{0.642}$
c. Cl_m : estimated from fitting a plot of %(1-ArCl) vs [TMAC]. %(1-ArCl)=11.75$[TMAC]^{0.771}$ [24]
d. S_w^{ToS} is obtained from fitting a plot of S_w^{ToS} vs [NaToS]: $S_w^{ToS} = 17.52[ToS_m]^{-0.275}$
e. $S_w^{Cl} = 6.42[Cl_m]^{-0.277}$ [24]
f. H_2O_m = (%16-ArOH)/(%16-ArToS + %16-ArCl)

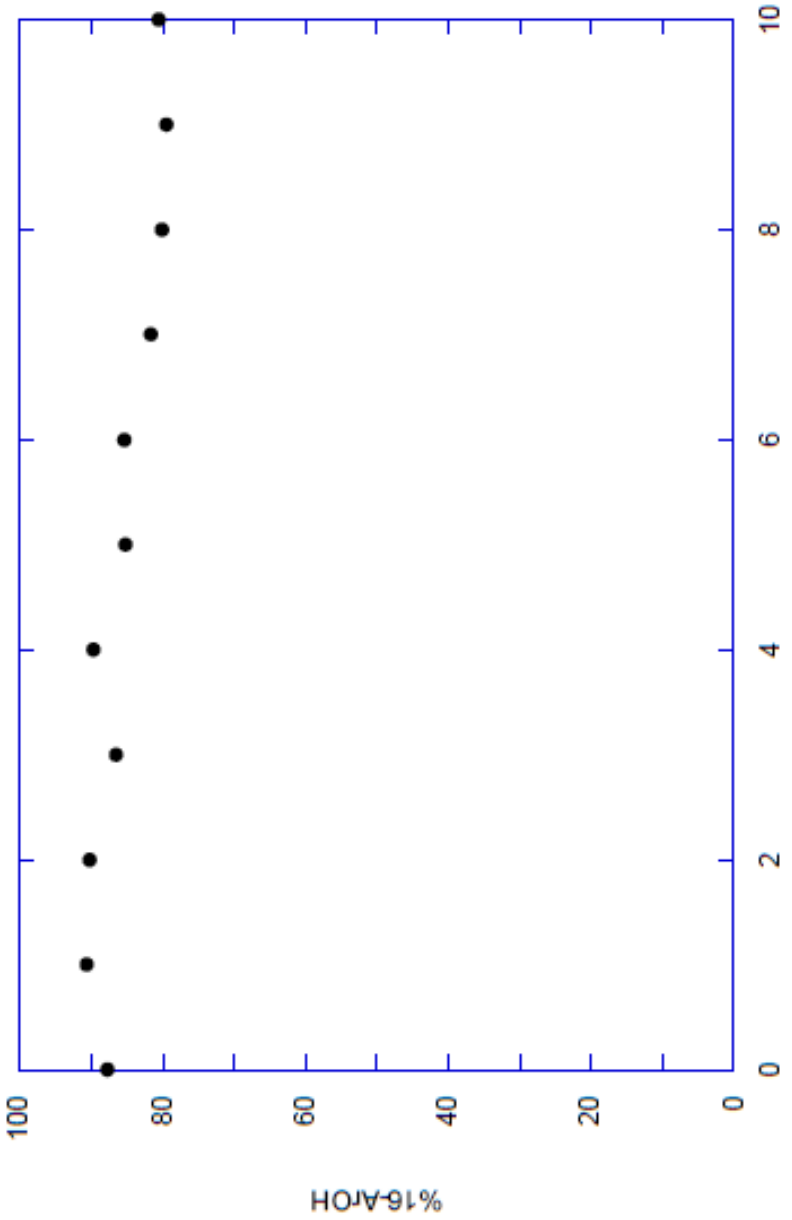

Figure 20. Plot of %16-ArOH vs. [CTATosS] for chemical trapping in CTATosS and CTAC mixed micelles with 2.5×10^{-4} M of 16-ArN_2^+ in 0.01 M of HCl at 25°C.

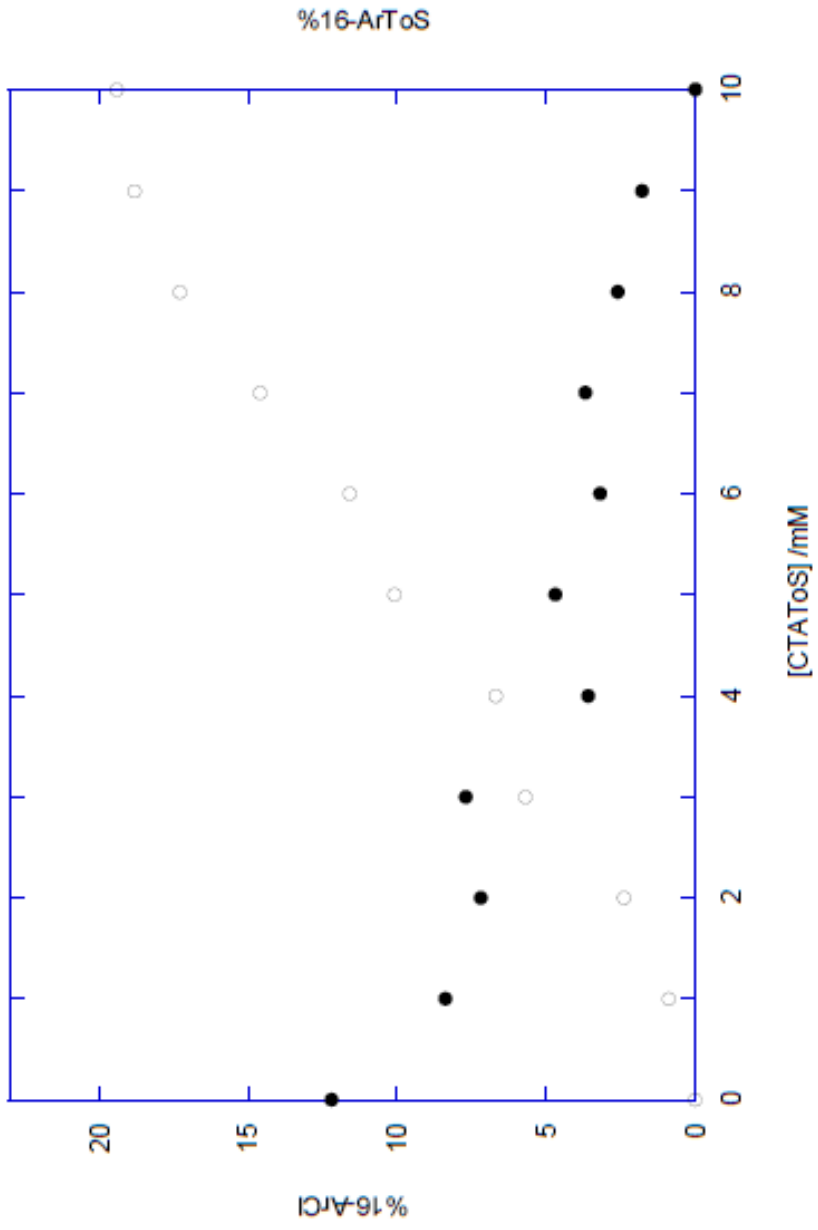

Figure 21. Plots of %16-ArCl and %16-ArToS vs. [CTAToS] for chemical trapping in CTAToS and CTAC mixed micelles with 2.5×10^{-4} M of 16-ArN_2^+ in 0.01 M of HCl at 25°C. (●) is 16-ArCl and (○) is 16-ArToS.

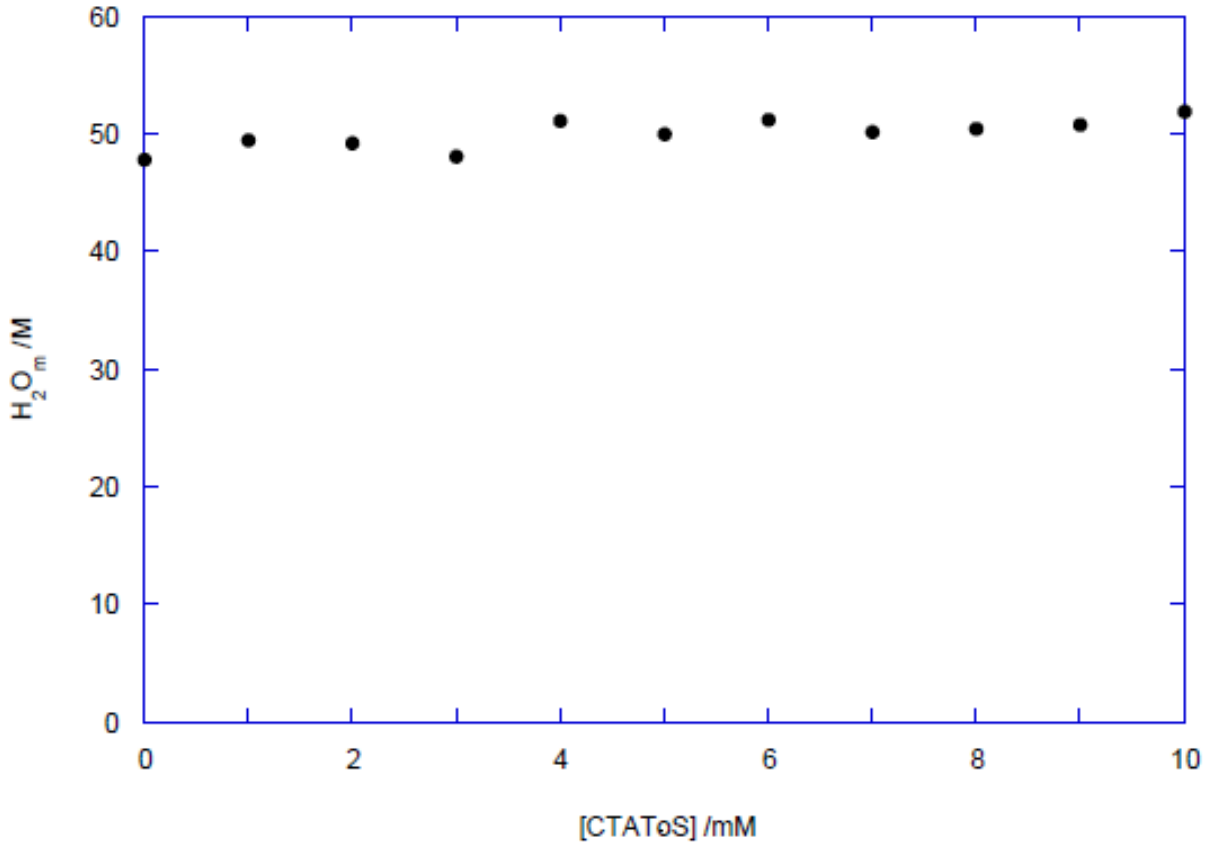

Figure 22. Plot of H_2O_m vs [CTAToS] for chemical trapping in CTAToS and CTAC mixed micelles with 2.5 x 10^{-4} M of 16-ArN_2^+ in 0.01 M of HCl at 25°C

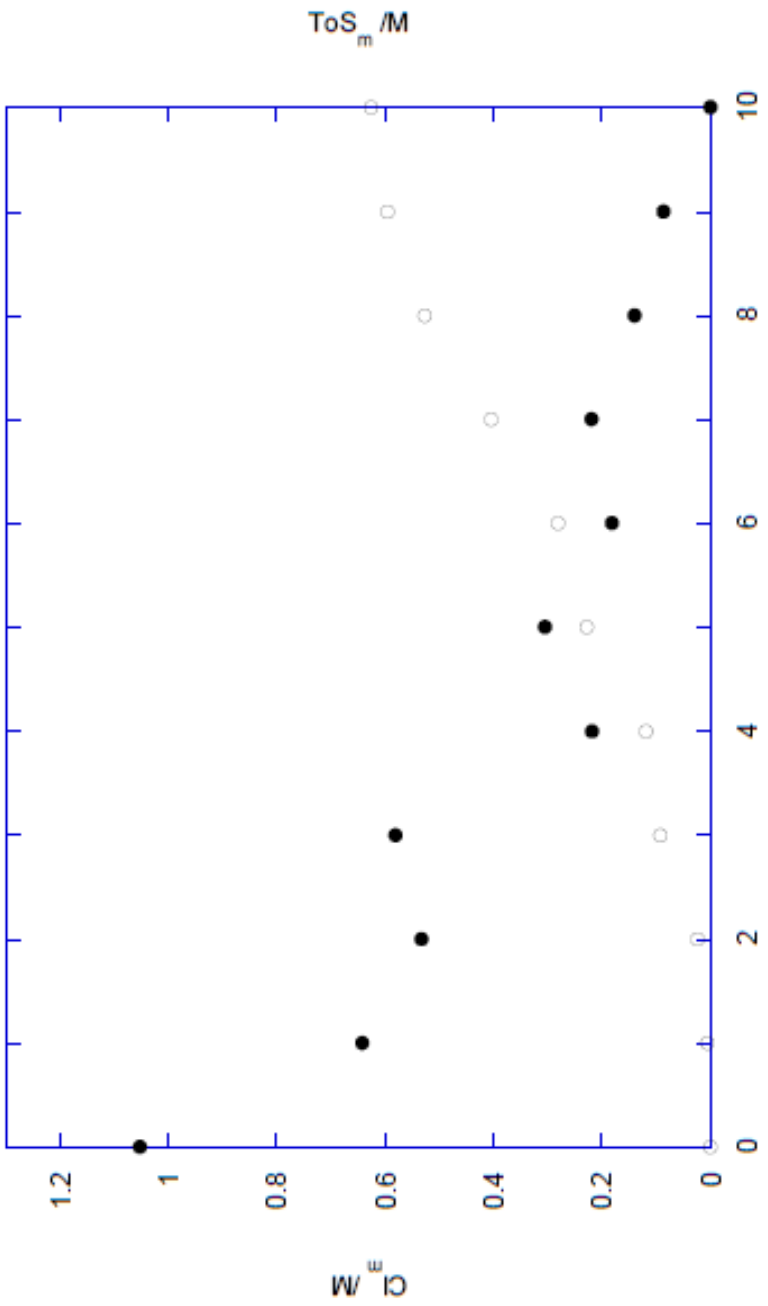

Figure 23. Plots of Cl_m and ToS_m vs. [CTAToS] for chemical trapping in CTAToS and CTAC mixed micelles with 2.5×10^{-4} M of 16-ArN_2^+ in 0.01 of M HCl at 25°C. (●) is 16-ArCl and (○) is 16-ArToS.

The total molarity of CTAToS and CTAC is 10 mM with [CTAToS] increasing from 0 to 1 mM and [CTAC] decreasing from 1 to 0 mM. The viscosity of the solutions increases visually, as [CTAToS] increases in the solution. The total yields of 16-ArOH, 16-ArToS and 16-ArCl are c.a. 100%. 16-ArOH yields have a tendency to decrease. %16-ArToS increases and %16-ArCl decreases when [CTAToS] increases in the mixed surfactant solutions. The molarities of ions in micellar interfacial regions are calculated from the equations in the footnotes of Table 6. ToS_m increases and Cl_m decreases when the mole fraction of CTAToS increases and the mole fraction of CTAC decreases. The changes indicate that ToS^- replaces Cl^- gradually in the micellar interfacial region.

Figure 20 -23 are a series of plots with data from Table 6, showing the effects when the CTAToS mole fraction increases in the mixed surfactant solutions. Figure 20 and 21 are the plots of normalized product yields versus [CTAToS]. When [CTAToS] increases, %16-ArOH decreases slightly, Figure 20, %16-ArCl decreases and %16-ArToS increases smoothly initially, following by a marked increase from 0.3 to 0.7 mM [CTAToS], then begins to plateau up to 10 mM CTAToS, Figure 21. Figure 22 and 23 are the plots of interfacial molarities calculated from percentage yields versus [CTAToS]. As [CTAToS] increases in aqueous solution, H_2O_m remains almost constant, Figure 22, Cl_m decreases and ToS_m increases smoothly at the beginning, followed by a marked increase, then finally a smooth increase again, Figure 23. The concentration changes of each ion in micellar interfacial region are similar to changes of product yields with that ion.

Compare the chemical trapping results on CTAOBz/CTAC solutions to the already discussed changes of ions in the interfacial region of CTAOBz/CTAC mixed surfactant solutions in Figure 17, the ToS_m curve is similar to the $3,5OBz_m$ curve with a marked increase, which indicates the sphere-to-rod transition, while the $2,6OBz_m$ increase smoothly. H_2O_m are close to constant during this process, different from the results in Figure 17, the reason of which is unknown at this point. But the ToS_m curve indicates that Tos^- replaces Cl^- in micellar interfacial region, and is consistent with a sphere-to-rod transition. Therefore, the chemical trapping method can be applied to pure CTAToS solution, to detect the changes of ToS_m when more Tos^- is added in the aqueous solution. Table 7 and 8 are the chemical trapping results of CTAToS solutions, which are plotted in Figures 24 and 25.

Table 7.
Chemical trapping in CTAToS surfactant with 2.5×10^{-4} M of 16-ArN_2^+ in ToSOH at 25°C [a]

[CTAToS] (mM)	[ToSOH] (M)	Total %yield	Normalized %yield		ToS_m [b] (M)	ToS_w [c] M	S_w^{ToS} [d]	H_2O_m [e] (M)
			16-ArOH	16-ArToS				
0.25	0.001	51.4	79.7	20.3	0.682	0.0013	19.8	52.9
0.5	0.001	59.2	79.9	20.1	0.671	0.0013	19.8	52.9
1	0.001	59.2	79.0	21	0.718	0.0014	19.5	52.7
2	0.001	69.3	78.5	21.5	0.744	0.0015	19.4	52.6
3	0.001	85.3	78.7	21.3	0.733	0.0016	19.4	52.7
4	0.001	93.3	78.4	21.6	0.749	0.0017	19.3	52.6
6	0.001	97.3	77.5	22.5	0.797	0.0020	19.1	52.3
0.25	0.01	91.1	77.8	22.2	0.781	0.0103	19.2	52.4
0.5	0.01	95.0	78.2	21.8	0.760	0.0103	19.3	52.6
1	0.01	72.8	81.8	18.2	0.575	0.0104	20.4	52.8
2	0.01	93.1	79.7	20.3	0.682	0.0105	19.8	52.9
3	0.01	100.0	78.5	21.5	0.744	0.0106	19.4	52.6
4	0.01	95.8	78.8	21.2	0.728	0.0108	19.5	52.7
6	0.01	92.3	78.4	21.6	0.749	0.0110	19.3	52.6

a. Reaction time 24 hours. Each sample injected in triplicate.
HPLC method: 55% methanol / 45% isopropanol. Flow rate = 0.4 mL/min over 80 min, λ = 220 nm, injection volume = 100 µL.
Typical retention times: 16-ArOH ~ 25 min, 16-ArToS ~ 36 min.
Calibration curve: $[16\text{-ArOH}] = 1.08 \times 10^{-10}$ (peak area)
$[16\text{-ArTOS}] = 4.78 \times 10^{-12}$ (peak area)
b. ToS_m: estimated from fitting a plot of %(1-ArToS) vs [NaToS]. $\%1\text{-ArToS} = 26.14[\text{NaToS}]^{0.642}$
c. ToS_w is obtained via the equation

$$[ToS_w] = \frac{\alpha\{([CTAToS] - cmc) + cmc + [ToSOH]}{1 - V[CTAToS]}$$

d. S_w^{ToS} is obtained from fitting a plot of S_w^{ToS} vs [NaToS]: $S_w^{ToS} = 17.52[ToS_m]^{-0.275}$
e. $H_2O_m = S_w^{ToS}[ToS]_m$ %16-ArOH / %16-ArToS

Table 8.
Chemical trapping in CTAToS surfactant with 2.5×10^{-4} M of 16-ArN_2^+ in 0.001 M of HBr at 25°C [a]

[CTAToS] (mM)	[NaToS] (M)	Total %yield	Normalized % yield 16-ArOH	Normalized % yield 16-ArToS	ToS_m [b] (M)	ToS_w [c] (M)	S_w^{ToS} [d]	H_2O_m [e] (M)
5	0	91.9	81.1	18.9	0.610	0.0009	20.2	52.9
7.5	0	97.4	80.4	19.6	0.646	0.0012	20.0	52.9
10	0	103.1	80.2	19.8	0.656	0.0015	19.9	52.9
15	0	102.4	79.3	20.7	0.702	0.0022	19.6	52.8
20	0	103.5	79.5	20.5	0.692	0.0029	19.7	52.8
5	0.02	105.6	77.7	22.3	0.786	0.0209	19.1	52.4
7.5	0.02	104.9	77.9	22.1	0.776	0.0213	19.2	52.5
10	0.02	109.0	78.5	21.5	0.744	0.0216	19.4	52.6
15	0.02	104.6	79.1	20.9	0.713	0.0223	19.6	52.8
20	0.02	110.1	78.8	21.2	0.728	0.0230	19.5	52.7
5	0.04	92.3	76.9	23.1	0.829	0.0410	18.9	52.1
7.5	0.04	94.9	77.6	22.4	0.791	0.0413	19.1	52.4
10	0.04	94.0	77.0	23	0.824	0.0417	18.9	52.2
15	0.04	92.4	77.3	22.7	0.807	0.0425	19.0	52.3
20	0.04	99.3	77.6	22.4	0.791	0.0432	19.1	52.4

a. Reaction time 24 hours. Each sample injected in triplicate.
HPLC method: 55% methanol / 45% isopropanol. Flow rate = 0.4 mL/min over 80 min, λ = 220 nm, injection volume = 100 µL.
Typical retention times: 16-ArOH ~ 25 min, 16-ArToS ~ 36 min.
Calibration curve: $[16\text{-ArOH}] = 1.08 \times 10^{-10}$(peak area)
$[16\text{-ArTOS}] = 4.78 \times 10^{-12}$(peak area)
b. ToS_m: estimated from fitting a plot of %(1-ArToS) vs [NaToS]. $\%1\text{-ArToS} = 26.14[NaToS]^{0.642}$
c. ToS_w is obtained via the equation

$$[ToS_w] = \frac{\alpha\{([CTAToS] - cmc) + cmc + [NaToS]}{1 - V[CTAToS]}$$

d. S_w^{ToS} is obtained from fitting a plot of S_w^{ToS} vs [NaToS]: $S_w^{ToS} = 17.52[ToS_m]^{-0.275}$
e. $H_2O_m = S_w^{ToS}[ToS]_m \%16\text{-ArOH} / \%16\text{-ArToS}$

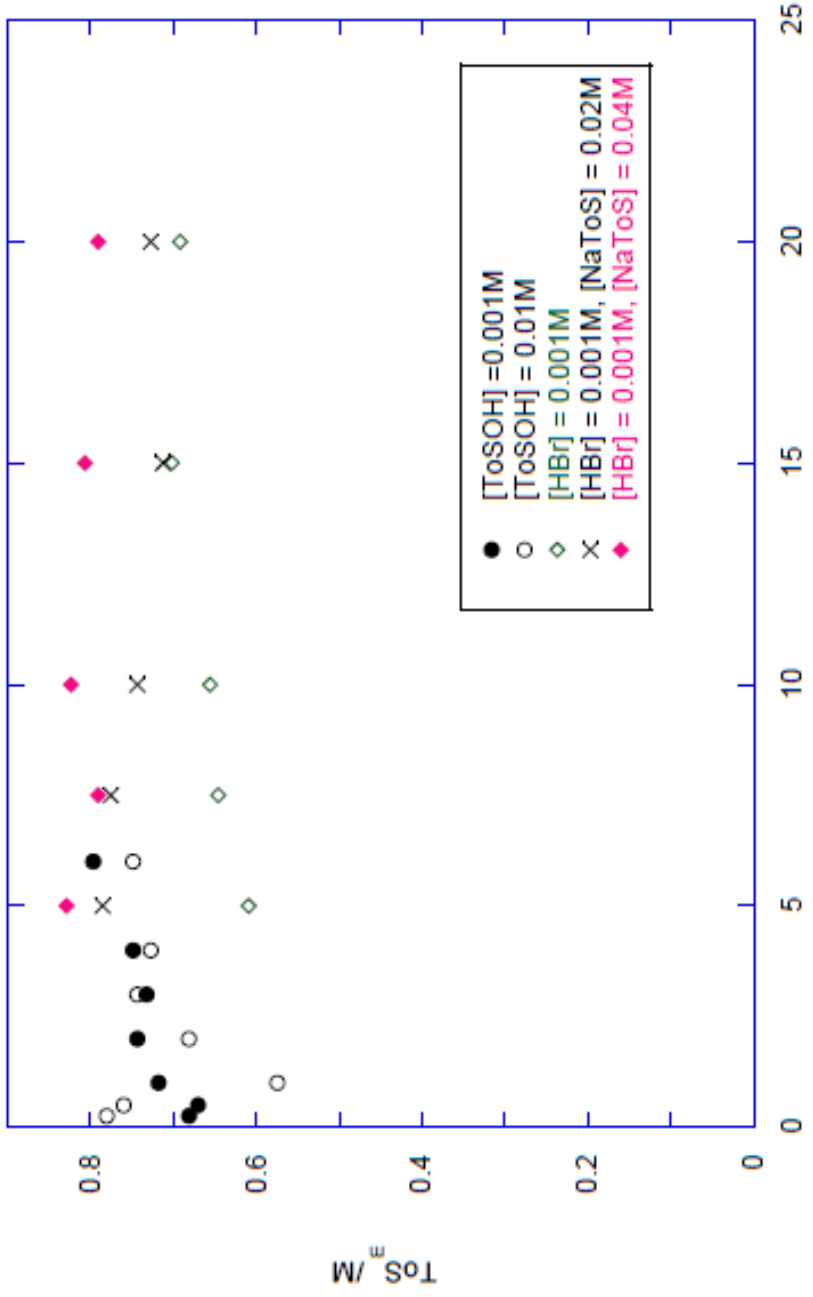

Figure 24. Plots of ToS_m vs [CTAToS] of chemical trapping in CTAToS surfactant with 2.5×10^{-4} M of 16-ArN_2^+ in 0.001 M of HBr at 25°C.

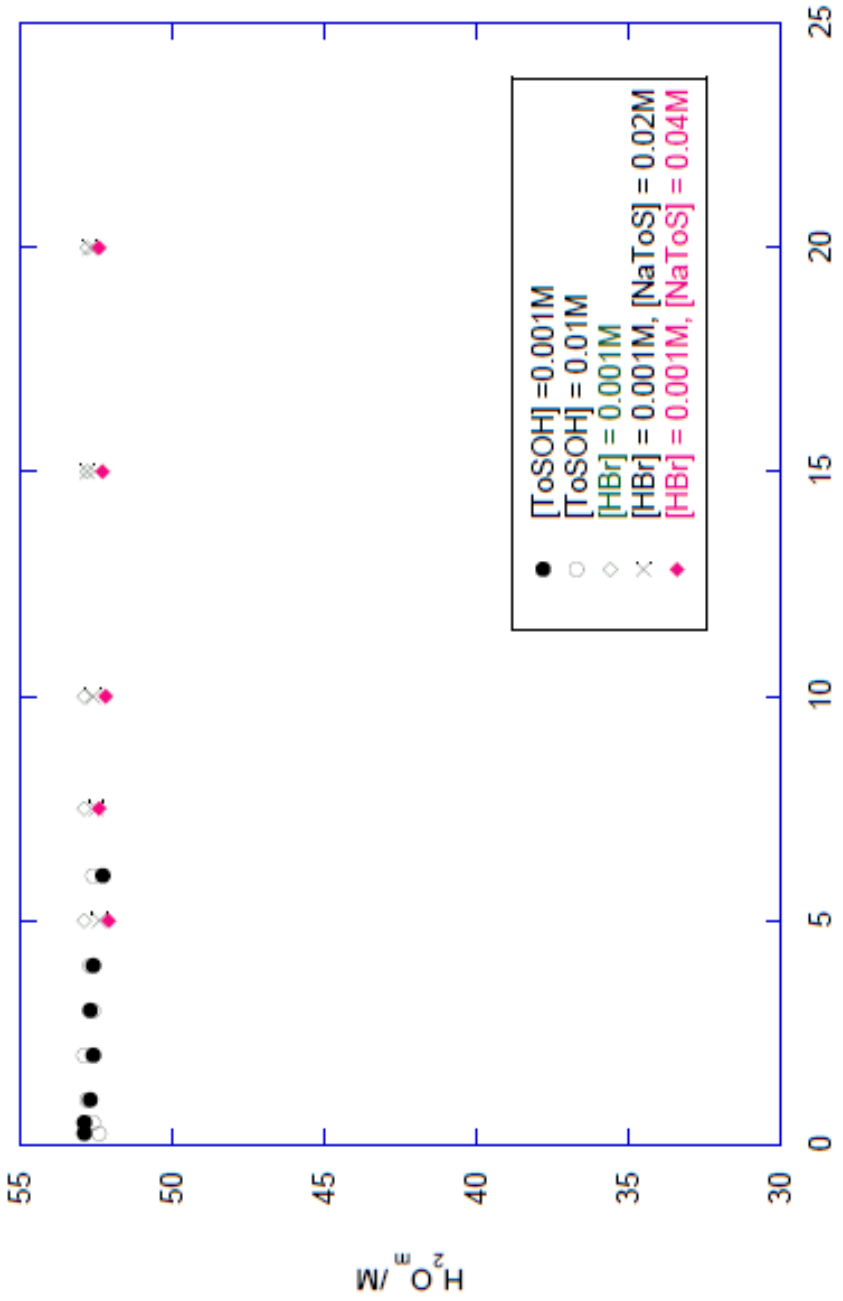

Figure 25. Plots of H_2O_m vs [CTAToS] of chemical trapping in CTAToS surfactant with 2.5×10^{-4} M of 16-ArN_2^+ in 0.001 M of HBr at 25°C.

In Table 7, ToSOH is used to make the solution acidic, and both 0.001 and 0.01 M acids effectively inhibited the formation of reduced products 16-ArOH. [CTAToS] increases from 0.25 M, which is the cmc, to 6 mM, which exceeds the 2nd cmc, 2 mM.[37] The total yields of products 16-ArToS and 16-ArOH for [CTAToS] at lower concentration, from 0.25 to 3 mM, with 0.001 M acid are much lower than 100% and for the rest of the solutions are close to 100%. The reasons for these differences are not known. The normalized yields of 16-ArOH decrease slightly, and the normalized yields of 16-ArToS increase slightly, so ToS_m and H_2O_m that calculated from the yields only change slightly.

In Table 8, as [NaToS] increases, the normalized %16-ArOH decreases slightly, the normalized %16-ArToS increases a little, and the corresponding ToS_m increases slightly too. However, H_2O_m remains essentially constant and independent of surfactant and counterion concentration added as salt.

Data in Table 7 and 8 are plotted in Figures 24 and 25. In these solutions, the viscosity increases when [CTAToS] and [NaToS] increase. Figure 24 is the plots of ToS_m versus [CTAToS]. When acid is ToSOH, data points are a little scattered. When HBr is used as acid, ToS_m with 0.04 M NaToS is higher than with 0.02 M NaToS, which is also higher than with no NaToS. The changes are consistent with the viscosity changes of the solutions. Figure 25 contains the plots of H_2O_m versus [CTAToS]. There is no significant change in H_2O_m with ToSOH or HBr as the acid. In this concentration range, the data show no sign of ToS^- replacing H_2O in the micellar interfacial region. Considering the 2nd cmc of CTAToS is rather small comparing to that of CTAB, and what have done on CTAToS are also around the 2nd cmc of CTAToS, we may want to know that when we

raise the concentration of CTAToS to a much higher level than its 2nd cmc, how the ToS_m and H_2O_m would change. Also we may know whether the definition about ToS_m provided in Equation 4 works in higher concentration. So the chemical trapping experiments are applied to CTAToS at higher concentrations. Because the CTAToS solid is difficult to dissolve at 25^{o}C and in higher concentration it has the viscosity problem, which makes the probe difficult to mix in the solution, the surfactant is replaced by mixing CTAB and NaToS bulk solutions. The data are shown in Table 9, and plotted from Figures 26 to 28.

Table 9.

Chemical trapping in CTAB with added NaToS and 2.5×10^{-4} M of 16-ArN_2^+ in HBr at 25°C [a]

[CTAB] (M)	[NaToS] (M)	[HBr] (M)	Total %yield	Normalized %yield		ToS_m [b] (M)	ToS_w [c] (M)	S_w^{ToS} [d]	H_2O_m [e] (M)
				%16-ArOH	%16-ArToS				
0.02	0.01	0.001	101.4	80	20	0.659		19.65	51.77
0.02	0.02	0.001	103.2	79.4	20.6	0.690	0.0029	19.40	51.58
0.02	0.03	0.001	105.3	79.1	20.9	0.705	0.0129	19.28	51.48
0.02	0.04	0.001	107.5	79.2	20.8	0.700	0.0230	19.32	51.52
0.02	0.05	0.001	99.9	76.8	23.2	0.830	0.0331	18.44	50.68
0.02	0.06	0.001	109.6	78.7	21.3	0.727	0.0432	19.13	51.35
0.05	0.02	0.001	99.1	78.5	21.5	0.737		19.05	51.28
0.05	0.04	0.001	100.5	77.4	22.6	0.797		18.65	50.90
0.05	0.05	0.001	99.9	77.1	22.9	0.813	0.0069	18.54	50.79
0.05	0.06	0.001	102.5	76.5	23.5	0.847	0.0171	18.34	50.56
0.05	0.08	0.001	103.9	76.1	23.9	0.870	0.0376	18.21	50.41
0.05	0.1	0.001	102.2	75.4	24.6	0.910	0.0580	17.98	50.14
0.05	0.15	0.01	96.9	72.5	27.5	1.082	0.1092	17.14	48.92
0.05	0.2	0.001	101.2	72.4	27.6	1.088	0.1604	17.12	48.87
0.05	0.25	0.01	98.6	70.4	29.6	1.214	0.2115	16.61	47.96
0.05	0.3	0.01	95.9	70	30	1.240	0.2627	16.51	47.77
0.05	0.35	0.01	99.4	68.5	31.5	1.338	0.3139	16.17	47.05
0.05	0.4	0.01	97.8	67.7	32.3	1.391	0.3650	16.00	46.65
0.05	0.5	0.01	100.3	66.4	33.6	1.479	0.4674	15.73	45.99
0.05	1	0.01	99.1	61.4	38.6	1.837	0.9790	14.82	43.31

a. Reaction time 24 hours. Each sample injected in triplicate. HPLC method: 55% methanol / 45% isopropanol. Flow rate = 0.4 mL/min over 80 min, $\lambda = 220$ nm, injection volume = 100 µL. Typical retention times: 16-ArOH ~ 25 min, 16-ArToS ~ 36 min. Calibration curve:[16-ArOH]=1.08×10^{-10}(peak area); [16-ArTOS]=4.78×10^{-12}(peak area)

b. ToS_m:estimated from fitting a plot of %(1-ArToS) vs [NaToS]. %1-ArToS = $26.14[NaToS]^{0.642}$

c. ToS_w is obtained via the equation

$$[ToS_w] = \frac{\alpha\{([CTAToS] - cmc) + cmc + [NaToS]}{1 - V[CTAToS]}$$

d. S_w^{ToS} is obtained from fitting a plot of S_w^{ToS} vs [NaToS]: $S_w^{ToS} = 17.52[ToS_m]^{-0.275}$

e. $H_2O_m = S_w^{ToS}[ToS_m]$ %16-ArOH / %16-ArToS

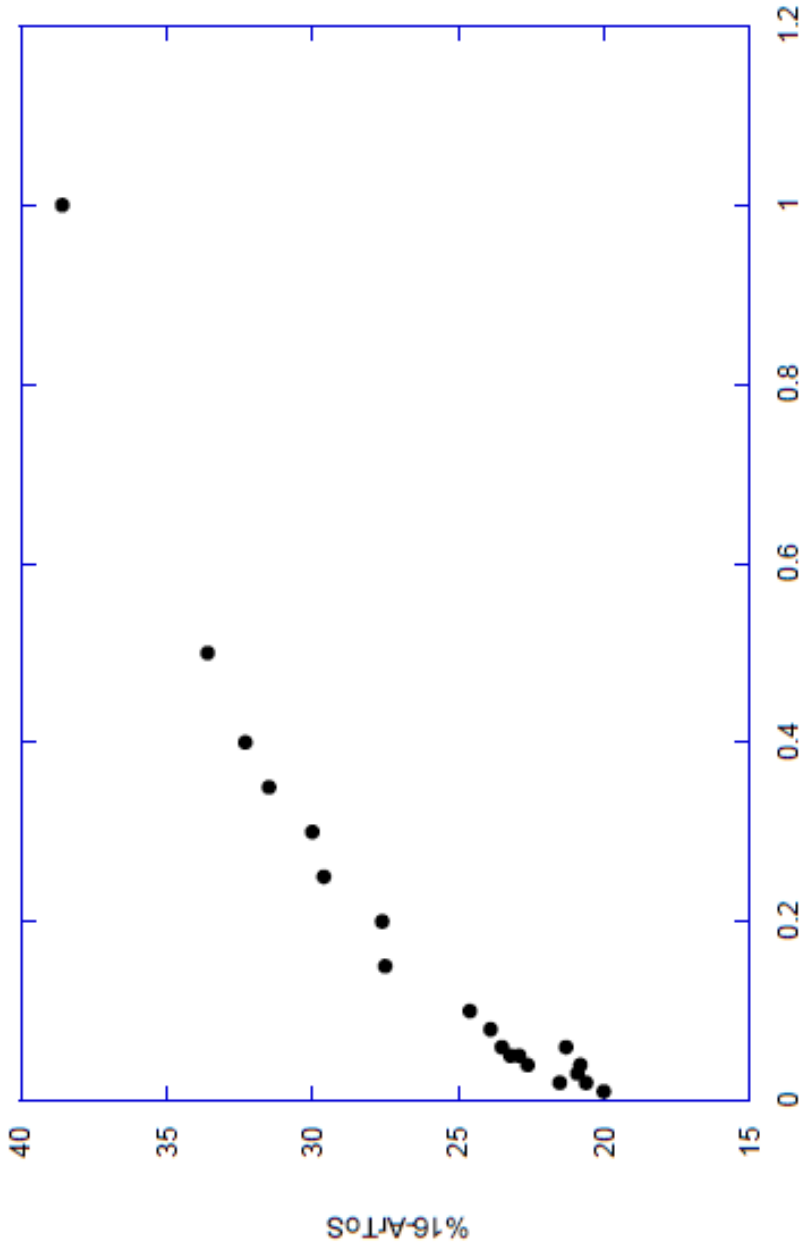

Figure 26. Plot of %16-ArToS vs [NaToS] of chemical trapping in CTAB surfactant and added salt NaToS with 2.5×10^{-4} M of 16-ArN_2^+ in HBr at 25°C

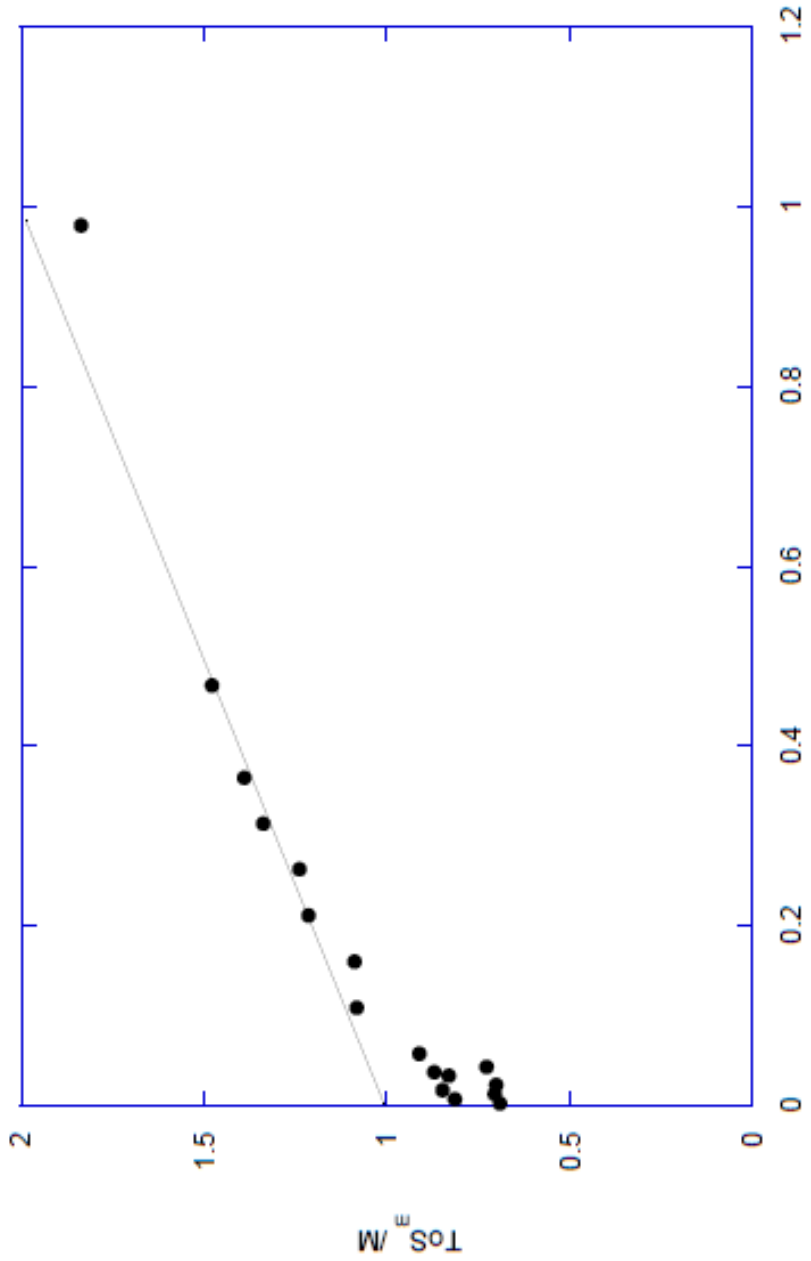

Figure 27. Plot of ToS_m vs $[ToS_w]$ of chemical trapping in CTAB surfactant and added salt NaToS with 2.5×10^{-4} M of 16-ArN_2^+ in HBr at 25°C. The straight line with slope 1 is used to aid the eye.

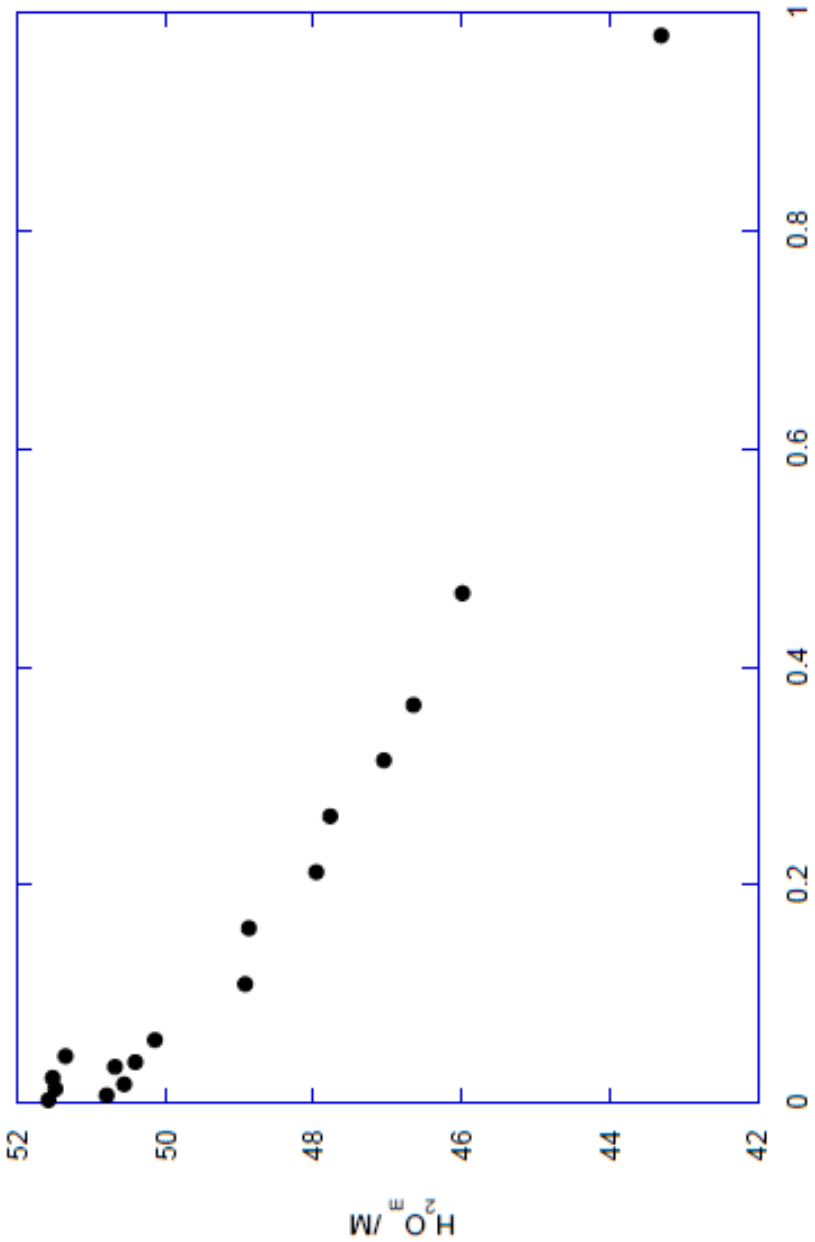

Figure 28. Plot of H_2O_m vs $[ToS_w]$ of chemical trapping in CTAB surfactant and added salt NaToS with 2.5×10^{-4} M of 16-ArN_2^+ in HBr at 25°C

ToS^- is the only counterion that is trapped by the probe. The 16-ArBr product is not observed by HPLC. The total yields of 16-ArToS and 16-ArOH products are 100 ± 5%, which are excellent. As [NaToS] increases, %16-ArOH decreases and %16-ArToS increases simultaneously. The calculated values of ToS_m show that as the ToS^- concentration increases, the ToS^- concentration in the micellar interfacial regions, ToS_m, also increases, with a concurrent decrease in H_2O_m.

The data are plotted from Figures 26 to 28. Figure 26 is the plots of %16-ArTos versus [NaToS]. As NaToS is added in the solution, %16-ArToS increases smoothly. Figure 27, a plot of ToS_m versus $[ToS_w]$, shows that as $[ToS_w]$ increases, ToS_m increases rapidly initially, and then falls on a straight line with slope of 1. An incremental increase of $[ToS_w]$ gives an equivalent increase in ToS_m. Figure 28 shows the corresponding decrease of H_2O_m, which is also on a smooth curve.

Figure 27 for ToS_m vs. $[ToS_w]$ and Figures 10 and 13, the Br_m versus $[Br_w]$ curve and the Cl_m versus $[Cl_w]$ curve, all contain regions in which X_m (X = Br, Cl, ToS) increases at the same rate of $[X_w]$, i.e. slope of 1. But Figure 27 and Figure 24 show no sign of an increase in ToS_m like those for Br_m and Cl_m. The probable explanation is that the sphere-to-rod transition of CTAToS occurs at a 2 mM, which is the reported 2nd cmc and the change in ToS_m is small comparing to CTAB. If the chemical trapping results are not 100% precise, a normal data fluctuation or tiny experimental error may have huge effect on the positions of data points on the ToS_m-$[ToS_w]$ graph, thus it would be difficult to identify the ToS_m break from the initially rapid increase of ToS_m.

The chemical trapping experiments were carried out in DTAB/NaToS for comparison. Adding NaToS to DTAB solution has the same effect as CTAB. As reported

in the literature, mixture of CTAB and NaToS solution viscosity increases to a maximam then starts to decreases.[42] Reducing the chain length reduces the hydrophobic effect and shifts the balance of forces, Section 1.3. The cmc of DTAToS is 4.4 mM,[43] higher than the cmc and 2nd cmc of CTAToS. The 2nd cmc of DTAToS is not reported, but must be higher than 4.4 mM. The degree of ionization of DTAToS is 0.13.[43] The results are shown in Table 10, and are plotted in Figures 29 and 30.

Table 10.

Chemical trapping in DTAB surfactant and added salt NaToS with 2.5×10^{-4} M of 16-ArN_2^+ in HBr at 25°C [a]

[DTAB] (M)	[NaToS] (M)	[HBr] (M)	Total %yield	Normalized %yield		$[ToS_w]$ [b] (M)	ToS_m [c] (M)	S_w^{ToS} [d]	H_2O_m [e] (M)
				%16-ArOH	%16-ArToS				
0.05	0.1	0.001	68.0	78.5	21.5	0.062	0.737	19.05	51.28
0.05	0.2	0.001	76.3	74.2	25.8	0.164	0.980	17.62	49.65
0.05	0.3	0.001	80.2	70.2	29.8	0.265	1.227	16.56	47.87
0.05	0.4	0.001	93.7	67.0	33.0	0.367	1.438	15.85	46.30
0.05	0.5	0.001	72.8	64.8	35.2	0.469	1.591	15.42	45.16
0.05	0.6	0.01	89.2	66.0	34.0	0.571	1.507	15.65	45.79
0.05	0.8	0.01	80.9	62.4	37.6	0.775	1.763	14.99	43.86

a. Reaction time 24 hours. Each sample injected in triplicate.
HPLC method: 55% methanol / 45% isopropanol. Flow rate = 0.4 mL/min over 80 min, $\lambda = 220$ nm, injection volume = 100 µL.
Typical retention times: 16-ArOH ~ 25 min, 16-ArToS ~ 36 min.
Calibration curve: $[16\text{-ArOH}] = 1.08 \times 10^{-10}$(peak area)
$[16\text{-ArTOS}] = 4.78 \times 10^{-12}$(peak area)

b. $[ToS_w]$ is calculated with the equation

$$[ToS_w] = \frac{\alpha\{([DTAToS] - cmc)\} + cmc + [NaToS]}{1 - V[DTAToS]}$$

where V is the molar volume of DTAToS in mole per liter assuming that the density of DTAToS is 1.0 g/mL. V is 0.389 L/mol for DTAToS.

c. ToS_m: estimated from fitting a plot of %(1-ArToS) vs [NaToS]. $\%1\text{-ArToS} = 26.14[NaToS]^{0.642}$

d. S_w^{ToS} is obtained from fitting a plot of S_w^{ToS} vs [NaToS]: $S_w^{ToS} = 17.52[ToS_m]^{-0.275}$

e. $H_2O_m = S_w^{ToS}[ToS_m]\ \%16\text{-ArOH} / \%16\text{-ArToS}$

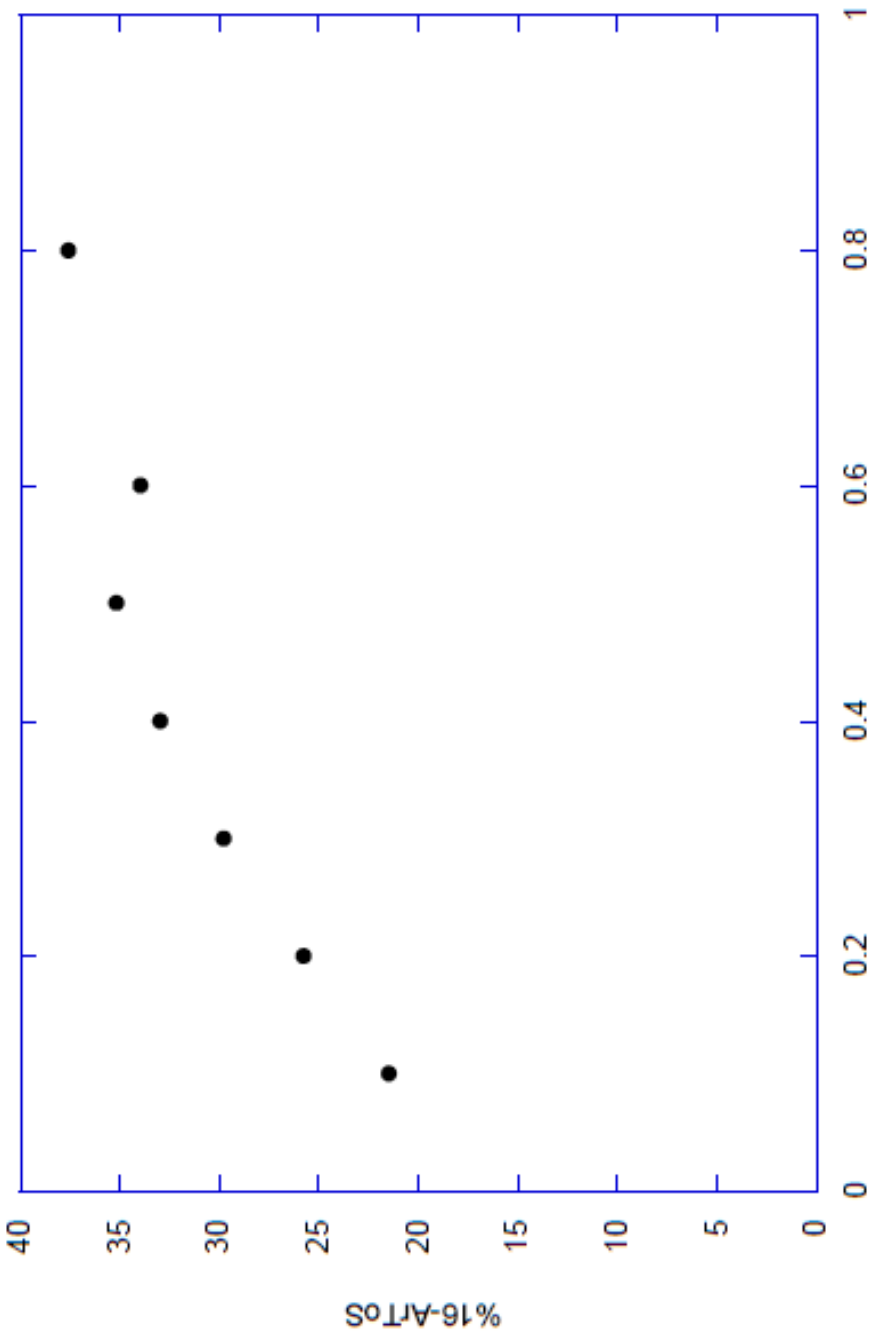

Figure 29. Plot of %16-ArToS vs [NaToS] of chemical trapping in DTAB surfactant and added salt NaToS with 2.5×10^{-4} M of 16-ArN_2^+ in HBr at 25°C.

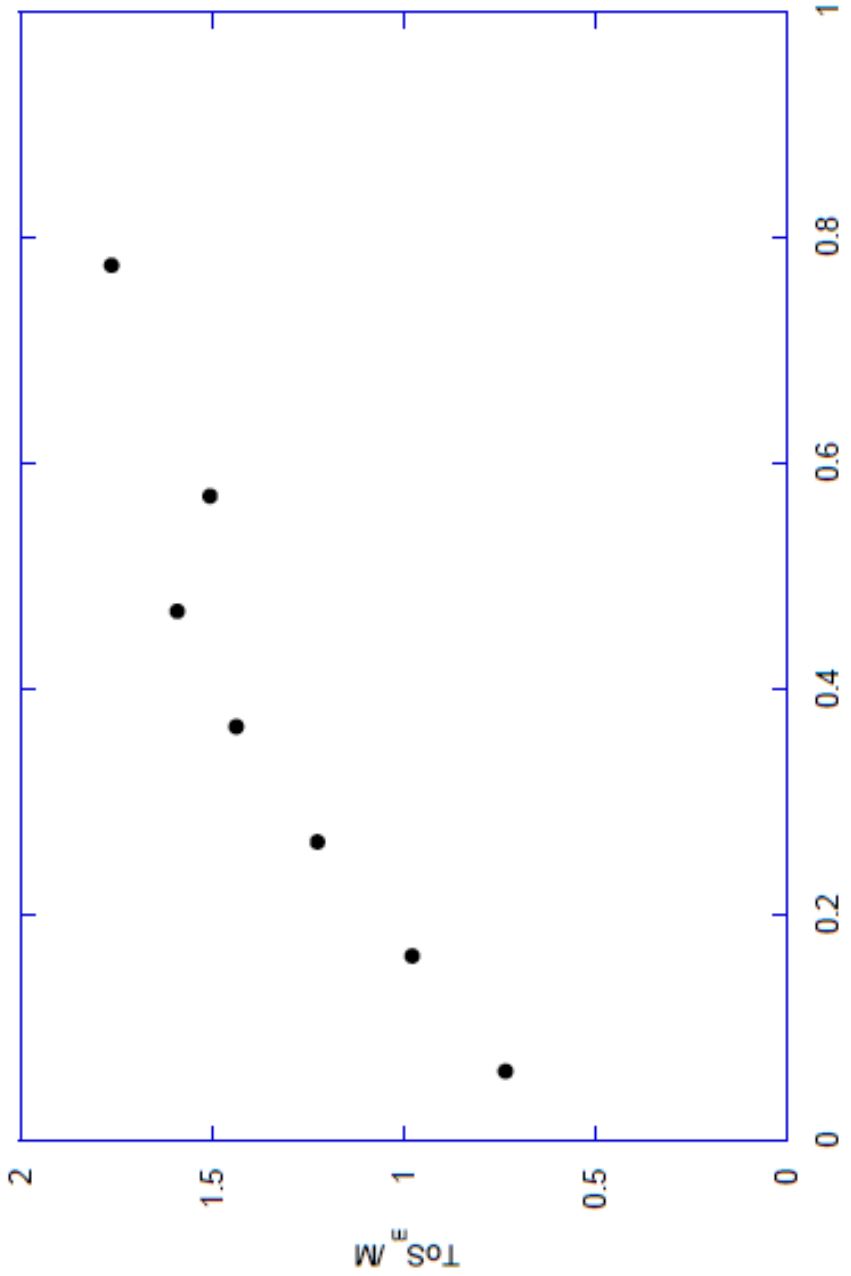

Figure 30. Plot of ToS_m vs $[ToS_w]$ of chemical trapping in DTAB surfactant and added salt NaToS with 2.5×10^{-4} M of 16-ArN_2^+ in HBr at 25°C.

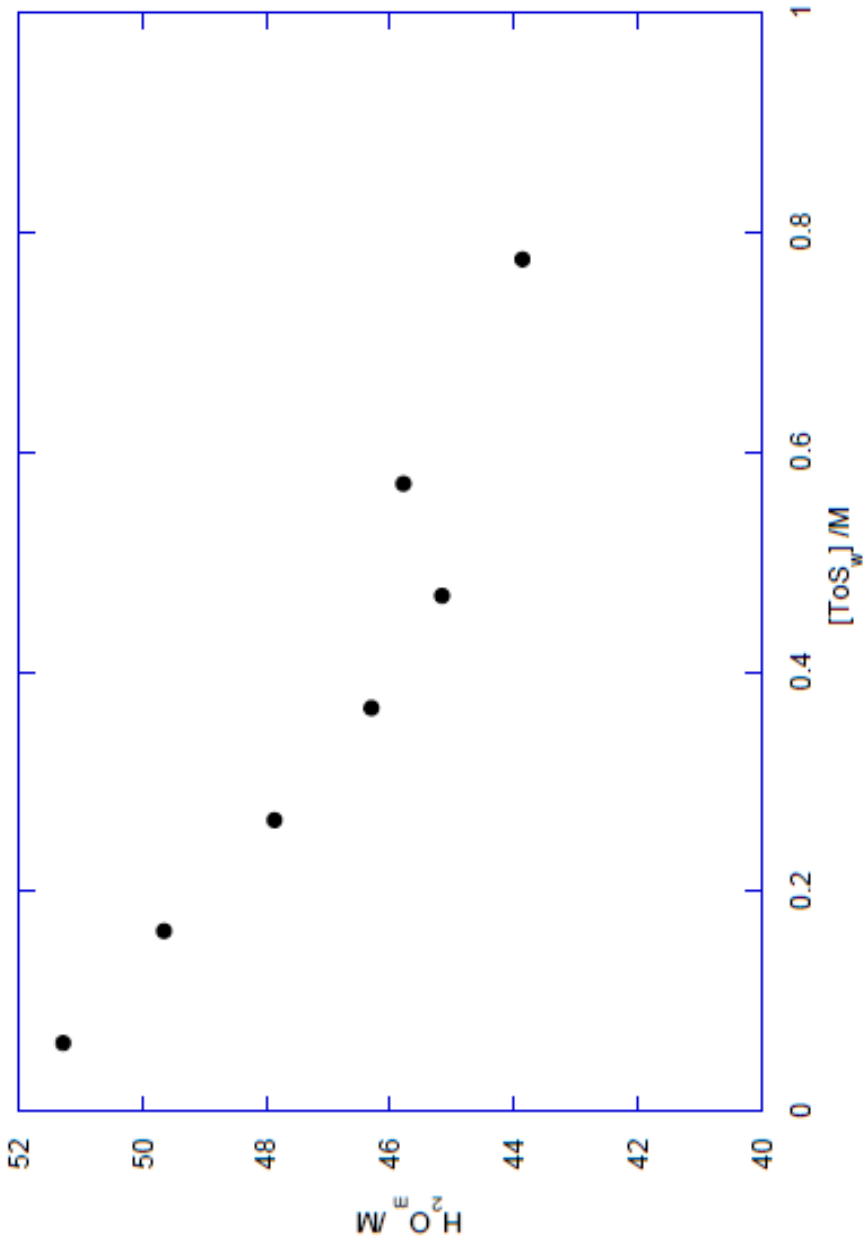

Figure 31. Plot of H_2O_m *vs* $[ToS_w]$ of chemical trapping in DTAB surfactant and added salt NaToS with 2.5×10^{-4} M of 16-ArN_2^+ in HBr at 25°C.

DTAB mixed with NaToS solutions are used instead of DTAToS. In all the solutions with 0.05 M DTAB and different concentrations of NaToS, the visual viscosities are the same as water. No viscosity maximum was observed visually.

Table 10 shows the chemical trapping results on 0.05 M DTAB with increasing [NaToS]. No bromo products was detected by HPLC, just as with CTAB/NaToS. The total yields of products are all a bit low. The normalized %16-ArOH decreases and the normalized %16-ArToS increases, which indicates that ToS^- replaces H_2O as more NaToS is added in the solution. The calculated increased ToS_m and decreased H_2O_m prove that too. $[ToS_w]$ is calculated with the equation provided in the footnote of the table.

Figure 29 plots %16-ArToS versus [NaToS]. As [NaToS] increases in the solution, %16-ArToS increases gradually, mostly on a smooth curve in the concentration range measured. The calculated ToS_m and $[ToS_w]$ are plotted in Figure 30. ToS_m increases almost smoothly as $[ToS_w]$ increases. The corresponding H_2O_m decreases on a smooth curve too, shown in Figure 31. However, the number of data shown in the figures is limited. It is difficult to identify the ToS_m break, if there is any. These data are a good start for the chemical trapping experiment on DTAToS.

2.4 Discussion

The pseudophase ion exchange model (PIE), and the ion-pairing model were introduced in the previous chapter. The PIE model explains specific ion effects on the rates and equilibria of chemical reactions in association colloids over a wide variety of experimental conditions.[21,29,44] However, limitations of the model were discovered as researchers applied it to interpret chemical reactions over larger ranges of ion concentrations. [25-27,44-46]

Bunton et al. discovered that the addition of cyanide ion to the 4 position of *N*-alkyl-3-carbamoylpyridinium bromides (alkyl = n-$C_{12}H_{25}$, n-$C_{14}H_{29}$, n-$C_{16}H_{33}$) were speeded in cationic micelles, and at high concentration of CTACN, the reaction rates became almost constant, Figure 32.[47]

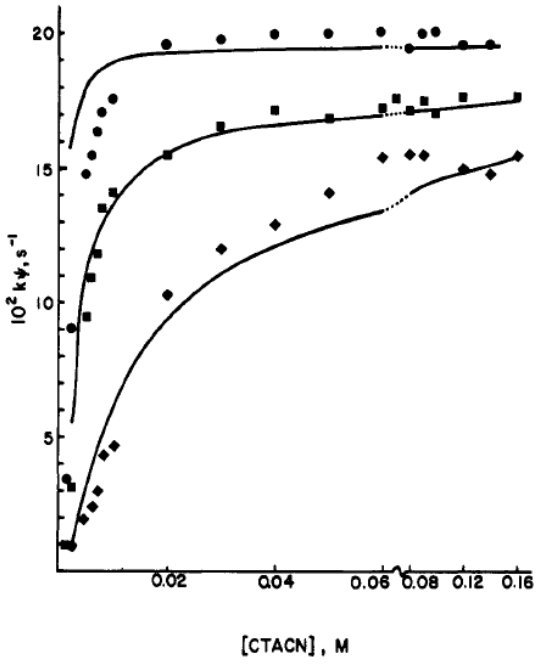

Figure 32. Variation of rate constants with CTACN: ♦, ■, ●, R = $C_{12}H_{25}$, $C_{14}H_{29}$, and $C_{16}H_{33}$, respectively.[47]

However, in reactive counterion surfactant solutions containing high concentrations of added reactive counterions, incremental increases of k_{obs} are observed for a variety of counterions, and neither maxima nor plateaus appear.[28,29,48] Nome et al. studied the dehydrochlorination of DDT, DDD and DDM with hydroxide ion in the presence of CTAOH, and discovered that k_{obs} increased linearly as a function of $[OH^-]$[49] Figure 33 is the example of DDM.

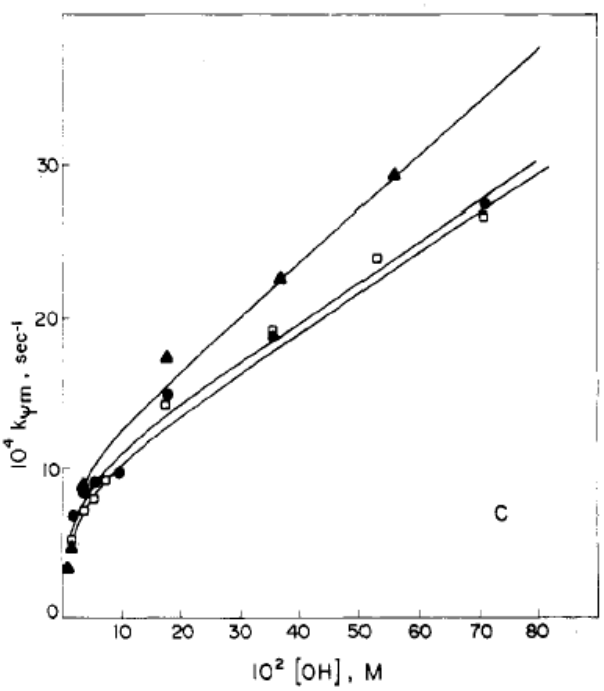

Figure 33. Plots of the observed pseudo-first-order rate constant of DDM vs. hydroxide ion concentration at constant added CTAOH, [CTAOH] = 8.78 x 10^{-4} (□), 1.46 x 10^{-3} (●), and 7.32 x 10^{-3} (▲) M.[49]

Another test of the PIE model was made by Zanette et al. for the acid-catalyzed hydrolysis of 2-(p-nitrophenyl)-1,3-dioxolane, acetyl p-methoxybenzaldoxime, and octanol p-methoxybenzaldoxime in the presence of SDS. Figure 34 compared the observed reaction rate from experiment for the hydrolysis of 2-(p-nitrophenyl)-1,3-

dioxolane with the calculated value of k_{ψ} based on the classical pseudophase model. According to the classical pseudophase model, the reaction rate should become constant at high [H^+], while the experimental observed reaction rate keeps increasing linearly without plateau.[50] This large deviation demonstrates the failure of pseudophase model clearly.

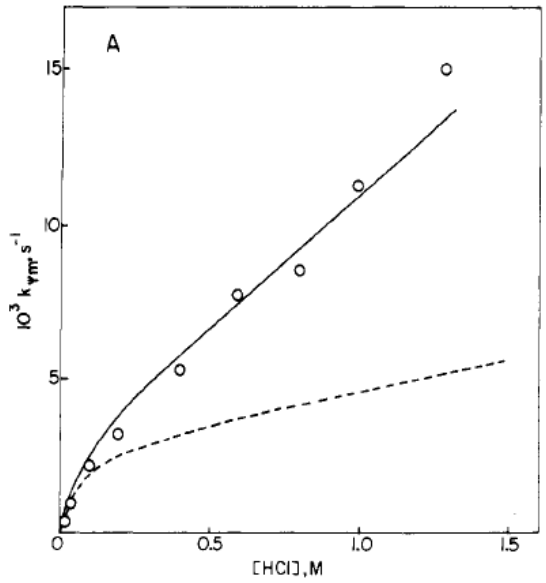

Figure 34. Variation of the pseudo-first-order rate constants for the hydrolysis of 2-(p-nitrophenyl)-1,3-dioxolane and increasing acid concentrations. [SDS] = 0.1 M. Full and broken lines correspond to theoretical curves.[50]

As described in Chapter 1, the chemical trapping method provides estimates of the interfacial water and counterion concentrations in micellar solutions with any surfactant and added salt above the cmc. Figures 10, 12-15, 17, 27 and 28 in Chapter 1 list these results for cationic surfactants with different tail lengths and several different counterions that were published previously and from my work.

The experimental results of counterion concentration in the micellar interfacial regions are plotted against aqueous counterion concentration, X_m vs. $[X_w]$. The plots are composed of at least two and sometimes three parts: (a) an initial rapid increase of X_m with increasing $[X_w]$; (b) a linear increase of X_m with increasing $[X_w]$ with a slope of 1; and (c) in some surfactants, a marked increase of X_m occurs at a range of $[X_w]$ close to the reported 2nd cmc, which indicates the sphere-to-rod transition of the micelles, and after that X_m keeps increasing linearly again with $[X_w]$. Figure 10 for CTAB and Figure 13 for CTAC show the results of Br_m vs. $[Br_w]$ with the three parts.[25] The chemical trapping method also provides estimates of interfacial H_2O molarities. Plotted against $[X_w]$, H_2O_m decreases with increasing $[X_w]$. This makes sense because the interfacial region is composed primarily of counterion, H_2O, and headgroups. The addition of surfactant or counterion as salt to the solutions produces an increase in interfacial counterion concentration and therefore a decrease of interfacial water concentration. The expected marked increases of X_m at the reported sphere-to-rod transitions are not always observed, such as in DTAB and CTAToS solutions, but this is probably caused by the limitation of experiments.

Figure 14 shows the increase of Br_m with increasing $[Br_w]$ in DTAB micelles. There is an initial rise up to 0.1 M $[Br_w]$, followed by a linear increase in Br_m with $[Br_w]$ to about 2.8 M $[Br_w]$, above which DTAB crystalizes out at room temperature. Note that Br_m is always greater than $[Br_w]$. For example, when $[Br_w]$ is 0.5 M, Br_m is 2.0 M; and when $[Br_w]$ is 1.0 M, Br_m is 2.5 M. This means that the interfacial counterion molarity is always higher than the aqueous counterion molarity, which makes sense because at high concentrations of added reactive counterion, Br_m is the sum of the initial Br_m associated

with the head groups and the salt cations, and the contribution of Br_m from added salt, as defined in Equation 4

$$Br_m = \frac{[Br_m]}{[D_n]V_m} = \frac{\beta}{V_m} + (1)\,[Br_w]$$

The coefficient of the equation indicates that the expected slope of the plots Br_m vs. $[Br_w]$ is 1. This equation accounts for the chemical trapping results on DTAB micelles. At low salt concentrations, the addition of surfactant DTAB increases the micelle concentration. When TMAB is added as counterion salt, both TMA^+ and Br^- add to the micellar interface and Br_m increases and H_2O_m decreases, Figures 14 and 15. The chemical trapping experiments on CTAToS give similar results, Figure 27. The ToS_m values above the initial rise increase linearly with increasing $[ToS_w]$ with slope of 1 up to 1.0 M, which is the same as the results of DTAB. The degree of association, β, is assumed to be constant to calculate $[Br_w]$ and $[ToS_w]$, but this assumption only has a small effect on the calculated values because the reported values of the degree of ionization, α ($\alpha = 1 - \beta$), are relatively small for both DTAB and CTAToS at 0.25,[51-53] and 0.13,[36] respectively.

Why should added counterions in the micellar solutions lead to a decrease of interfacial water molarity? Ranganathan has made a point that when micelles form, hydrocarbon/water interactions in the interfacial region still exist.[54,55] However, water molecules associate more strongly to each other than to hydrocarbon. So the increase of counterion concentration in the interfacial region may reduce the amount of water contacting with hydrocarbon, and decrease the molarity of water in the interfacial region.

The initial rise in interfacial counterion concentration has been observed in a number of cases such as CTAC, CTAB, DTAB, CTAToS and some hexadecyl surfactants with different sizes of head groups.[24,25] The resulted X_m vs $[X_w]$ plots all show an initial rise followed by a linear increase of X_m with a slope of 1. All of the initial rises occur at low $[X_w]$, and no sphere-to-rod transition was reported in these concentration ranges. The reason for the initial rise is not straightforward. A possible explanation is that β and V_m are assumed to be constant for a particular surfactant, or it is not sensitive to aqueous counterion concentration.[25-27,56-58] At low $[X_w]$, the ratio of β/V_m determines the value of X_m, Equation 4. However, how β and V_m are affected by increasing $[X_w]$ is unknown, which leaves the appearance of initial rise an unsolved problem.

The plots of X_m vs $[X_w]$ for CTAB and CTAC are similar in shape, but there are some differences, see Figures 10 and 13.[25] Both Br_m versus $[Br_w]$ and Cl_m versus $[Cl_w]$ plots show marked increase in Br_m and Cl_m and marked decrease in H_2O_m at the reported sphere-to-rod transition ranges, e.g. 0.1 M $[Br_w]$ for CTAB and 1.0 M $[Cl_w]$ for CTAC. These breaks are consistent with the theory that the trimethylammonium head groups form ion pairs with the counterions and release water to the aqueous pseudophase.[59] The slopes return to 1 after the breaks for both surfactants. The two breaks are also consistent with the specific ion-ion and ion-water interactions with these two ions. For example, Br^- is bigger in size, more polarized and less strongly hydrated than Cl^-. The experimental results are consistent with forming Br^- ion pairs with head groups at a lower interfacial concentration than Cl^-.[18] The fact that the slope returns to 1 suggests that once the sphere-to-rod transition is complete and the dominant aggregate structure in the micellar solution is a rod shape, adding counterion salts to the solution still increases the counterion

concentration and decreases the water concentration in the interfacial region in the same way as below the sphere-to-rod transition.

The same marked increase in interfacial counterion concentrations and decrease in interfacial water concentrations are also observed for gemini surfactants with ethylene spacers, 12-2-12•2Br, close to the reported sphere-to-rod transition range, while the gemini surfactants with propylene and butylene spacers show incremental increase in interfacial counterion concentrations without any marked increase.[14] The marked increase is also observed with benzoate counterions.[32] By adding 3,5-dichlorobenzoate surfactant to CTAC micelles, the interfacial 3, 5-dichlorobenzoate concentration showed a marked jump at the reported sphere-to-rod concentration range. But when 2, 6-dichlorobenzoate surfactant was added to CTAC solutions, no marked jump is observed, which indicates that the mixed micelles of CTAC/CTA2,6-dichlorobenzoate remain spherical at all mole fractions (0 to 1).

The chemical trapping experimental results for DTAB with added TMAB, Figure 14, and for CTATos with added NaToS, Figure 27, show smooth increase for Br_m and ToS_m respectively, with no marked jump. However, the 2nd cmcs of 1.8 M and 2.0 mM respectively, are reported for both surfactants.[37,60] The sphere-to-rod transition of DTAB occurs at a higher concentration than that of CTAB because DTAB is less hydrophobic than CTAB, and much more Br^- is needed in the interfacial region to shift the balance of forces to form rod-shape micelles. CTAToS is much more hydrophobic than CTAB, and less ToS^- is needed to balance the forces toward rod-shape micelles and the sphere-to-rod transition concentration of CTAToS is much lower than that of CTAB.

The lack of observed concentration breaks is probably caused by limitations of the chemical trapping method. In the CTAC results, Figure 13, the Cl_m jump occurs over a broader range of $[Cl_w]$ and smaller values of Cl_m than those of CTAB results. So in the DTAB results, the reported sphere-to-rod transition occurs at a much higher concentration than CTAC, and at such high salt concentrations, the Br_m jump is not observed because the ion pairing occurs over an even broader $[Br_w]$ concentration range, and the increase of Br_m at the transition is too small to be observed in the presence of a large excess of added Br^-. CTAToS has a smaller 2nd cmc than CTAB, the transition with added ToS^- is not observed because it occurs at a very low concentration and it becomes part of the initial rise of ToS_m with increasing $[ToS_w]$.

To summarize, there are three regions observed in X_m versus $[X_w]$ plots in the chemical trapping results: (a) an initial rise in X_m consistent with partial dehydration and /or an increase in β of the interfacial region induced by added salt; (b) a progressive increase in X_m with a slope of 1 and a concomitant decrease in H_2O_m with increasing $[X_w]$ below the sphere-to-rod transition; and (c) a marked increases in X_m and decreases in H_2O_m when rod-like micelles are formed at the reported sphere-to-rod transition concentration when the transition concentration is neither too low nor too high. All these results are consistent with continued dehydration of the methylene groups in the vicinity of the micellar interface; exchange of interfacial water by added salt; and, consistent with the ion pair/dehydration model, the formation of ion pairs at an added salt concentration that depends on anion type after sufficient water has been displaced from the micellar interface.

2.5 Conclusions

The chemical trapping method is the only method at present that can determine the ion molarities in the micellar interfacial region. By applying the trapping method on surfactants with shorter chain length, DTAB, and with bigger head group, CTAToS, the molarities of counterions and water in micellar interfacial regions are determined, and the X_m vs. $[X_w]$ plots are drawn. Comparing to the published results of CTAB and CTAC, the plots for DTAB and CTAToS are similar in the initial rises and the finally continuous increases following a straight line with slope of 1 with no plateau, and different with no abrupt increases when the sphere-to-rod transition occurs. The reasons for the smooth increases are different for DTAB and CTAToS, and they are explained. Surfactants with shorter chain lengths have lower counterion concentrations in the micellar interfacial regions given the same surfactant and added salt concentrations. However, surfactants with bigger head groups do not have to have higher interfacial counterion concentrations given the same conditions. The head groups may become part of the hydrophobic core and change the compositions in the micellar interfacial regions. The relative interfacial water concentrations of DTAB and CTAToS are determined by the chemical trapping method for the first time, and the changes are the reverse of the counterion changes.

2.6 Future work

The chemical trapping method was applied to CTAB and CTAC, and obvious counterion breaks were observed in the results at the sphere-to-rod transition concentrations. However, the counterion breaks were not observed on DTAB and CTAToS. Possible explanations were proposed from the dependence of the cmc and 2nd cmc of CTAB, CTAC, DTAB and CTAToS on chain length and counterion type. Experiments are proposed to test those explanations.

First, the chemical trapping method can be applied to TTAB (tetradecyltrimethylammonium bromide) solution. TTAB has a chain length longer than DTAB but shorter than CTAB, and the hydrophobicity of TTAB is stronger than DTAB and weaker than CTAB. The reported cmc and 2nd cmc of TTAB are 3.8 mM[61,62] and 0.12 M,[63] both of which are higher than those of CTAB and lower than those of DTAB, Table 1. The chemical trapping results will show the change of Br_m as $[Br_w]$ increases. The sphere-to-rod transition concentration of TTAB is lower than CTAC (1M), which shows the Cl_m break, so we may observe the Br_m break from the chemical trapping result of TTAB. The transition range of $[Br_w]$ may be measured and compared to that of CTAB. If the transition range of $[Br_w]$ is broader in TTAB than in CTAB, then the result would support the tentative conclusion that the Br_m break of DTAB is difficult to observe from the Br_m vs $[Br_w]$ graph because the transition range of $[Br_w]$ is too broad.

Second, chemical trapping experiments in DTAToS. DTAToS has a cmc of 4.4 mM[43] but the sphere-to-rod transition concentration is not reported. The chemical trapping experiment has applied on some CTAB/NaToS solutions with selected concentrations, and the products, 16-ArToS and 16-ArOH, are analyzed with HPLC.

DTAB/NaToS solutions with wider concentration range may be selected, for example, from 4.4 mM up to the solubility limit of surfactants. We may see the counterion concentration changes in micellar interfacial region when the sphere-to-rod transition occurs. The results may compare with the trapping result of CTAToS, CTAB and DTAB, and find the composition difference of counterion and water in interfacial region when hydrophobic chain length and counterion type are different.

Chapter 3. Crystal Studies of 1-n-1•2Br Bolaform Salts

Conventional surfactants and their properties were introduced in Chapter 1. This chapter introduces a short project with twin tailed gemini surfactants 12-n-12•2Br (n = 2, 3, 4), and their short-chain analogs, bolaform salts 1-n-1•2Br (n = 2, 3, 4). Research on gemini surfactants has increased dramatically over the last decade.[64-69] The physical properties of twin-tailed gemini surfactants in solutions are significantly different from those of single-chain surfactants. X-ray analysis can be used to obtain the crystal structures of such surfactants and the interactions between the bromine ion, water, and the alkyl group of the dications, and whether the interactions meet the requirement of weak hydrogen bonds as expressed by bond lengths and bond angles. Bolaform salts 1-n-1•2Br (n = 2, 3, 4) have similar and simpler structures than 12-n-12•2Br (n = 2, 3, 4). The crystals of these bolaform salts were prepared and analyzed by single crystal X-ray analysis, and the location of water molecules and weak hydrogen bonds were identified.

3.1 Introduction to gemini surfactants and bolaform salts

In 1991, Menger and Littau created the name gemini surfactant for what, at that time, was a relatively new kind of surfactant.[70] Ionic gemini surfactants are composed of two headgroups, two hydrophobic tails connected with a spacer group, and two counterions,[64,67,70,71] Figure 35.

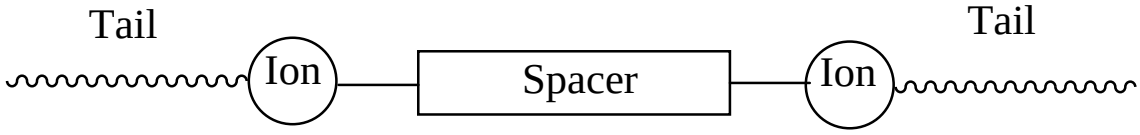

Figure 35. Schematic representation of a gemini surfactant.[70]

The spacer group of gemini surfactant may be as simple as ethylene, or a complicated rigid structure, such as an imidazolidinium ring.[4,72] The most popular cationic gemini surfactants are the alkanediyl-α,ω-(dimethydodecylammonium bromides), or 12-n-12•2Br for short, n = 2, 3, 4, Figure 36.[73]

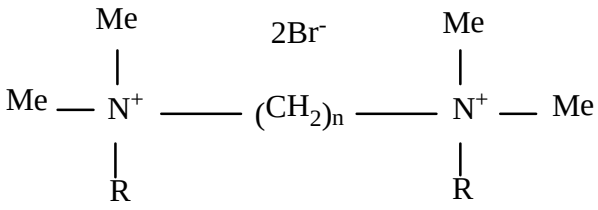

Figure 36. Structure of R-n-R•2Br, R = $C_{12}H_{25}$, CH_3, n = 2, 3, 4.

Solutions of gemini surfactants become viscous at lower concentrations than their single-chained analogs, and the 1st and 2nd cmcs of 12-2-12•2Br, which have been defined in Chapter 1, are much lower compared to its single-chained analog DTAB, Table 11.

Surfactants	Cmc/mM	2nd cmc
DTAB	16[60]	1.8 M[60]
12-2-12•2Br	0.84[74,75]	4.2 mM[76]
12-3-12•2Br	0.91[74,75]	N/A[65,77]
12-4-12•2Br	1.00[74,75]	N/A[65,77]

Table 11. 1st and 2nd cmcs of DTAB and 12-n-12•2Br (n = 2, 3, 4).

12-2-12•2Br forms rod-like micelles at 4.2 mM, about 5 times its 1st cmc.[76] Micelles of 12-3-12•2Br and 12-4-12•2Br stay spherical up to much higher concentrations.[65,73,74,76,77] Chemical trapping experiments were carried out on gemini micellar solutions to measure interfacial ion concentrations.[14,73] Romsted et al. proposed that in the micellar interface of 12-2-12•2Br, the quaternary ammonium head groups bind Br^- strongly to form ion pairs at the 2nd cmc. The trapping results are consistent with concomitant ion-pair formation and release of water of hydration during the sphere-to-rod transition of 12-2-12•2Br at 2.2 mM of [12-2-12•2Br].[14] However, sphere-to-rod transitions were not observed for either 12-3-12•2Br or 12-4-12•2Br,[14,73] which have longer spacer lengths. The association constants, K_s, for the binding of the first Br^- were estimated by chemical trapping in bolaform salts and by Br^- NMR. By chemical trapping, K_s decreases with increasing spacer length (16.7 for 12-2-12•2Br, 5.79 for 12-3-12•2Br, and 1.75 for 12-4-12•2Br), while K_s for the binding of the second Br^- were assumed to be the same for all three gemini surfactants.[14]

The state of surfactants in aqueous solutions is very different from their crystalline state. Surfactants in solutions undergo translational, rotational, and vibrational motions. However in a crystalline environment, many of these motions are absent. Substantial experimental evidence indicates that the crystal structures of surfactants have weak hydrogen bonds between charged ions.[4,78-83] As discussed in previous chapters, such interactions between head groups and counterions may contribute to the sphere-to-rod transition of micelles.

Single crystal X-ray diffraction is a technique for determining molecular structures.[78,79,81,84-89] The positive charged cations interact with anionic halide ions

electrostatically and specifically because the structures are different for different anions. Gaussian calculations show that when the atoms are close, weak hydrogen bonds are stronger than the Van der Waals interactions because they have shorter interaction distances (sum of H-X radii) and the C-H⋯X angle is close to 180^{o}.[4,79-81,89] Steiner et al. concluded that a fundamental difference between hydrogen bonds and Van der Waals interactions is their different directionality characteristics.[89] However, their study of the weak hydrogen bonds could not determine whether weak hydrogen bonds determine the geometry of the interactions.[4,89]

Gemini surfactants have long twin tails that complicate crystal structures. The short-chain analogs of gemini surfactants, called bolaform salts, are simple models for the surfactant head groups and were used to grow crystals from aqueous solutions. Understanding the nature of weak hydrogen bonds between methyl and methylene protons and bromide ions may eventually help us to understand the nature of bolaform salt crystals and headgroups, counterions and water interactions in the interfacial regions of micelles.

Aqueous solutions of 1-n-1•2Br (n = 2, 3, 4) bolaform salts with the same concentrations as the interfacial regions of gemini surfactant solutions have been used as models for the head group and counterion interactions in the interfacial regions of gemini surfactant solutions.[59]

3.2 Crystal structures of bolaform salts

Bolaform salts have high solubilities in water. No bolaform crystals precipitate from cooling their concentrated solutions. McPherson used aqueous poly (ethylene)

glycol solutions to precipitate macromolecules because the glycol competed for water and dehydrated macromolecules.[90,91] X-ray diffraction confirmed that the macromolecule crystals were in their native condition probably because glycol did not enter the crystals and did not contact the interior atoms.[90,91] Because tetra (ethylene glycol) dimethyl ether has similar structure to poly (ethylene) glycol and it is convenient to obtain, it was added to the aqueous bolaform salt solution as a precipitant. Bolaform salts crystallized out as expected. Three crystal structures of 1-n-1•2Br (n = 2, 3 and 4) were determined by single crystal X-ray diffraction analysis, Tables 12 – 14, and views of the crystal structures were prepared using ORTEP3v2 for windows, Figures 37 to 39.

Table 12. Crystal and structure refinement data for 1-2-1•2Br

Formula	$C_8H_{22}N_2Br_2•H_2O$
Color	Colorless
Formula weight	324.11
Temperature, ^oK	100(2)
Wavelengh, Å	0.71073
Crystal system	Monoclinic
Space group	P 2_1/c
Unit cell dimensions, Å	a = 12.4725(10)
	b = 7.3893(6)
	c = 15.3247(12)
	β = 108.760(1)
Volume, $Å^3$	1337.34(19)
Z	4
Calculated density, Mg m^{-3}	1.610
Absorption coefficient mm^{-1}	6.035
θ range for data collection	2.76-31.60
Limiting indices (h, k, l)	-18/18, -10/10, -22/22
Reflections collected/unique	16275/4484
Data/restraints/parameters	4484/0/215
Goodness-of-fit on F^2	1.003
Final R/wR_2 [$I > 2\sigma(I)$]	0.0293/0.0686
Final R/wR_2 (all data)	0.0363/0.0711
Largest diff. Peak and hole, e $Å^{-3}$	0.980/-0.855

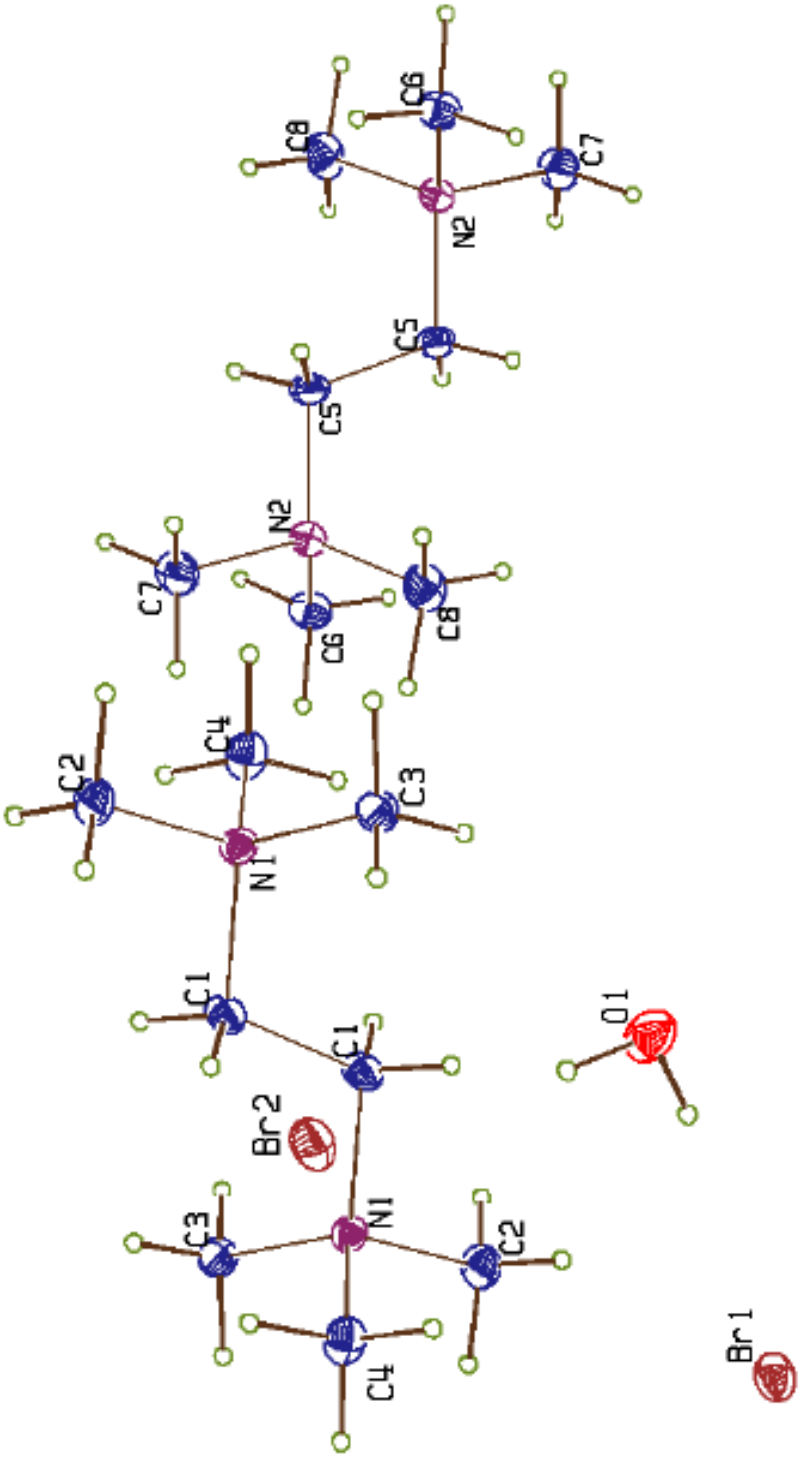

Figure 37. ORTEP view of 1-2-1•2Br crystal.

Table 13. Crystal and structure refinement data for 1-3-1•2Br

Formula	$C_9H_{24}Br_2N_2O_{0.75}$
Color	Colorless
Formula weight	333.63
Temperature, ^oK	100(2)
Wavelengh, Å	0.71073
Crystal system	Monoclinic
Space group	$P2_1/c$
Unit cell dimensions, Å	a = 11.8739(11)
	b = 28.503(3)
	c = 12.8151(11)
	β = 93.465(2)
Volume, $Å^3$	4329.3(7)
Z	12
Calculated density, Mg m^{-3}	1.530
Absorption coefficient mm^{-1}	5.619
θ range for data collection	1.74-30.64
Limiting indices (h, k, l)	-16/17, -40/40, -18/18
Reflections collected/unique	49616/13269
Data/restraints/parameters	13269/12/427
Goodness-of-fit on F^2	1.001
Final R/wR_2 [$I > 2\sigma(I)$]	0.0354/0.0703
Final R/wR_2 (all data)	0.0485/0.0739
Largest diff. Peak and hole, e $Å^{-3}$	0.979/-0.541

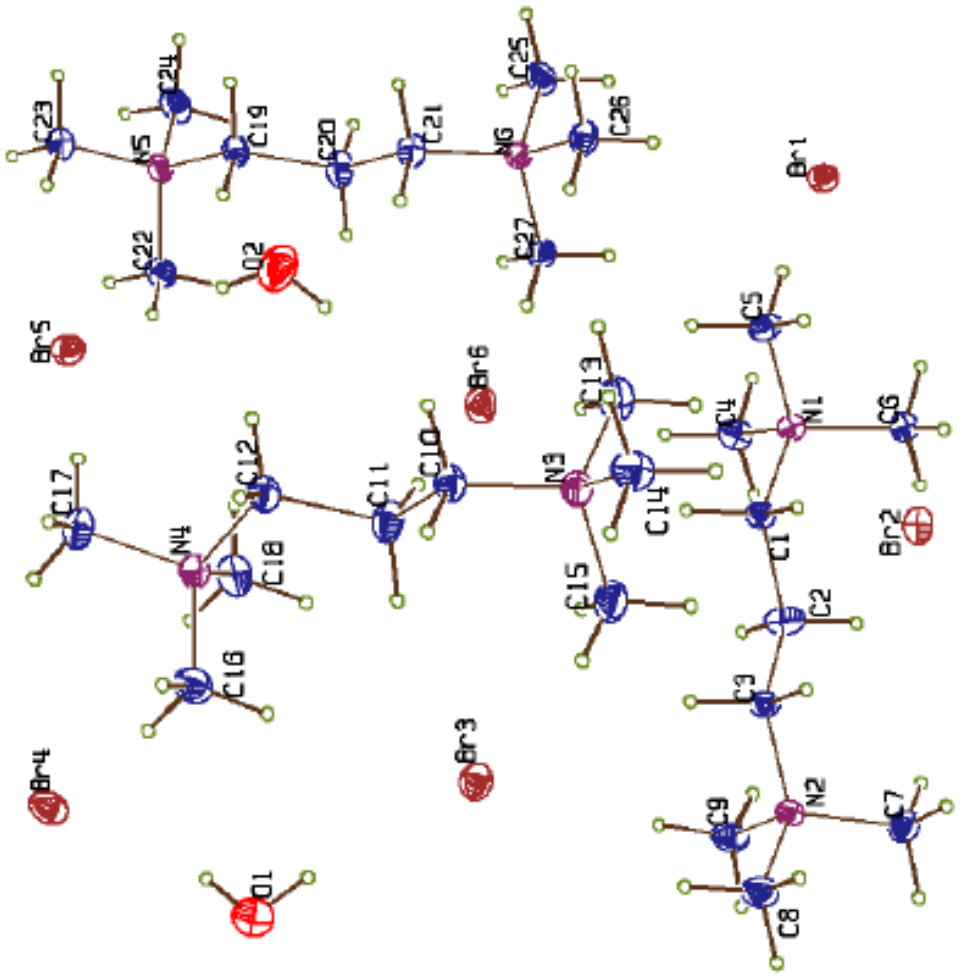

Figure 38. ORTEP view of 1-3-1•2Br crystal

Table 14. Crystal and structure refinement data for 1-4-1•2Br

Formula	$C_{12}H_{30.54}Br_2N_2O_{2.27}$
Color	Colorless
Formula weight	374.95
Temperature, ^oK	100(2)
Wavelengh, Å	0.71073
Crystal system	Monoclinic
Space group	C2/m
Unit cell dimensions, Å	a = 21.128(3)
	b = 7.0476(10)
	c = 5.6476(9)
	β = 101.094(4)
Volume, $Å^3$	825.2(2)
Z	2
Calculated density, Mg m^{-3}	1.524
Absorption coefficient mm^{-1}	4.903
θ range for data collection	1.96-31.56
Limiting indices (h, k, l)	-30/30, -10/10, -6/8
Reflections collected/unique	4102/1458
Data/restraints/parameters	1458/129/96
Goodness-of-fit on F^2	1.005
Final R/wR_2 [$I > 2\sigma(I)$]	0.0210/0.0532
Final R/wR_2 (all data)	0.0222/0.0538
Largest diff. Peak and hole, e $Å^{-3}$	0.689/-0.246

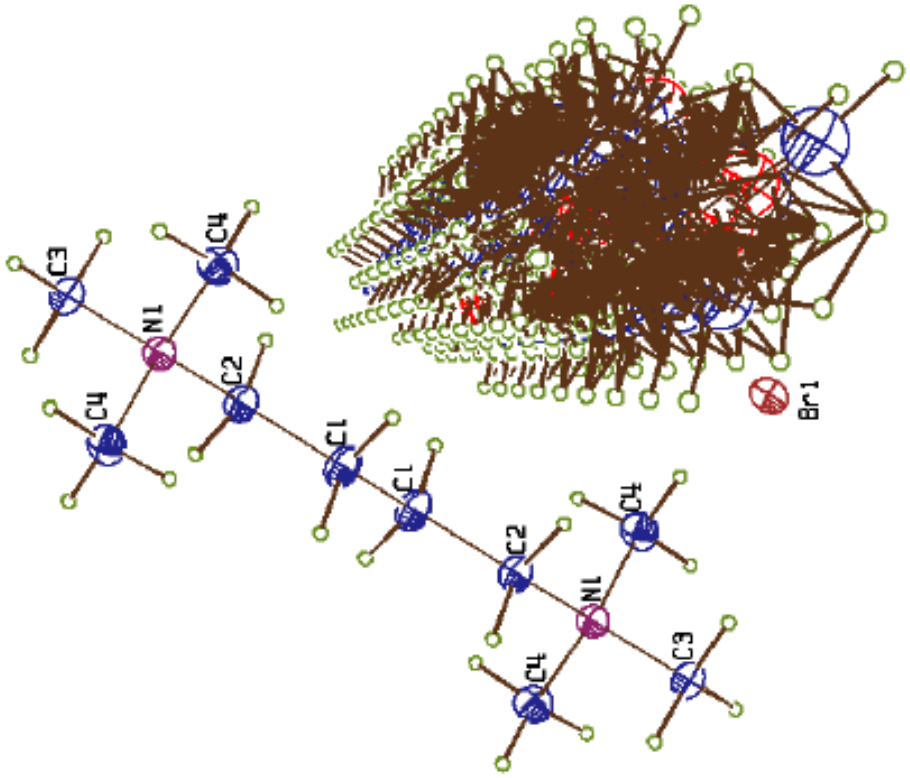

Figure 39. ORTEP view of 1-4-1•2Br crystal

All three crystals are colorless, and the crystal systems are monoclinic. The crystal formulas show that all three crystals contain water of hydration. The crystals were prepared repeatedly, and they always contain water. These results suggest that the anhydrous crystals of the bolaform salts can not be obtained by this process.

A space group is a symmetry group that describes the symmetry of a crystal.[92,93] There are 230 unique types of space groups in three dimensions, and the monoclinic system includes 13 of the space group types.[92] 1-2-1•2Br and 1-3-1•2Br have the same space group, $P2_1/c$, while 1-4-1•2Br has space group as C2/m.

Figures 37 and 38 show the structures of 1-2-1•2Br and 1-3-1•2Br. In Figure 39, the cylinder-like structure adjacent to 1-4-1•2Br exhibits substantial disorder. Numerous attempts were made to determine the composition of the disordered section of the unit by NMR and IR, but no conclusion is made. The asymmetric unit of the structure provides an interpretation for the composition. An asymmetric unit is the smallest unit of the crystal. While growing the asymmetric unit by the symmetry of the space group, the unit cell can be produced. Figure 40 shows the asymmetric unit of the crystal view in Ortep 3.2V.

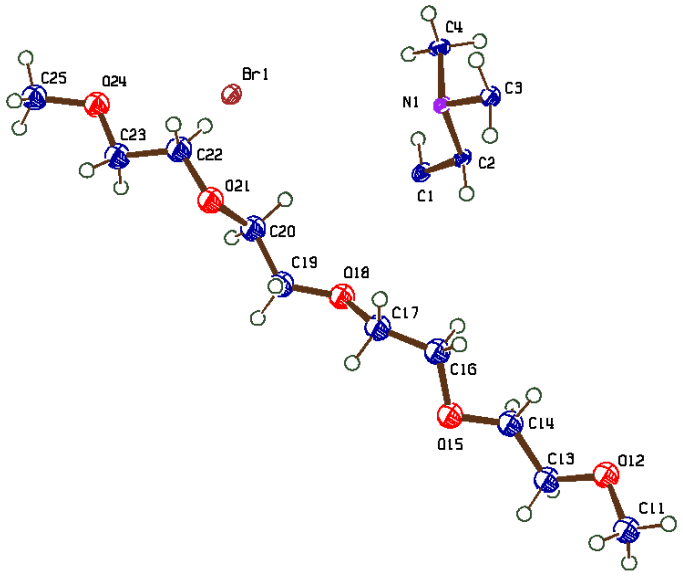

Figure 40. The asymmetric unit of 1-4-1•2Br crystal

The asymmetric unit of 1-4-1•2Br crystal contains structures of half of 1-4-1 dication and glycol ether. The unit cell is generated by the symmetry of the space group C2/m, which contains only the 1-4-1 and the cylinder-like structures. The cylinder-like structure is only composed of disordered glycol ether.

Restraint is commonly used for the refinement of crystal structures.[94,95] The use of restraint reduces the variable parameters, such as bond length and bond angle.[94,96] To model the disordered cylinder in the 1-4-1•2Br structure, a large number of restraints (129) were required. However, no restraints were required for the 1-2-1•2Br dication and its counterions, which were well ordered. Because of the disorder in 1-4-1•2Br, only the 1-2-1•2Br and 1-3-1•2Br crystals will be analyzed and compared.

The 1-2-1•2Br and 1-3-1•2Br crystals both contain water. Formulas show that each 1-2-1•2Br contains 1 H_2O, and each 1-3-1•2Br contains 0.75 H_2O. There are three

water sites in the 1-3-1•2Br lattice, two fully occupied and one about a quarter occupied, which makes 0.75 H_2O on average.

Both the Br^- counterions and the water molecules are distributed around the dications, and interact with them. The commonly accepted Van Der Waal radii are 1.85 Å for Br^- and 1.20 Å for H,[97,98] so any Br^-•••H distance shorter than 3.05 Å is considered a short contact. Tables 15 and 16 list short Br^-•••H contacts and C-H•••Br^- interaction angles respectively for 1-2-1•2Br and 1-3-1•2Br. There are three Br^- in the crystal view of 1-3-1•2Br, and there are only two Br^- in that of 1-2-1•2Br, so many more short Br^-•••H contacts are listed for 1-3-1•2Br than for 1-2-1•2Br.

Hydrogen	Br^-	Distance (Å)	Angle (^{o})
H(3B)	Br(2)	2.90	166
H(4A)	Br(1)	2.98	152

Table 15. Short contact distances and angles in 1-2-1•2Br crystal.

Hydrogen	Br^-	Distance (Å)	Angle (^{o})
H(1A)	Br(2)	2.70	169
H(23A)	Br(5)	2.83	159
H(11B)	Br(6)	2.84	171
H(13B)	Br(6)	2.89	172
H(27A)	Br(6)	2.89	158
H(3B)	Br(3)	2.92	158
H(5B)	Br(6)	2.92	155
H(8A)	Br(3)	2.92	156
H(15A)	Br(2)	2.93	157
H(26A)	Br(1)	2.94	160
H(15B)	Br(3)	2.98	136
H(16A)	Br(4)	2.99	159
H(4A)	Br(1)	3.00	158
H(22A)	Br(5)	3.03	149
H(18A)	Br(4)	3.04	156
H(5A)	Br(1)	3.04	156

Table 16. Short contact distances and angles in 1-3-1•2Br crystal.

Tables 15 and 16 list the short contacts of Br^-•••H less then 3.05 Å, and both tables show that only two of the C-H•••Br angles are less than 150^o, i.e. most are approaching linearity. According to Gaussian calculations, those short contacts are weak hydrogen bonds. For 1-2-1•2Br in Table 15, there are C-H•••Br bonds with H•••Br

distances of 2.90 Å and 2.98 Å with H(3B) and H(4A), and angles of 166 ^{o} and 152 ^{o} respectively. Both H(3B) and H(4A) are part of methyl groups attached to the nitrogen. For 1-3-1•2Br in Table 16, the shortest C-H•••Br bond is 2.70 Å between Br^{-} and H(1A), which is part of the bridging propylene group, and the angle is 169 ^{o}, almost linear, which indicates the presence of weak hydrogen bond. The methyl hydrogens also have short contacts with Br^{-}, e.g. H(8A) and Br(3) at 2.92 Å and 156 ^{o}. Comparison of the contact data of 1-2-1•2Br and 1-3-1•2Br crystals, the primary difference is that the bridging propylene group of 1-3-1•2Br has a short contact with Br^{-}, but the bridging methylene group of 1-2-1•2Br does not.

3.3 Discussion

The crystal structures of 1-2-1•2Br and 1-3-1•2Br are similar, though the number of 1-3-1•2Br molecules in the crystal is more than that of 1-2-1•2Br molecules due to the slight differences among the molecules in a molecular view. The 1-3-1•2Br structure contains three 1-3-1 dications, each of which is almost in the 'all trans' confirmation, to different extents. The crystal structures demonstrate that there are a number of C-H•••Br bonds with H•••Br distances shorter than the Van der Waal radii sum of 3.05 Å, and C-H•••Br angles close to 180^{o} for 1-2-1•2Br and 1-3-1•2Br bolaform salts. The short interaction distances and the nearly linear angles are consistent with weak hydrogen bonds, which have been reported a number of times for other quaternary ammonium salts.[79,84,99-101]

The strengths of hydrogen bonds depend mainly on the electronegativity of the acceptor and the electropositivity of the donor.[79,82] Brammer's review shows that C-H

bond is generally the weakest donor goup.[79] The acceptor group has strength order of I^-< Br^- < Cl^- < F^- for halide ions.[79] The bolaform salt crystals prepared in this chapter have the same donor group and acceptor group. Therefore, the hydrogen bond strengths for both 1-2-1•2Br and 1-3-1•2Br are similar. There are also differences between the hydrogen bonds of these two salts. First, the number of weak hydrogen bonds is higher for 1-3-1•2Br than for 1-2-1•2Br. Second, there is short contact between the propylene group and the Br^- for 1-3-1•2Br, but there is no short contact between the methylene group and the Br^- for 1-2-1•2Br.

Regler obtained the crystal structure of *N*,*N*,*N*',*N*'-tetramethylimidazolidinium dibromide methanolate from methanol/acetone, and the short H•••Br distance and nearly 180^o C-H•••Br angles support the formation of weak hydrogen bonds.[4] In that crystal structure, each imidazolidinium C-H has at least one short contact with Br ions or methanol, except one hydrogen. In the imidazolidinium dibromide methanolate and bolaform crystals, the number of weak hydrogen bonds in dibromide methanolate is more than those in the bolaform salt crystals, and the ring structure has more short contacts with bromine ion than the chain structure.

3.4 Conclusions/ Future Directions

The analysis of crystal structures by single crystal X-ray diffraction provides evidence of weak hydrogen bonds in bolaform salt crystals. Other methods may be used to confirm the evidence. For example, IR spectral measurements indicate that when hydrogen bonds become stronger, C-H stretch bands shift to a lower frequency.[84] ^{1}H

NMR spectra of surfactant solutions in D_2O also used to study hydrogen bonding by shifting the interacting proton downfield.[4]

Reference

(1) Rosen, M. J. *Surfactants and Interfacial Phenomena*; 3rd ed.; John Wiley & Sons: New York, 2004.

(2) Evans, D. F.; Wennerstrom, H. *The Colloidal Domain: Where Physics, Chemistry, Biology and Technology Meet*; VCH Publishers: New York, 1994.

(3) Bunton, C.; Nome, F.; Quina, F. H.; Romsted, L. S. *Acc. Chem. Res.* **1991**, *24*, 357-374.

(4) Regler, B. Ph.D., Rutgers, The State University of New Jersey, 2005.

(5) Chaudburi, A.; Romsted, L. S.; Yao, J. *J. Am. Chem. Soc.* **1993**, *115*, 8362-8367.

(6) Ezrahi, S.; Tuval, E.; Aserin, A. *Advances in Colloid and Interface Science* **2006**, *128 - 130*, 77-102.

(7) Israelachvili, J. *Intermolecular and Surface Forces*; 2nd ed.; Academic Press: London, 1991.

(8) Israelachvili, J. *Langmuir* **1994**, *10*, 3774-3781.

(9) Duval, F. P.; Zana, R.; Warr, G. G. *Langmuir* **2006**, *22*, 1143-1149.

(10) Israelachvili, J. N.; Mitchell, D. J.; Ninham, B. W. *Journal of the Chemical Society, Faraday Transactions 2* **1976**, *72*, 1525-1568.

(11) Porter, M. R. *Handbook of Surfactants*; 2nd edition ed.; Springer, 1994.

(12) Tanford, C. *The Hydrophobic Effect: Formation of Micelles and Biological Membranes*; 2nd ed.; Wiley: New York, 1980.

(13) Tanford, C. *J. Phys. Chem.* **1972** *76*, 3020-3024.

(14) Geng, Y.; Romsted, L. S.; Menger, F. *J. Am. Chem. Soc.* **2006**, *128*, 492-501.

(15) Marcus, Y. *Journal of Physical Chemistry B* **2005**, *109*, 18541-18549.

(16) Tanford, C. *The Journal of Physical Chemistry* **1974**, *78*, 2469-2479.

(17) Romsted, L. S. *Langmuir* **2007**, *23*, 414-424.

(18) Hofmeister, F. *Naunyn-Schmiedebergs Arch. Exp. Pathol. Parmakol. (leipzig)* **1888**, *24*, 247-260.

(19) Ferreira, L. C. M.; Zucco, C.; Zanette, D.; Nome, F. *The Journal of Physical Chemistry* **1992**, *96*, 9058-9061.

(20) Bunton, C. A.; Gan, L.-H.; Moffatt, J. H.; Romsted, L. S. *The Journal of Physical Chemistry* **1981**, *85*, 4118-4125.

(21) Romsted, L. S. Ph.D., Indiana University, 1975.

(22) Romsted, L. S. In *Reactions and Synthesis in Surfactant Systems*; Texter, J., Ed.; Marcel Dekker: New York, 2001, p 265-294.

(23) Romsted, L. S. In *Adsorption and Aggregation of Surfactants in Solution*; Mittal, K. L., Shah, D. O., Eds.; Marcel Dekker: New York, 2002, p 149-170.

(24) Chaudhuri, A.; Loughlin, J. A.; Romsted, L. S.; Yao, J. *J. Am. Chem. Soc.* **1993**, *115*, 8351-8361.

(25) Soldi, V.; Keiper, J.; Romsted, L. S.; Cuccovia, I. M.; Chaimovich, H. *Langmuir* **2000**, *16*, 59-71.

(26) Romsted, L. S. In *Micellization, Solubilization and Microemulsions*; Mittal, K. L., Ed.; Plenum Press: New York, 1977; Vol. 2, p 489-530.

(27) Romsted, L. S. In *Surfactants in Solution*; Mittal, K. L., Lindman, B., Eds.; Plenum Press: New York, 1984; Vol. 2, p 1015-1068.

(28) Bunton, C. A.; Romsted, L. S.; Savelli, G. *Journal of the American Chemical Society* **1979**, *101*, 1253-1259.

(29) Neves, M. F. S.; Zanette, D.; Quina, F.; Moretti, M. T.; Nome, F. *The Journal of Physical Chemistry* **1989**, *93*, 1502.

(30) Zollinger, H. *Diazo Chemistry I: Aromatic and Heteroaromatic Compounds*; VCH Publishers, Inc.: Weinheim, 1994.

(31) Zollinger, H. *Angewandte Chemie: International Edition in English* **1978**, *17*, 141-220.

(32) Geng, Y.; Romsted, L. S.; Froehner, S.; Zanette, D.; Magid, L. J.; Cuccovia, I. M.; Chaimovich, H. *Langmuir* **2005**, *21*, 562-568.

(33) Cuccovia, I. M.; da Silva, I. N.; Chaimovich, H.; Romsted, L. S. *Langmuir* **1997**, *13*, 647-652.

(34) Bacaloglu, R.; Bunton, C. A.; Ortega, F. *J. Phys. Chem* **1989**, *93*, 1497-1502.

(35) Thebaud, B., Carnegie Mellon University, 1998.

(36) Gamboa, C.; Rios, H.; Sepulveda, L. *Journal of Physical Chemistry* **1989**, *93*, 5540-5543.

(37) Truong, M. T.; Walker, L. M. *Langmuir* **2000**, *16*, 7991-7998.

(38) Imae, T.; Ikeda, S. *Colloid and Polymer Science* **1987**, *265*, 1090-1098.

(39) Mata, J.; Varade, D.; Bahadur, P. *Thermochimica Acta* **2005**, *428*, 147 - 155.

(40) Bunton, C. A.; Minch, M. J.; Hidalgo, J.; Sepulveda, L. *Journal of the American Chemical Society* **1973**, *95*, 3262.

(41) Bunton, C. A.; Minch, M. J.; Hidalgo, J.; Sepulveda, L. *J. Am. Chem. Soc* **1973**, *95*, 3262-3272.

(42) Bunton, C. A.; Cowell, C. P.; Nome, F.; Romsted, L. S. *Journal of Physical Organic Chemistry* **1990**, *3*, 239-247.

(43) Berlot, I.; Chevalier, Y.; Labbe, P.; Moutet, J.-C. *Langmuir* **2001**, *17*, 2639 - 2646.

(44) Quina, F. H.; Chaimovich, H. *The Journal of Physical Chemistry* **1979**, *83*, 1844-1850.

(45) Dougherty, S. J.; Berg, J. G. *Colloid interface Sci.* **1974**, *49*, 135 - 138.

(46) Berezin, I. V.; Martinek, K.; Yatsimirskii, A. K. *Russian Chemical Reviews* **1973**, *42*, 787-802.

(47) Bunton, C. A.; Romsted, L. S.; Thamavit, C. *Journal of the American Chemical Society* **1980**, *102*, 3900-3903.

(48) Bunton, C. A.; Romsted, L. S. In *Solution Behavior of Surfactants: Theoretical and Applied Aspects*; Mittal, K. L., Ed.; Plenum Press: New York, 1982; Vol. 2, p 975-991.

(49) Stadler, E.; Zanette, D.; Rezende, M. C.; Nome, F. *Journal of Physical Organic Chemistry* **1984**, *88*, 1892-1896.

(50) Gonsalves, M.; Probst, S.; Rezende, M. C.; Nome, F.; Zucco, C.; Zanette, D. *The Journal of Physical Chemistry* **1985**, *89*, 1127-1130.

(51) Jones, M. N.; Piercy, J. *J. Chem. Soc., Faraday Trans. 1* **1972**, *68*, 1839 - 1848.

(52) Causi, S.; De Lisi, R.; Milioto, S.; Tirone, N. *Journal of Physical Chemistry* **1991**, *95*, 5664-73.

(53) De Lisi, R.; Fisicaro, E.; Milioto, S. *J. Solution Chem.* **1988**, *17*, 1015 - 1041.

(54) Ranganathan, R.; Okano, L. T.; Yihwa, C.; Quina, F. H. *Journal of Colloid and Interface Science* **1999**, *214*, 238-242.

(55) Ranganathan, R.; Tran, L.; Bales, B. L. *The Journal of Physical Chemistry B* **2000**, *104*, 2260-2264.

(56) Stigter, D. *Progress in Colloid and Polymer Science* **1978**, *65*, 45-52.

(57) Gunnarsson, G.; Gustavsson, H. *Journal of the Chemical Society, Faraday Transactions 1* **1982**, *78*, 2901-2910.

(58) Linse, P.; Gunnarsson, G.; Jonsson, B. *The Journal of Physical Chemistry* **1982**, *86*, 413-421.

(59) Geng, Y.; Romsted, L. S. *J. Phys. Chem. B* **2005**, *109*, 23629-23637.

(60) Klevens, H. B. *J. Phys. Chem.* **1948**, *52*, 130-148.

(61) Bakshi, M. S.; Kaur, I.; Sood, R.; Singh, J.; Singh, K.; Sachar, S.; Singh, K. J.; Kaur, G. *J. Colloid Interface Sci.* **2004**, *271*, 227 - 231.

(62) Evans, D. F.; Allen, M.; Ninham, B. W.; Fouda, A. *Journal of Solutions Chemistry* **1984**, *13*, 87-101.

(63) Imae, T.; Ikeda, S. *The Journal of Physical Chemistry* **1986**, *90*, 5216-5223.

(64) Nayak, B. B.; Patel, S.; Behera, P. K.; Mishra, B. K. *ARKIVOC* **2006**, 22 - 27.

(65) Zana, R.; Xia, J. *Gemini Surfactants: Synthesis, Interfacial and Solution-Phase Behavior, And Applications*; Marcel Dekker: New York, 2004; Vol. 117.

(66) Jiang, N.; Li, P.; Wang, Y.; Wang, J.; Yan, H.; Thomas, R. K. *Journal of Physical Chemistry B* **2004**, *108*, 15385-15391.

(67) Hait, S. K.; Moulik, S. P. *CURRENT SCIENCE* **2002**, *82*, 1101 - 1111.

(68) Camesano, T. A.; Nagarajan, R. *Colloids and Surfaces A: Physicochemical and Engineering Aspects* **2000**, *167*, 165-177.

(69) Oda, R.; Panizza, P.; Schmutz, M.; Lequeux, F. *Langmuir* **1997**, *13*, 6407-6412.

(70) Menger, F. M.; Littau, C. A. *J. Am. Chem. Soc.* **1991**, *113*, 1451 - 1452.

(71) Rosen, M. J. *Chemtech* **1993**, 30-33.

(72) Regler, B.; Emge, J. T.; Elliot, J. J.; Sauers, R. R.; Potenza, J.; Romsted, L. S. *Journal of Physical Chemistry B* **2007**, *111*, 13668-13674.

(73) Menger, F. M.; Keiper, J. S.; Mbadugha, B. N. A.; Caran, K. L.; Romsted, L. S. *Langmuir* **2000**, *16*, 9095-9098.

(74) Zana, R.; Benrraou, M.; Rueff, R. *Langmuir* **1991**, *7*, 1072-1075.

(75) Alami, E.; Beinert, G.; Marie, P.; Zana, R. *Langmuir* **1993**, *9*, 1465-1467.

(76) Bernheim-Groswasser, A.; Zana, R.; Talmon, Y. *J. Phys. Chem. B* **2000**, *104*, 4005-4009.

(77) Zilman, A.; Tlusty, T.; Safran, S. A. *Journal of Physics: Condensed Matter* **2003**, *15*, S57-S64.

(78) Abdallah, D. J.; Bachman, R. E.; Perlstein, J.; Weiss, R. G. *J. Phys. Chem. B* **1999**, *103*, 9269-9278.

(79) Brammer, L.; Bruton, E. A.; Sherwood, P. *Crystal Growth and Design* **2001**, *1*, 277-290.

(80) Kolle, P.; Dronskowski, R. *Inorg. Chem.* **2004**, *43*, 2803-2809.

(81) Lutz, H. D. *Journal of Molecular Structure* **2003**, *646*, 227-236.

(82) Szafran, M.; Dega-Szafran, Z.; Jaskolski, M.; Addlagatta, A.; Dulewicz, E. *Journal of Molecular Structure* **2005**, *741*, 171-181.

(83) Meot-Ner, M. *Chem. Rev.* **2005**, *105*, 213-284.

(84) Harmon, K. M.; Gennick, I.; Madeira, S. L. *J. Phys. Chem.* **1974**, *78*, 2585-2591.

(85) Milburn, G. H. *X-ray Crystallography. An Introduction to the Theory and Practice of Single-Crystal Analysis*; Butterworth: London, 1973.

(86) Ladd, M. F. C. *Structure Determination by X-Ray Crystallography; 4th ed.*; Plenum Press: New York, 2003.

(87) Gennick, I.; Harmon, K. M.; Potvin, M. M. *Inorg. Chem.* **1977**, *16*, 2033-2040.

(88) Khan, M. A.; Peppe, C.; Tuck, D. G. *Canadian Journal of Chemistry* **1984**, *62*, 1662-1665.

(89) Steiner, T.; Desiraju, G. R. *Chemistry Communications* **1998**, 891-892.

(90) McPherson, A. J. *J. Bio. Chem.* **1976**, *251*, 6300 - 6303.

(91) McPherson, A. J. *Eur. J. Biochem* **1990**, *189*, 1 - 23.

(92) Hahn, T. *International Tables for Crystallography, Volume A: Space Group Symmetry*; 5th ed.; Springer-Verlag, 2002.

(93) Fedorov, E. S. *Symmetry of Crystals, ACA Monograph*; American Crystallographic Association, 1971.

(94) Immirzi, A. *J. Appl. Cryst.* **2009**, *42*, 362-364.

(95) Sheldrick *Acta Cryst. A* **2008**, *64*, 112-122.

(96) Bennett, D. W. *Understanding Single-Crystal X-Ray Crystallography*; Wiley-VCH, 2010.

(97) Zhao, Y. H.; Abraham, M. H.; Zissimos, A. M. *J. Org. Chem* **2003**, *68*, 7368-7373.

(98) Rowland, R. S.; Taylor, R. *J. Phys. Chem.* **1996**, *100*, 7384-7391.

(99) Strauss, I.; Symons, M. C. R. *Chemical Physics Letters* **1977**, *45*, 423-424.

(100) Desiraju, G. R.; Steiner, T. *The Weak Hydrogen Bond in Structural Chemistry and Biology*; Oxford University Press: London, 1999.

(101) Wilson, C. C. *Single Crystal Neutron Diffraction from Molecular Materials*; World Scientific, 2000, 2000.

Experimental

1. Synthesis method

1.1 4-n-Hexadecyl-2,6-dimethylbenzenediazonium Tetrafluoroborate (16-ArN_2BF_4) synthesis

16-ArN_2BF_4 is synthesized using an anhydrous method. About 10 mL of THF was injected into a three-neck 100-mL round-bottom flask fitted with septum caps and a magnetic stirrer. The system was cooled to -15^oC in an ice/MeOH bath for 10 min. 1.13 mL (9.2 mmol) of $BF_3 \cdot Et_2O$ was added by syringe, and the mixture was stirred for 5 min. then 2 g (5.8 mmol) of 16-$ArNH_2$ dissolved in 10 mL of THF was added via syringe, giving a clear solution, and 0.87 mL (7.4 mmol) of tert-butyl nitrite in 10 mL of THF was added via syringe over a 2-min period. After 15 min of stirring, the temperature was increased to 0^oC and the solution was stirred for 6 h. a white precipitate began forming after about 20 min. the reaction mixture was transferred to a 500-mL beaker and 80 mL of cold pentane was added. The white solid was collected on a Buchner funnel, recrystallized three times by dissolving it in CH_3CN and forced it from solution with cold anhydrous Et_2O, and then dried under vacuum for 24h. Yield: 1.3 g (50%) of white crystals which were stored in the freezer in the dark. This arenediazonium salt decomposes slowly in the solid state, probably because of periodic exposure to light or moisture, and it must be recrystallized periodically. ^1H NMR ($CDCl_3$) δ (ppm) 0.87 (3 H, t, RCH_3), 1.24 (26 H, Br s, -$(CH_2)_{13}$-), 1.73 (2 H, br, -CH_2-), 2.72 (8 H, s with shoulder, *o*-$ArCH_3$ and *p*-$ArCH_2$-), 7.23 (2 H, s, Ar H).

1.2 Synthesis of 2,4,6-Trimethylbenzenediazonium Tetrafluoroborate (1-ArN_2BF_4)

About 30 mL of THF was injected into a three-neck 250-mL round-bottom flask fitted with septum caps and a magnetic stirrer. The system was cooled to -15^oC in an ice/MeOH bath for 10 min. 10 mL (82.8 mmol) of $BF_3 \cdot Et_2O$ was added by syringe, and the mixture was stirred for 5 min. then 7.4 mL (53 mmol) of 1-$ArNH_2$ dissolved in 30 mL of THF was added via syringe, giving a clear solution, and 7.8 mL (66 mmol) of tert-butyl nitrite in 30 mL of THF was added via syringe over a 2-min period. After 15 min of stirring, the temperature was increased to 0^oC and the solution was stirred for 6 h. A white precipitate began forming after about 20 min. the reaction mixture was transferred to a 500-mL beaker and 100 mL of cold pentane was added. The white solid was collected on a Buchner funnel, recrystallized three times by dissolving it in CH_3CN and forced it from solution with cold anhydrous Et_2O, and then dried under vacuum for 24h. Yield: 3.3 g (27%) of white crystals which were stored in the freezer in the dark. This arenediazonium salt decomposes slowly in the solid state, probably because of periodic exposure to light or moisture, and it must be recrystallized periodically. ^1H NMR ($CDCl_3$) δ (ppm) 2.54 (3 H, s, p-$ArCH_3$), 2.75 (6 H, s, *o*-$ArCH_3$), 7.54 (2 H, s, Ar H).

1.3 Synthesis of 4-n-Hexadecyl-2,6-dimethylphenol (16-ArOH) and 4-n-hexadecyl-2,6-dimethylchlorobenzene (16-ArCl).

Both compounds were synthesized at the same time because they are formed simultaneously in the dediazoniation reaction. DTAC (5.2 g) was stirred with 200 mL of 1 M HCl in a 500 mL three-neck round bottom flask in 60^oC for 1 hour to dissolve the

solid DTAC. 16-ArN_2BF_4 (1 g) was added, stirred for more than 6h, and cooled to room temperature. $NaClO_4 \cdot H_2O$ (3.8 *g*) dissolved in 100 *g* water was added, giving a white solid precipitate of (CTA)ClO_4 containing the dediazoniation products. The precipitates were collected in a buchner funnel, washed with copious amounts of water several times, air (2 h) and vacuum-dried (overnight). The dried solid was ground to a fine powder and extracted with 250 mL of ether with vigorous stirring three times. The extracts were collected, combined, and rotoevaporated, giving a white solid. The solid was chromatographed in a 40 mm x 135 mm column packed with 200 mL silica gel. The column was eluted first with 200 mL pure hexane then with 200 mL 20%EtOAc/80%hexane (v/v) to separate 16-ArCl and 16-ArOH. 16-ArCl was isolated as a white solid, with retention time of 22 min by HPLC. 16-ArOH was isolated as a light yellow solid. After recrystallization twice from MeOH, a white solid was isolated, with HPLC retention time at 11 min. Percentage yield for 16-ArOH is 5%, for 16-ArCl 30%. ^{1}H NMR ($CDCl_3$) δ (ppm) 16-ArOH: 0.85 (3 H, t, RCH_3), 1.25 (26H, br s, -$(CH_2)_{13}$-), 1.55 (2 H, m, -CH_2-), 2.22 (6 H, s, o-$ArCH_3$), 2.45 (2 H, t, p-$ArCH_2$-), 4.40 (1H, s, br, ArOH), 6.78 (2H, s, ArH); 16-ArCl: 0.87 (3 H, t, RCH_3), 1.25 (26H, br s, -$(CH_2)_{13}$-), 1.55(2 H, m, -CH_2-), 2.37(6 H, s, o-$ArCH_3$), 2.47(2 H, t, p-$ArCH_2$-), 6.88(2 H, s, Ar-H).

16-ArBr was synthesized by the same procedure, using DTAB instead of DTAC. Pure 16-ArOH was also obtained. Percentage yield of 16-ArBr is 12%. ^{1}H NMR ($CDCl_3$) δ (ppm) 16-ArBr: 0.87 (3 H, t, RCH_3), 1.25 (26H, br s, -$(CH_2)_{13}$-), 1.55(2 H, m, -CH_2-), 2.37(6 H, s, o-$ArCH_3$), 2.47(2 H, t, p-$ArCH_2$-), 6.88(2 H, s, Ar-H).

1.4 Synthesis of 4-n-hexadecyl-2,6-dimethyltoluenesulfonate (16-ArToS)

16-ArOH synthesized using the method above, is the starting material for making 16-ArToS. Mix 0.250 g (0.72 mM) of 16-ArOH and 0.132 g (0.69 mM) of toluene-p-sulphonyl chloride in 500 uL of pure pyridine in a two-necked flask under nitrogen. Then, heat it to 90^{o}C for 2 days. After that, 2.0 mL of water was added and stirred until the oil solidified. The precipitate was filtered and washed with cold 0.1 M of HCl to remove the pyridine. Finally the product was washed with water again and get product. The product was identified as mixture of mostly 16-ArToS and small percentage of 16-ArOH by chromatography column. The calibration curve of 16-ArOH is known, so the effect of 16-ArOH in measuring calibration curve of 16-ArToS can be eliminated by calculation.

1.5 Synthesis of Cetyltrimethylammonium *p*-toluenesulfonate (CTAToS)

N,N-dimethylhexadecylamine(20 mL, 0.059 mol) and methyl *p*-toluenesulfonate (10 mL, 0.066 mol) were added to 25 mL 1-propanol in a 250 mL round bottom flask. Heat the flask to reflux. Solid was formed immediately. Filter the product, and recrystallize by dissolving in hot 1-propanol then forcing it out with cold ether. The white solid was put in vacuum for 24 hours. (yield: 85%).

1.6 Synthesis of *N,N*-bis(trimethyl)-α,ω-ethylenediammonium dibromide (1-2-1·2Br)

Tetramethylethylenediamine (34.2 mL, 0.23 mol) was added to 120 mL methanol in a 500 mL round bottom flask, cooled to -10^{o}C in ice/methanol bath, and stirred. 66.4 mL (2.3 mol) bromomethane in chilled canister was pour into a prechilled graduated

cylinder. Bromomethane was in ten moles excess to ensure complete tetradisubstitution of the diamine. Bromomethane was added rapidly to the round bottom flask and fitted with a cold water reflux condenser. The solution was brought to room temperature slowly over 4 hours and after 2 more hours at room temperature, was heated to a mild reflux and a white precipitate appeared. The solution was refluxed for another 24h, cooled to room temperature, and the precipitate was washed with copious amount of diethyl ether. The white solid was recrystallized three times from hot methanol, and dried under vacuum overnight. 15 g of product was obtained (yield: 21%). ^{1}H NMR (D_2O): δ (ppm) 3.20 (s, 18H), 3.95 (s, 4H).

1.7 Synthesis of *N*,*N*-bis(trimethyl)-α,ω-propenediammonium dibromide (1-3-1·2Br)

Tetramethyl-1,3-propanediamine (27.1 mL, 0.16 mol) was added to 120 mL methanol in a 500 mL round bottom flask, cooled to -10^{o}C in ice/methanol bath, and stirred. 46.2 mL (1.6 mol) bromomethane in chilled canister was pour into a prechilled graduated cylinder. Bromomethane was in ten moles excess to ensure complete tetradisubstitution of the diamine. Bromomethane was added rapidly to the round bottom flask and fitted with a cold water reflux condenser. The solution was brought to room temperature slowly over 4 hours and after 2 more hours at room temperature, was heated to a mild reflux. A white precipitate soon appeared. The solution was refluxed for another 24h, cooled to room temperature, and the precipitate was washed with copious amount of diethyl ether. The white solid was recrystallized three times from hot methanol, and dried

under vacuum overnight. 15 g of product was obtained (yield: 29%). ^{1}H NMR (D_2O): δ (ppm) 3.10 (s, 18H), 3.35 (t, 4H), 2.25 (m, 2H).

1.8 *N,N*-bis(trimethyl)-α,ω-butenediammonium dibromide (1-4-1·2Br)

Tetramethyl-1,4-butanediamine (22.8 mL, 0.125 mol) was added to 120 mL methanol in a 500 mL round bottom flask, cooled to -10^{o}C in ice/methanol bath, and stirred. 36.1 mL (1.25 mol) bromomethane in chilled canister was pour into a prechilled graduated cylinder. Bromomethane was in ten moles excess to ensure complete tetradisubstitution of the diamine. Bromomethane was added rapidly to the round bottom flask and fitted with a cold water reflux condenser. The solution was brought to room temperature slowly over 4 hours and after 2 more hours at room temperature, was heated to a mild reflux. A white precipitate soon appeared. The solution was refluxed for another 24h, cooled to room temperature, and the precipitate was washed with copious amount of diethyl ether. The white solid was recrystallized three times from hot methanol, and dried under vacuum overnight. 15 g of product was obtained (yield: 36%). ^{1}H NMR (D_2O): δ (ppm)

1.9. Preparation of DTAB

DTAB obtained from Sigma Aldrich was recrystallized three times by dissolving in hot methanol, and forced from solution with ether. The white solid was dried in vacuum, then made into aqueous solution to measure surface tension. Figure E1 shows the surface tension of DTAB solutions as a function of logarithm of concentrations before and after recrystallization. The minimum of surface tension disappears after

recrystallization, which means the impurity has been removed by recrystallization, and the DTAB surfactant is pure enough to use.

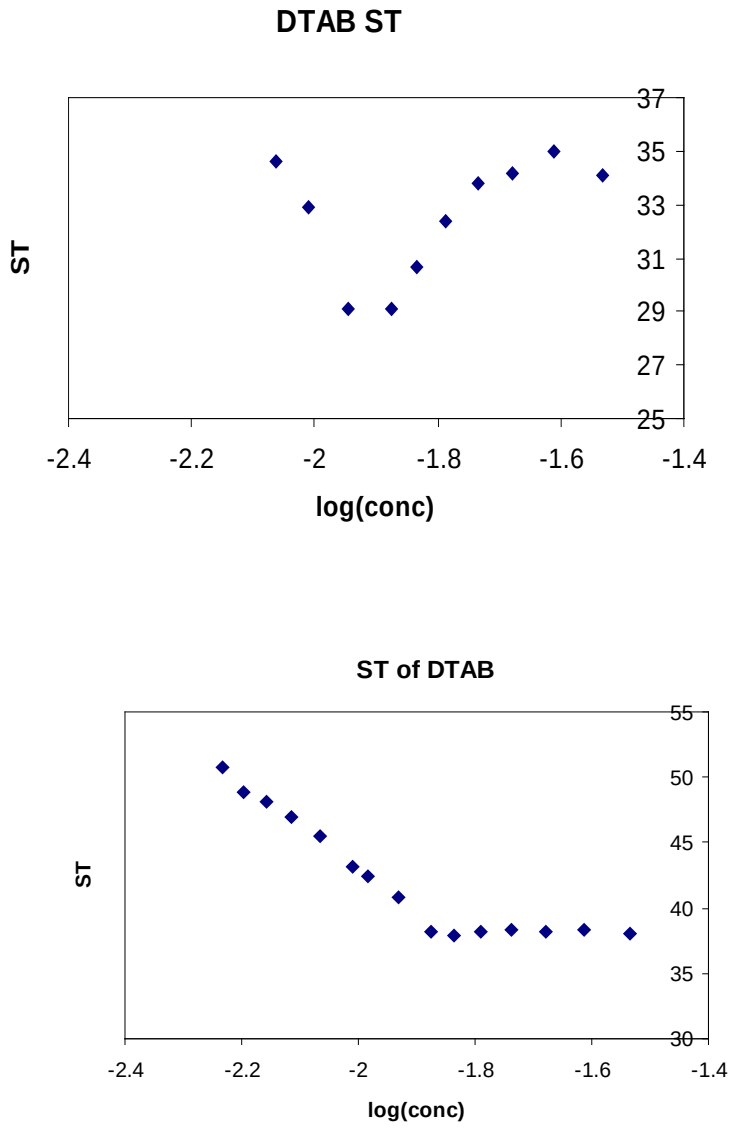

Figure E1. Surface tension measurement of DTAB solutions versus logarithm of DTAB concentrations before (top) and after (bottom) recrystallization.

2. Dediazoniation reaction

2.1 Dediazoniation of 16-ArN_2BF_4

The CTAX and HX with needed concentrations were added to a 2 mL test tube, and the solution was equilibrated in 25^oC water bath. 0.01 g 16-ArN_2BF_4 solid was dissolved in 1 mL methanol to make stock solution of 0.025 M. 20 μL stock solution was injected into the 2 mL test tube immediately with syringe, to initiate the dediazoniation reaction. The solution was mixed well, capped and sealed with parafilm, and left in 25^oC water bath. The half life of the reaction is about 90 mins at 25^oC. After 24 h, the test tube was removed from the water bath, analyzed by HPLC. Conditions for product separation on the Perkin Elmer HPLC were as follows: a Varian Microsorb-MV C18 reverse-phase colume (4.6 mm x 25 cm; 5 μm particle size); mobile phase 55% methanol / 45% isopropanol; flow rate 0.4 mL/min; λ = 220 nm; inject volume = 100 μL; run time 60 min.

2.2 Dediazoniation of 1-ArN_2BF_4

The TMAX and HX with needed concentrations were added to a 2 mL test tube, and the solution was equilibrated in 25^oC water bath. 0.01 g 1-ArN_2BF_4 solid was dissolved in 1 mL methanol to make stock solution of 0.05 M. 20 μL stock solution was injected into the 2 mL test tube immediately with syringe, to initiate the dediazoniation reaction. 20 μL cyclohexane was layered via syringe on top of the reaction mixture, to prevent the loss of products by vaporizing. The stopper was sealed with parafilm, and the solution was put in 25^oC water bath. After 24 h, the solution was removed to a 5 mL flask, and methanol was filled to the label to make a homogenous solution. The product was analyzed by HPLC. Conditions for product separation were as follows: a Varian

Microsorb-MV C18 reverse-phase colume (4.6 mm x 25 cm; 5 μm particle size); mobile phase 80% methanol / 20% water; flow rate 0.8 mL/min; λ = 230 nm; inject volume = 100 μL; run time 40 min.

3. Recrystallization from aqueous tetra (ethylene glycol) dimethyl ether

3.1. Recrystallization of *N*,*N*-bis(trimethyl)-α,ω-ethenediammonium dibromide (1-2-1·2Br)

1-2-1·2Br solid is placed in a vial, dissolved with hot water. The solution is translucent. Tetra (ethylene glycol) dimethyl ether in equivalent volume of the solution is added. Mix well and let stand. Clear crystals appear at the bottom of the vial after overnight.

3.2. Recrystallization of *N*,*N*-bis(trimethyl)-α,ω-propenediammonium dibromide (1-3-1·2Br)

1-3-1·2Br solid is placed in a vial, dissolved with hot water. The solution is translucent. Tetra (ethylene glycol) dimethyl ether in equivalent volume of the solution is added. Mix well and let stand. Clear crystals appear at the bottom of the vial after overnight.

3.3. Recrystallization of *N*,*N*-bis(trimethyl)-α,ω-butenediammonium dibromide (1-4-1·2Br)

1-4-1·2Br solid is placed in a vial, dissolved with hot water. The solution is translucent. Tetra (ethylene glycol) dimethyl ether in equivalent volume of the solution is added. Mix well and let stand. Clear crystals appear at the bottom of the vial after overnight.

APPENDIX

1. Calibration curves

1.1 Calibration curve of 1-ArOH

[1-ArOH] /M	peak area
0.00001	237063.85
0.00002	433972.16
0.00004	903658.13
0.00006	1373803.52
0.00008	1885081.67
0.0001	2377659.10
0.001	19167038.07

Table A1. data for calibration curve of 1-ArOH (from Aldrich).

Each sample injected in triplicate. HPLC method: 80% methanol / 20% H_2O. Flow rate = 0.8 mL/min over 30 min, λ = 230 nm, injection volume = 10 µL.

Typical retention times: 1-ArOH ~ 6 min.

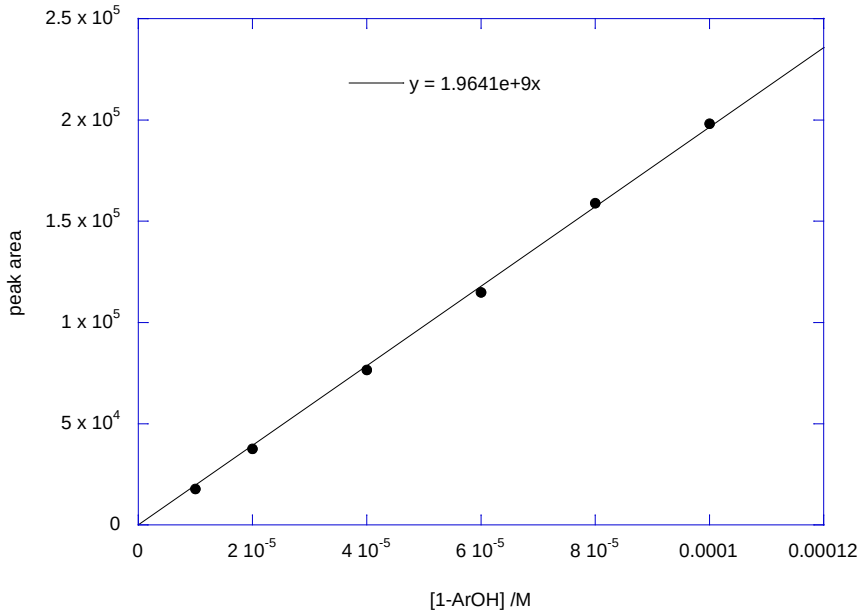

Figure A1. calibration curve of 1-ArOH.

(peak area) = 1.96 x 10^9 [1-ArOH]

1.2 Calibration Curve of 1-ArBr

[1-ArBr] /M	peak area
0.00001	32793.745
0.00002	56262.95
0.00004	113439.41
0.00006	172589.19
0.00008	228776.68
0.0001	280906.56

Table A2. data for calibration curve of 1-ArBr.

Each sample injected in triplicate. HPLC method: 80% methanol / 20% H_2O. Flow rate = 0.8 mL/min over 30 min, λ = 230 nm, injection volume = 10 µL.

Typical retention times: 1-ArBr ~ 21 min.

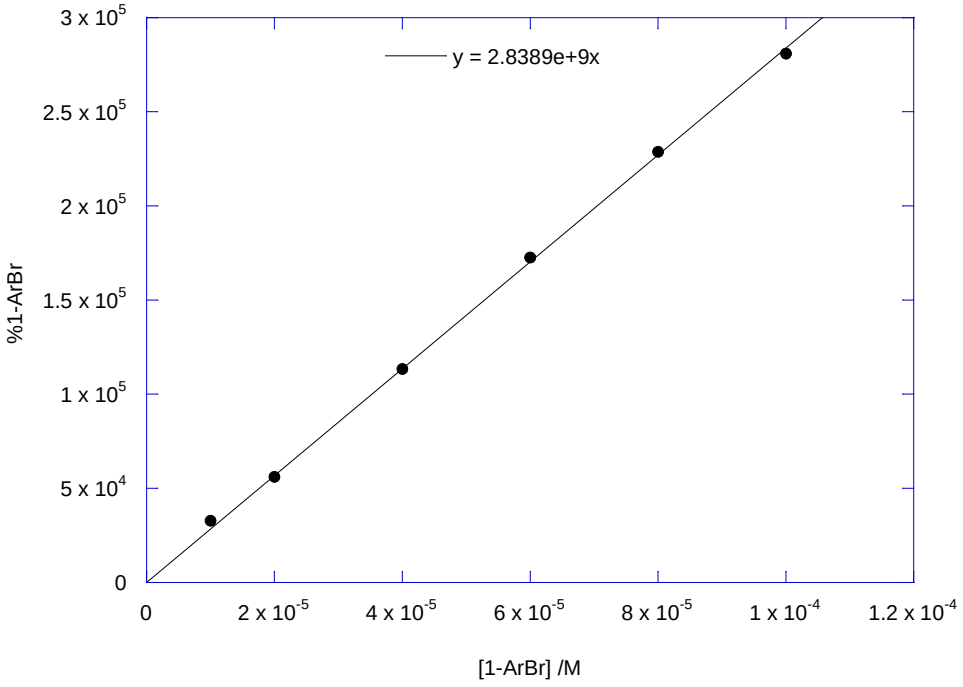

Figure A2. calibration curve of 1-ArBr.

(peak area) = 2.84 x 10^9 [1-ArBr]

1.3 Calibration curve of 1-ArH

[1-ArH]/M	peak area
0.00001	4903.54
0.00002	12904.75
0.00004	27116.89
0.00006	40846.29
0.00008	56943.24
0.0001	71309.23

Table A3. data for calibration curve of 1-ArH.

Each sample injected in triplicate. HPLC method: 80% methanol / 20% H_2O. Flow rate = 0.8 mL/min over 30 min, λ = 230 nm, injection volume = 10 µL.

Typical retention times: 1-ArH ~ 13 min.

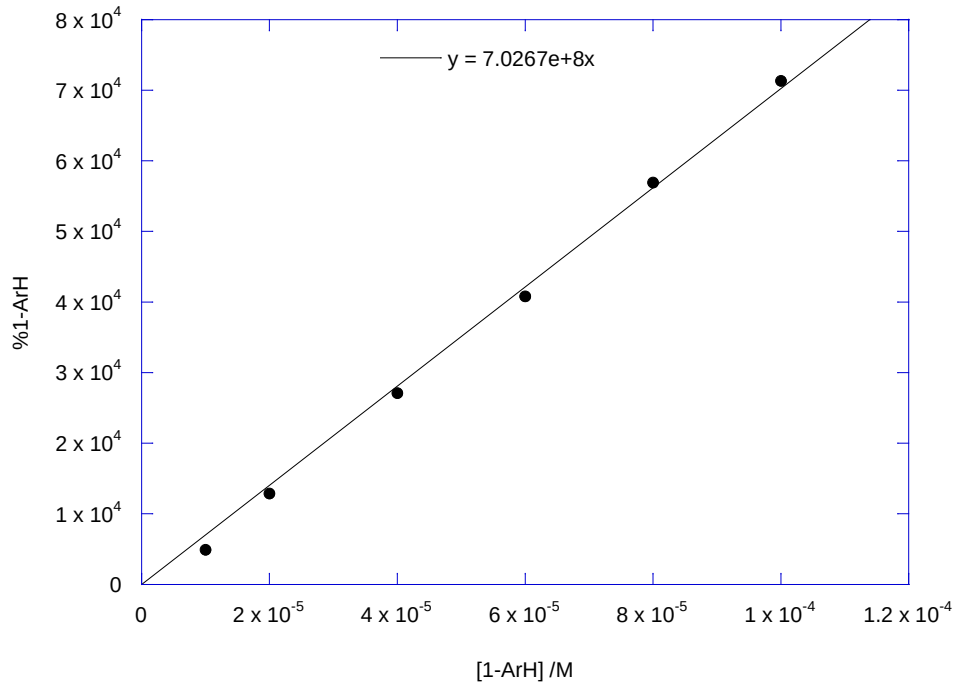

Figure A3 . calibration curve of 1-ArH.

(peak area) = 7.027 x 10^8 [1-ArH]

1.4 Calibration curve of 1-ArToS

[1-ArToS]/M	peak area
0.00001	176158.29
0.00002	372870.79
0.00004	746473.40
0.00006	1075433.01
0.00008	1467727.22
0.0001	1935464.93

Table A4. data for calibration curve of 1-ArToS.

Each sample injected in triplicate. HPLC method: 80% methanol / 20% H_2O. Flow rate = 0.8 mL/min over 20 min, λ = 230 nm, injection volume = 20 µL.

Typical retention times: 1-ArToS ~ 4.5 min.

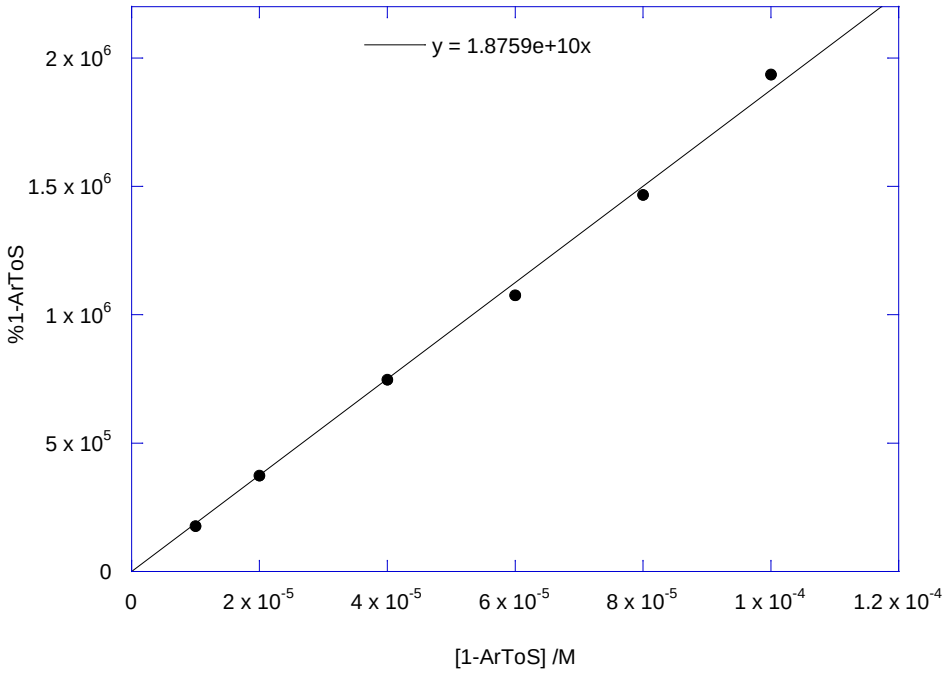

Figure A4. calibration curve of 1-ArToS.

(peak area) = 1.88 x 10^{10} [1-ArToS]

1.5 Calibration curve of 16-ArOH

[16-ArOH] /M	Peak area
0.00001	83047.71
0.00002	171383.22
0.00004	355688.90
0.00006	540859.63
0.00008	727668.45
0.0001	925655.56

Table A5. data for calibration curve of 16-ArOH.

Each sample injected in triplicate. HPLC method: 55% methanol / 45% isopropanol. Flow rate = 0.4 mL/min over 40 min, λ = 220 nm, injection volume = 10 µL.

Typical retention times: 16-ArOH ~ 10 min.

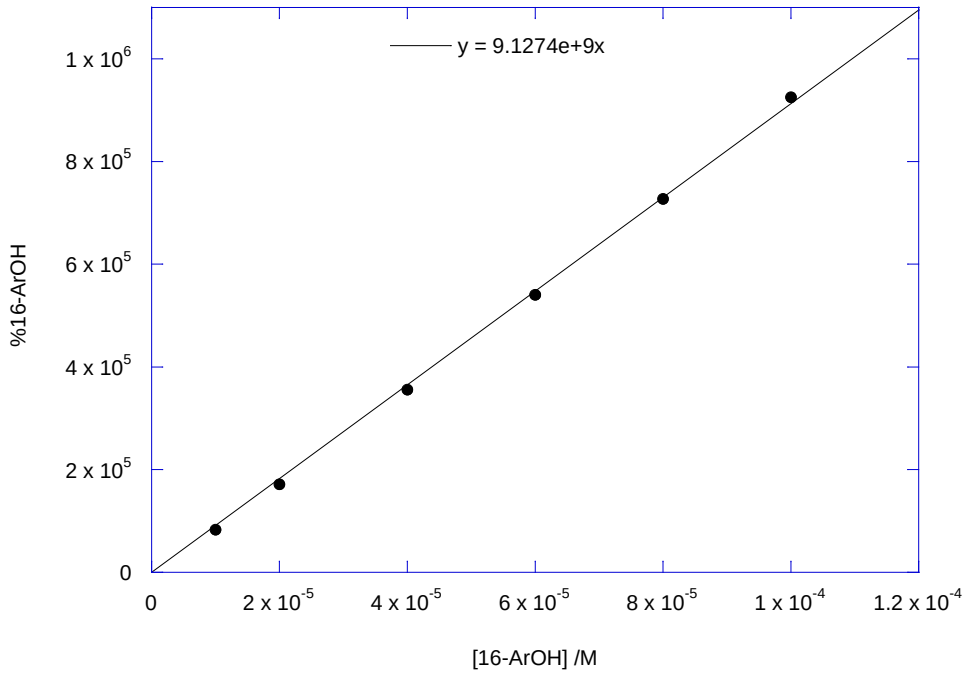

Figure A5 . calibration curve of 16-ArOH.

(peak area) = 9.13×10^9 [16-ArOH]

1.6 Calibration curve of 16-ArBr

[16-ArBr]/M	Peak area
0.00002	252235.11
0.00004	515439.47
0.00006	776464.96
0.00008	1014358.90
0.0001	1327966.25

Table A6. data for calibration curve of 16-ArBr.

Each sample injected in triplicate. HPLC method: 55% methanol / 45% isopropanol. Flow rate = 0.4 mL/min over 40 min, λ = 220 nm, injection volume = 10 μL.

Typical retention times: 16-ArBr ~ 35 min.

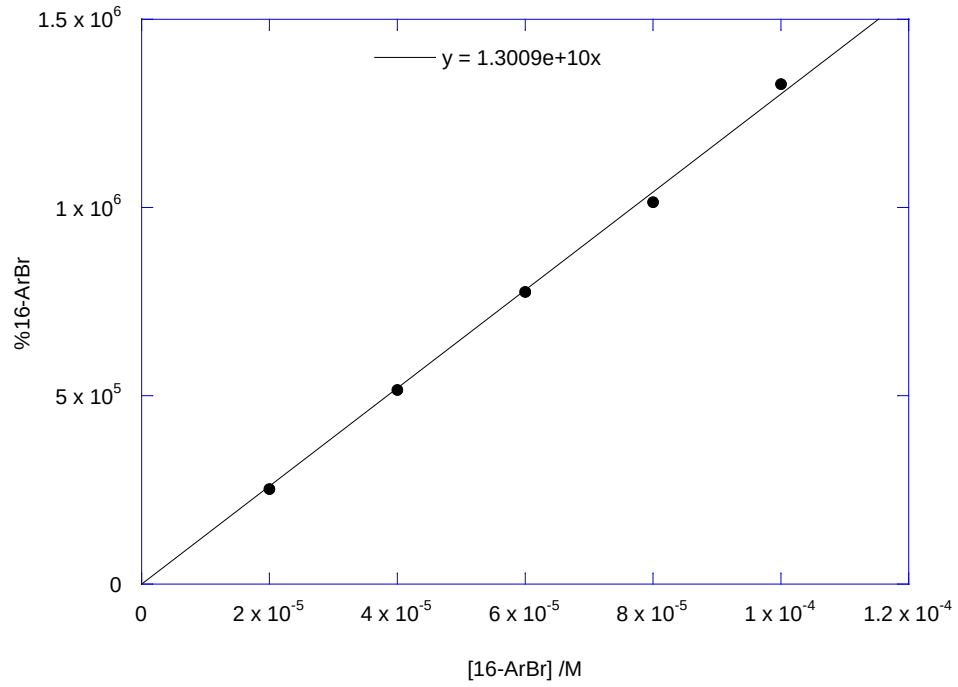

Figure A6. calibration curve of 16-ArBr.

(peak area) = 1.30 x 10^{10} [16-ArBr]

1.7 Calibration curve of 16-ArToS

[16-ArToS]/M	peak area
0.0000167	3544044
0.0000418	8852913
0.0000622	13540497
0.000089	18189417

Table A7. data for calibration curve of 16-ArToS.

Each sample injected in triplicate. HPLC method: 55% methanol / 45% isopropanol. Flow rate = 0.4 mL/min over 40 min, λ = 220 nm, injection volume = 100 µL.

Typical retention times: 16-ArToS ~ 27 min.

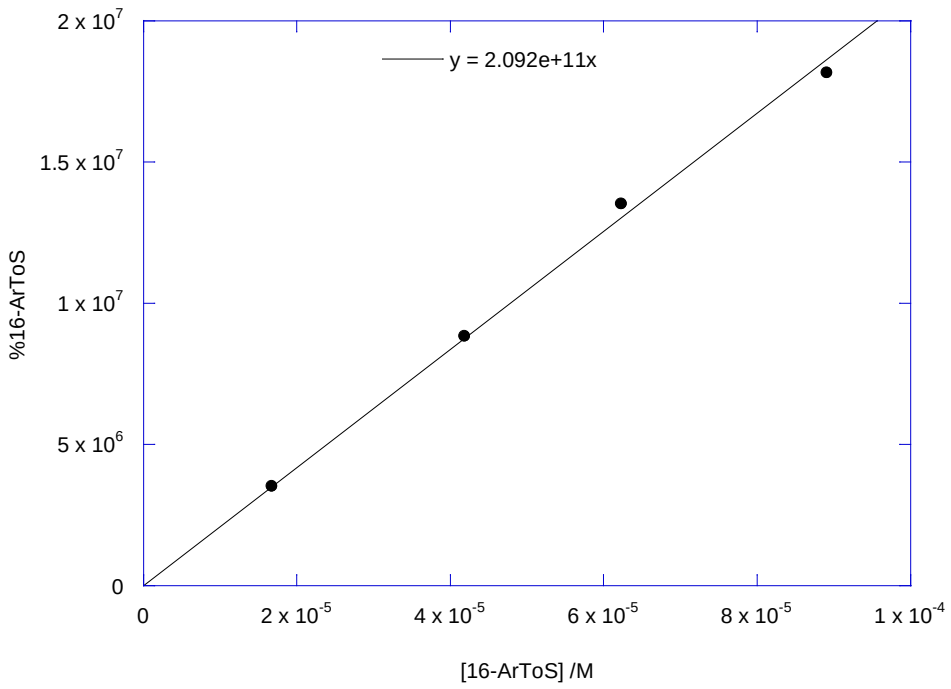

Figure A7. calibration curve of 16-ArToS.

(peak area) = 2.09 x 10^{11} [16-ArToS]

2. Chemical Trapping Experiment Original Data

Table A8. HPLC peak areas and observed yields for the Reaction of DTAB solution and added TMAB with 2.5 x 10^{-4} M of 16-ArN_2BF_4 in 0.001 M HBr at 25°C (refer to Table 4)

[TMAB] (M)	[DTAB] (M)	Inject Volume (µL)	Peak Area (µV•s)			Observed %Yields			
			16- ArOH	16-ArH	16-ArBr	16-ArOH	16-ArH	16-ArBr	Total
0	0.05	20	1164406.1	78119.6	495010.73	68.5	4.8	19.9	98.0
0	0.1	10	589971.3	38566.1	286035.3	66.5	4.5	22.0	97.5
0	0.2	10	579539.4	45900.9	315626.6	65.3	5.4	24.3	100.4
0	0.3	20	1010554.8	124125.0	608316.2	59.5	7.6	24.5	99.3
0	0.4	20	984946.7	136004.2	611329.0	57.9	8.3	24.6	99.1
0	0.5	10	535452.6	67698.1	370105.9	60.3	8.0	28.5	104.8
0.1	0.05	20	1037529.8	148155.0	633572.5	60.9	9.1	25.5	104.6
0.2	0.05	20	982482.1	156009.0	695479.2	57.8	9.6	28.0	105.0
0.3	0.05	20	943711.8	173224.2	695755.6	55.5	10.6	28.0	104.7
0.4	0.05	20	843727.3	194207.6	723300.6	49.6	11.9	29.1	102.5
0.5	0.1	10	534880.0	46946.7	431273.5	60.3	5.5	33.2	104.5
0.5	0.4	10	485685.5	70933.8	477145.6	54.8	8.4	36.8	108.4
0.6	0.05	20	851631.9	191685.1	731195.9	50.1	11.8	29.4	103.1
1	0.05	10	495616.2	24206.8	522639.0	55.3	2.8	38.6	99.5
1	0.1	10	480084.7	82057.9	504160.5	54.1	9.6	38.8	112.1
1	0.5	10	433600.2	88346.6	505870.0	48.9	10.4	39.0	108.7
1.5	0.05	10	442991.0	28841.0	517014.6	49.9	3.4	39.8	96.5
1.5	0.1	10	444965.3	49306.9	529220.5	50.2	5.8	40.7	102.5
1.5	0.3	10	414465.6	65141.0	576189.3	46.7	7.6	42.6	104.5
2	0.05	10	439876.1	43744.3	579490.2	49.5	5.1	44.6	104.3
2	0.1	10	400480.0	50095.8	556771.4	45.1	5.9	42.8	99.7
2.5	0.05	10	389558.7	46019.4	627335.9	43.9	5.4	48.3	103.0
2.5	0.1	10	369899.4	55208.7	621346.9	41.7	6.5	47.9	102.6
2.5	0.2	10	347292.1	62203.5	644937.1	39.2	7.3	49.6	103.4

Table A9. Average deviation of peak area

[TMAB] (M)	[DTAB] (M)	Inject Volume (µL)	Peak Area (µV•s)			Average Deviation		
			16- ArOH	16-ArH	16-ArBr	16-ArOH	16-ArH	16-ArBr
0	0.05	20	1164406.1	78119.6	495010.73	51961	0	3760
0	0.1	10	589971.3	38566.1	286035.3	1986	549	3044
0	0.2	10	579539.4	45900.9	315626.6	3634	358	3393
0	0.3	20	1010554.8	124125.0	608316.2	119	5899	17037
0	0.4	20	984946.7	136004.2	611329.0	12988	833	6289
0	0.5	10	535452.6	67698.1	370105.9	984	252	6927
0.1	0.05	20	1037529.8	148155.0	633572.5	1413	1672	7256
0.2	0.05	20	982482.1	156009.0	695479.2	5924	1917	20890
0.3	0.05	20	943711.8	173224.2	695755.6	7828	10158	23136
0.4	0.05	20	843727.3	194207.6	723300.6	13020	8765	4517
0.5	0.1	10	534880.0	46946.7	431273.5	218	1028	4318
0.5	0.4	10	485685.5	70933.8	477145.6	387	349	5588
0.6	0.05	20	851631.9	191685.1	731195.9	7645	16836	32742
1	0.05	10	495616.2	24206.8	522639.0	0	0	0
1	0.1	10	480084.7	82057.9	504160.5	1525	313	4334
1	0.5	10	433600.2	88346.6	505870.0	2585	528	1647
1.5	0.05	10	442991.0	28841.0	517014.6	247	1481	20563
1.5	0.1	10	444965.3	49306.9	529220.5	5003	129	4992
1.5	0.3	10	414465.6	65141.0	576189.3	5769	70	2394
2	0.05	10	439876.1	43744.3	579490.2	837	379	1315
2	0.1	10	400480.0	50095.8	556771.4	180	550	9722
2.5	0.05	10	389558.7	46019.4	627335.9	687	619	18338
2.5	0.1	10	369899.4	55208.7	621346.9	1874	511	3634
2.5	0.2	10	347292.1	62203.5	644937.1	3996	439	12969

Table A10. HPLC peak areas and observed and normalized yields for the Reaction of NaToS solution with 1-ArN_2BF_4 in 0.01 M HBr at 25°C, solution diluted 10 times and inject volume is 100 µL (refer to Table 5)

[NaToS]	Peak Area (μV•s)		Observed %Yields			Normalized %Yields	
(M)	1-ArOH	1-ArToS	1-ArOH	1-ArToS	total	1-ArOH	1-ArToS
0.5	1908888.9	1738324.9	63.2	12.6	75.8	83.4	16.6
*	201608.1	165579.6	52.0	10.1	62.1	83.7	16.3
1.0	1503660.1	2583518.4	59.6	22.0	81.6	73.0	27.0
	1660627.6	2781463.8	55.0	19.7	74.7	73.6	26.4
**	461468.3	779714.0	46.6	16.7	63.3	73.6	26.4
1.5	1454141.7	3564216.3	48.1	25.0	73.1	65.8	34.2
2.0	1177029.6	3835122.6	46.6	32.2	78.8	59.1	40.9
	1324312.8	4346954.6	42.8	30.4	74.2	59.0	41.0
2.5	759326.1	3087386.9	36.9	32.0	68.9	53.6	46.4

* solution diluted 10 times and inject volume 20 μL

**solution diluted 5 times and inject volume 20 μL

Table A11. HPLC peak areas and observed yields for the Reaction of CTAToS and CTAC mixture surfactants with 16-ArN_2^+ 2.5×10^{-4} M in 0.01 M HCl at 25°C, injection volume 20 μL (Refer to Table 6)

[CTAToS]	[CTAC]	Peak Area (μV•s)				Observed %Yields				
(mM)	(mM)	16-ArOH	16-ArToS	16-ArH	16-ArCl	16-ArOH	16-ArToS	16-ArH	16-ArCl	total
0	10	19942782.5	0	361022.6	4683305.9	89.5	0	1.6	12.2	101.3*
1	9	3190305.7	144348.6	198065.2	519472.8	73.3	0.8	4.8	7.2	90.9
2	8	3207486.7	263968.0	204720.5	451513.4	73.7	2.1	4.9	6.3	91.9
3	7	19960166.5	3254495.3	523277.1	3033035.0	86.0	5.8	2.4	7.9	104.5*
4	6	3210794.7	590619.3	0	218755.2	73.8	5.5	0	3.0	82.3
5	5	19414226.6	5566643.4	662592.8	1825772.8	83.6	10.3	3.0	4.8	104.7*
6	4	3353387.3	1117323.1	163890.5	213630.0	77.1	11.0	3.9	3.0	98.8
7	3	3206873.8	1324242.1	0	239148.23	73.7	13.2	0	3.3	90.2
8	2	18719743.3	9542890.5	656665.1	1029676.2	80.6	18.1	3.0	2.7	107.4*
9	1	18698439.9	10473235.7	850154.5	737509.0	80.5	19.9	3.8	1.9	109.9*
10	0	3367212.3	1847800.5	0	0	77.4	18.6	0	0	96.0

*injection volume 100 μL

Table A12. HPLC peak areas and observed yields for the Reaction of CTAToS surfactant with 2.5×10^{-4} M of 16-ArN_2^+ in ToSOH at 25°C (Refer to Table 7)

[CTAToS]	[ToSOH]	Peak Area (μV•s)			Observed %Yields			
(mM)	(M)	16-ArOH	16-ArToS	16-ArH	16-ArOH	16-ArToS	16-ArH	total
0.25	0.001	1606318.1	1041964.1	137689.1	35.2	9.8	3.2	51.4
0.5	0.001	1876271.3	1191501.4	148939.2	41.2	11.2	3.4	59.2
1	0.001	1897615.8	1249882.9	125818.3	41.6	11.8	2.9	59.2
2	0.001	2481845.6	1559897.0	0	54.4	14.9	0	69.3
3	0.001	3057496.0	1893355.8	0	67.1	18.2	0	85.3
4	0.001	3186354.2	2045538.1	79206.0	69.9	19.8	1.8	93.3
6	0.001	3350385.6	2231641.4	49808.2	73.5	21.6	1.1	97.3
0.25	0.01	6849222.4	4898892.7	420574.8	63.6	19.3	4.1	91.1
0.5	0.01	7299969.0	5032462.7	380774.0	67.7	19.9	3.7	95.0
1	0.01	5943252.8	3350177.2	250088.0	55.2	12.8	2.4	72.8
2	0.01	7435872.5	4648421.3	301298.8	69.0	18.3	2.9	93.1
3	0.01	7977724.9	5293891.9	259332.5	74.0	21.0	2.5	100.0
4	0.01	7884649.7	5051321.5	131772.9	73.2	20.0	1.3	95.8
6	0.01	7466653.2	4958260.7	172924.5	69.3	19.6	1.7	92.3

Table A13. HPLC peak areas and observed yields for the Reaction of CTAToS surfactant with 2.5 x 10^{-4} M of 16-ArN_2^+ in 0.001 M of HBr at 25°C (Refer to Table 8)

[CTAToS] (mM)	[NaToS] (M)	Peak Area (μV•s)			Observed %Yields			
		16-ArOH	16-ArToS	16-ArH	16-ArOH	16-ArToS	16-ArH	total
5	0	6848371.6	3884195.4	102061.4	72.5	17.2	1.1	91.9
7.5	0	7190021.1	4242340.4	112265.9	76.1	18.9	1.2	97.4
10	0	7472473.4	4475517.6	183132.4	79.1	20.0	2.0	103.1
15	0	7216994.4	4595454.1	245076.1	76.4	20.6	2.7	102.4
20	0	7249563.4	4598179.2	278027.7	76.7	20.6	3.1	103.5
5	0.02	7070946.8	5016524.6	372264.6	74.8	22.6	4.1	105.6
7.5	0.02	6815602.5	4878837.9	487489.2	72.1	22.0	5.4	104.9
10	0.02	7040729.2	4910770.3	560077.8	74.5	22.1	6.2	109.0
15	0.02	6807405.4	4599449.6	543221.4	72.0	20.6	6.0	104.6
20	0.02	6816570.8	4812139.6	742466.4	72.1	21.6	8.2	110.1
5	0.04	6851885.1	5080449.3	336421.0	65.1	20.6	3.3	92.3
7.5	0.04	7172122.1	5095172.2	311782.0	68.1	20.6	3.1	94.9
10	0.04	7378141.0	5247340.8	127516.8	70.1	21.3	1.3	94.0
15	0.04	7517063.7	5170561.9	0	71.4	21.0	0	92.4
20	0.04	7615008.0	5314243.0	268047.2	72.3	21.6	2.7	99.3

3. Normalization of products

The chemical trapping experiments applied to surfactants have three products, 16-ArOH, 16-ArX (X = Br, Cl, ToS, etc.), and 16-ArH which is the reduced product of 16-ArOH and unreacted 16-ArN_2^+. To determine normalized %yield of 16-ArX and 16-ArOH, the total yield of 16-ArN_2^+ is considered to consume in two reactions:

$$\%16\text{-}ArN_2^+ = \%16\text{-}ArN_2^+{}_h + \%16\text{-}ArN_2^+{}_{Ox/Red}$$

$\%16\text{-}ArN_2^+{}_h$ is the percentage of 16-ArN_2^+ that undergoes heterolytic reaction

$$\%16\text{-}ArN_2^+{}_h = \%16\text{-}ArOH_h + \%16\text{-}ArX_h$$

and $\%16\text{-}ArN_2^+{}_{Ox/Red}$ is the percentage of $\%16\text{-}ArN_2^+$ that reduces 16-ArOH.

$$\%16\text{-}ArN_2^+{}_{Ox/Red} + \%16\text{-}ArOH_{Ox/Red} = \%16\text{-}ArH_{Ox/Red} + \%16\text{-}ArOX_{Ox/Red}$$

This equation shows that one equivalent of 16-ArH produced consumes one equivalent of 16-ArOH and one of 16-ArN_2^+. So $\%16\text{-}ArN_2^+$ is given by

$$\%16\text{-}ArX_h + \%16\text{-}ArOH_h + 2 * (\%16\text{-}ArH_{Ox/Red}) = \%16\text{-}ArN_2^+{}_T$$

where $2 * (\%16\text{-}ArH_{Ox/Red}) = \%16\text{-}ArOH_{Ox/Red} + \%16\text{-}ArH_{Ox/Red}$

the total product yield from the heterolytic pathway becomes

$$\%16\text{-}ArX_h + \%16\text{-}ArOH_h + \%16\text{-}ArH_{Ox/Red} = \%16\text{-}ArN_2^+{}_h$$

All three items on the left of equation are obtained directly from HPLC results.

Definition of normalized product yields are listed as

$$\%16\text{-}ArOH_N = (\%16\text{-}ArOH_h + \%16\text{-}ArH_{Ox/Red}) / \%16\text{-}ArN_2^+{}_h$$

$$\%16\text{-}ArX_N = \%16\text{-}ArX_h / \%16\text{-}ArN_2^+{}_h$$

subscript N means normalized yields.

The normalized yields of 16-ArOH and 16-ArX are used to calculate the concentrations of X^- and H_2O in micellar interfacial region.

$$Br^-_m = (\%16\text{-}ArBr_N / 19.95)^{1.439}$$

$$S_w^{Br} = 12.01 \times Br^-_m{}^{-0.272}$$

$$Br^-_w = \{ \alpha ([CTAB] - cmc) + cmc + [HBr] + [TMAB] \} / (1 - V [CTAB])$$

$$H_2O_m = S_w^{Br} Br^-_m \%16\text{-}ArOH_N / \%16\text{-}ArBr_N$$

$$ToS_m = (\%16\text{-}ArToS_N / 26.14)^{1.56}$$

$$S_w^{ToS} = 17.52 \times ToS_m^{-0.275}$$

$$ToS_w = \{ \alpha ([CTAT] - cmc) + cmc + [NaToS] \} / (1 - V [CTAT])$$

$$H_2O_m = S_w^{ToS} ToS_m \%16\text{-}ArOH_N / \%16\text{-}ArToS_N$$

curriculum vitae

Yan Cai

Education

2003-3013 Rutgers University, New Brunswick, NJ
Ph.D., Department of Chemistry and Chemical Biology

1999-2003 Nanjing University, Nanjing, China
B.S. Chemistry

Publication

Ning Bao, Jing-Juan Xu, Yue-Hua Dou, **Yan Cai**, Hong-Yuan Chen, and Xing-Hua Xia; "Electrochemical Detector for Microchip Electrophoresis of Poly(dimethylsiloxane) with a Three-dimensional Adjustor"; *Journal of Chromatography A*; 2004; 1041(1-2) pp 245-248.